University of Stavanger

Faculty of Science and Technology

MASTER'S THESIS

Study program/ Specialization: Offshore Technology – Marine and Subsea Technology	Spring semester, 2015 Restricted access
Writer: Knut Erik Gluggvasshaug	…… (Writer's signature)
Faculty supervisor: Ove Tobias Gudmestad External supervisor(s): Tor-Bjørn Idsøe Næss – Subsea 7	
Thesis title: Study of the Module Handling System on Seven Viking	
Credits (ECTS): 30	
Key words: - Module Handling System - Lifting operations - Subsea modules - Moonpool - Sensitivity analysis - SIMO	Pages: 133 + enclosure: 10 Stavanger, 15.06.2015 Date/year

University of Stavanger

Study of the Module Handling System on Seven Viking

Knut Erik Gluggvasshaug

June 2015

MASTER THESIS

Supervisor 1: Tor-Bjørn Idsøe Næss, Subsea 7

Supervisor 2: Ove Tobias Gudmestad, UiS

Abstract

Subsea installations is a vital part of the oil and gas industry, but as have also been a major cost factor. When the oil price decline, subsea installations are one of the first fields to be affected. The priority to cost optimize have never been more important. Using module-based subsea installations allows for simplified maintenance and fast replacement, thus minimizing downtime. Subsea modules allows for easier installations compared to fully integrated subsea equipment as the modules are smaller and lighter. This allows for a wider range of construction vessels to be considered for installation.
Light construction, intervention and Inspection, Maintenance and Repair (IMR) vessel may all be considered for installations of subsea modules. A normal feature of these vessels is the use of a Module Handling System (MHS). The MHS is a system that allows for a safe and predictable deployment and recovery of modules. Subsea modules can be of such a size that the capacity of the vessel is challenged.

In this thesis a study of the MHS has been completed. The main part of the study has been to use Simulation of Marine Operations (SIMO) to simulate and analyse the critical phase where a module is suspended in air from the MHS tower. A literature study presenting the previous work done by Subsea 7 where the critical aspects of deployment and recovery through moonpool is presented and discussed.

The analysis show that resonance between vessel motion and module motion is a major issue when the module is suspended in air. This cause limitation in operability. Analysis show that the operative sea state can increase if the design of guidance system on the MHS is modified. The sea state can be further increased by adding means to equalize the resonance.

Previous work done by Subsea 7 show that clearance between the modules and the moonpool walls are critical for modules that is in the vicinity of the capacity limit of the MHS.
Based on the results from the analysis presented in this thesis and from previous work by Subsea 7, the technical requirements stated by Statoil in TR1231 for MHS seem unrealistic and are unlikely to be met.

Preface

This thesis is the concluding part of my MSc program in Offshore Technology at the University of Stavanger (UiS). This thesis was proposed and carried out in cooperation with Subsea 7. The work has been conducted during the spring semester 2015. The purpose of this thesis is to investigate the critical aspects of the MHS on Seven Viking. Special focus have been put on the critical phase where a module is suspended in air.
Subsea 7 have provided me with a simulation software and relevant data of the vessel and the lifting system, which enabled me to analyse the deployment of modules.
A lot of time has been put into learning the simulation software SIMO and Matlab. Numerous trials and errors have been made to get qualitative analysis. This thesis includes expressions and jargon used in marine technology and lifting operations, and the expected reader should have the knowledge representative for a master student in marine technology.
During the work with this thesis I have received help from numerous people. First of all I would like to thank my supervisor at Subsea 7, Tor-Bjørn Idsøe Næss for helping my define the topics of the thesis and providing me with all relevant data concerning the simulations and great inputs and advice during the analysis. I would also like to thank Marius Milch for giving me the opportunity to write this thesis for Subsea 7 and the IMR department for inputs and advice during my work. I would also like to thank my faculty supervisor, Ove Tobias Gudmestad, who have provided me with fast responses and guidance, and also my fellow students for educational discussion and good support during the work with the thesis. My smart and generous girlfriend, Ragnhild Bechmann also deserve praise for her constant motivation, great advice and her expertise in Matlab, which have helped me many times.

Stavanger, 2015-15-06

Knut Erik Gluggvasshaug

Contents

List of Figures

List of Tables

Chapter 1

Introduction

1.1 Background

In times when cost efficiency have become a major concern in the oil and gas industry, subsea module installations from IMR vessels have become more relevant. When it comes to size and mass of subsea modules, they challenge the lifting capacity of IMR vessels. Seven Viking have a dedicated MHS for deployment and recovery of modules up to $70Te$. Subsea 7 and Statoil have a frame agreement for the IMR vessel Seven Viking. According to this agreement the MHS should be designed according to the technical requirements TR1231. When the MHS was designed the requirements to the MHS was not clearly stated. After the completion of Seven Viking, a revised version of TR1231 where defined requirements are stated, have been issued. The main requirements are:

- Significant Wave Height (H_S) of $5.0m$
- Heading = $\pm 15°$
- Module CoG = $3.0m$ below the below the top of the funnels
- Module CoG at maximum $6.0m$ above main deck

- Module footprint = $6x6m$

These requirements does not concern Seven Viking, but future vessels. It is still of interest to investigate whether the MHS meet these requirements and what the limitations of the MHS are.

During the work with the Gullfaks Subsea Compression (GSC) modules up to the capacity of the MHS have been put through analysis to investigated what the limitations for the specific modules are. The most important components of the MHS is the cursor system which provides movement control during deployment and recovery and the skidding system that transport the modules on deck.

A critical phase of the deployment is when the module is hanging in air. During this phase the module will be suspended from the vessel by a main lift wire and docked to a cursor guide frame that restrain lateral movement. The docking have a clearance that allows for some lateral and rotational motion. Because of the clearance the suspended module act as a pendulum. The length of the main lift wire to the CoG of the module will be of such a nature that the interference between vessels period and eigen period of the module may cause resonance. If resonance occurs, the rotation motion of the module increase, and thereby increasing the forces that is exerted on the MHS.

There are basically to options for dealing with this problem:

1. Design the MHS to withstand the loads applied
2. Design the MHS to prevent resonance

Sensitivity analysis of the phase where the module is suspended in air remains to be done. Special emphasis will be put into understanding the resonance of the system and examining means to reduce and equalize resonance in the system.

Det Norske Veritas (DNV) standards and Norsk sokkels konkurranseposisjon (NORSOK) standard deal with general operations. With lifting operations using the MHS on Seven Viking

there has been done research regarding special operations. The Subsea 7 internal document, MODULES DEPLOYMENT AND RECOVERY ANALYSES, [15] and HANDLING OF STRUCTURES IN MOONPOOL, [14] both discuss the MHS with special emphasis on the deployment through moonpool. A complete literature study will be presented in chapter 4. Since operations are different on different on different vessels, it is difficult to find relevant information from other publication other than the specific standards.

1.2 Objectives

The main objectives of this Master's thesis are:

1. Find the sea state where the MHS can safely operate
2. Compare the original prong setup with the new PILT design
3. Examine the effect of module CoG and footprint
4. Improve the MHS

1.3 Limitations

The objective of the thesis is not to check whether SIMO gives the right output or not. It is assumed that the methods used by SIMO is correct, and they will not by checked by manual calculations as it would be highly complicated and time consuming.

The Joint North Sea Wave Observation Project (JONSWAP) spectrum is used in the sensitivity analysis. As realistic sea may consist of both wind sea and swell with different directions Torsethaugen spectrum or double-peaked JONSWAP spectrum should would be preferable when describing the irregular sea.

The extreme value is estimated using a Gumbel distribution. The distribution may not fit all scenarios equally. The values should therefore be used as guidelines for further work and not as a design basis.

1.4 Approach

To reach the objectives in section 1.2 sensitivity analysis of the MHS using the SIMO software to simulate the deployment of the module will be performed together with a literature study of previous work done by Subsea 7.

1.5 Structure of the Report

The rest of the thesis is organized as follows:

- Chapter 2 gives an introduction to the vessel and marine operations
- Chapter 3 provides an introduction to the MHS
- Chapter 4 is a literature study of the MHS with focus on the previous work done by Subsea 7
- Chapter 5 describe the methodology for the sensitivity analysis
- Chapter 6 present and discuss the results obtained by the sensitivity analysis

Chapter 2

Seven Viking and Marine Operations

2.1 Chapter overview

This thesis concern a marine operation where a module is deployed and recovered. Marine operations, such as offshore lifting operations have been extensively documented, researched and studied. There have also been put great effort into making standards to aid in planning different aspects of marine operations. This chapter aims to give an introduction to marine operations and give an overview of aspects relevant to the analysis to be performed. This thesis is based on earlier research done regarding Seven Viking.

2.2 The vessel - Seven Viking

Seven Viking was at the end of January 2013 delivered to Eidesvik Seven, a joint venture between Eidesvik Offshore and Subsea 7. The vessel is under a long term, all-year frame agreement with Statoil for subsea IMR services in the North Sea, Norwegian Sea and Barents Sea.
Seven Viking is a state-of-the-art vessel, specially designed to meet the high demands of IMR,

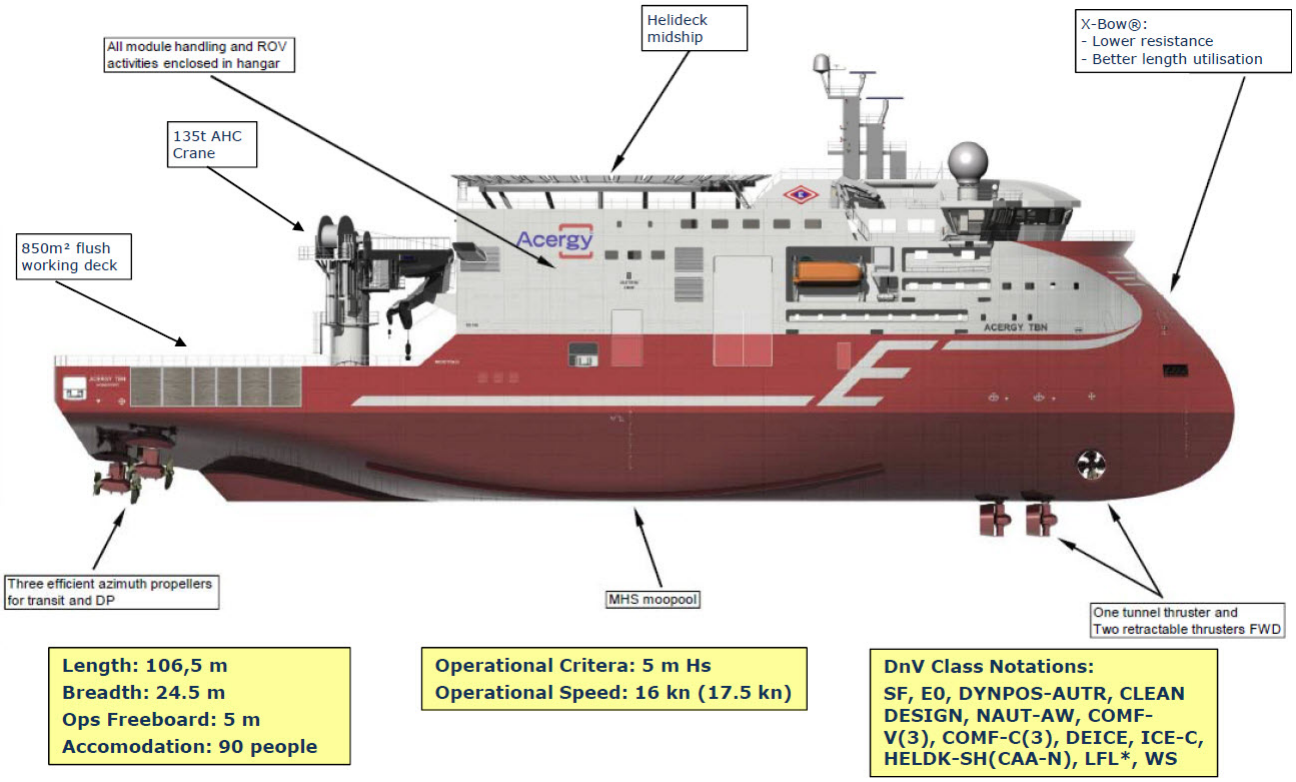

Figure 2.1: Seven Viking main data overview [12]

survey and light construction in harsh environments. The vessel is also on the top ten list of environmental friendly ships according to World Ports Climate Initiative (WPCI) [20]. All the solutions are developed to ensure safe and secure operations, including a tailored MHS integrated in the hangar. Integrated MHS contributes to prevent hazardous working situations. An illustration of the vessel and its main data is given in fig. 2.1 and the dimensions of the vessel is given in table 2.1. A presentation of the main data is given in appendix A.

Table 2.1: Dimensions of Seven Viking

Dimensions	
Length overall	106.5m
Breadth moulded	24.5m
Draught - operational	6.5m
Draught - max	8.0m
Freeboard at operational draught	5.0m
Freeboard at max draught	3.5m

The vessel has a Dynamic Positioning (DP) system and is certified to class DYNPOS AUTR in

compliance with [6]. The class notation state that to achieve the classification DYNPOS AUTR the dynamic positioning system must have redundancy in technical design and with an independent joystick system back-up.
The principles of dynamic positioning are the same regardless of the manufacturer, type of system hardware or complexity of vessel. A DP system controls a vessel's position and heading automatically.
The active control of thrusters and propellers counteracts the effects of environmental forces and enables the vessel to remain on location at or very near to a specified point. An illustration of a basic dynamic positioning system is given in fig. 2.2

The shape of the vessel makes it very efficient during transit, but is sensitive to roll motions. In the autumn of 2014 new anti roll tanks was installed by Eidesvik. The new anti roll tanks can be activated during operations to decrease the roll motions. However, the new anti roll tanks also caused an increase in pitch motion. The new Response Amplitude Operators (RAOs) for roll, pitch and heave is illustrated in figs. 2.3 to 2.5 respectively. The RAOs for yaw, surge and sway can be found in appendix B

The wave direction relative to the vessel is following the definitions illustrated in fig. 2.6.

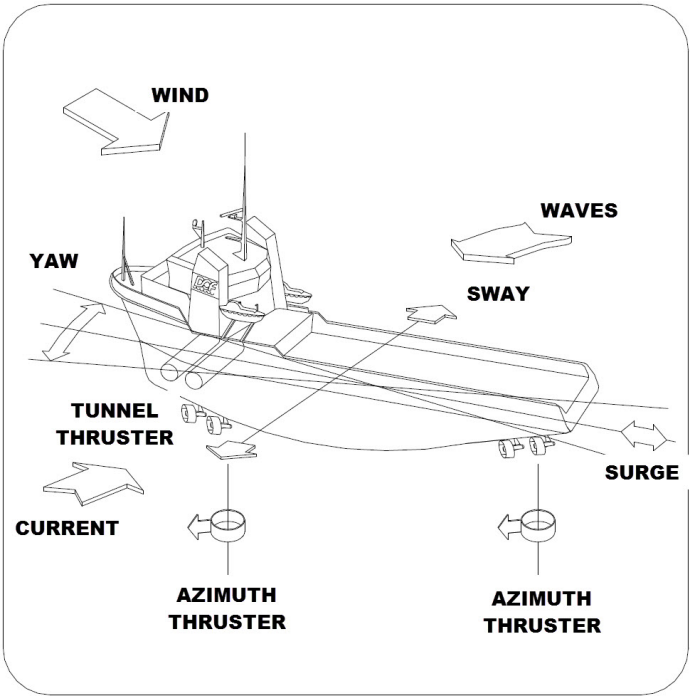

(a) A sea going vessel is subject to wind, wave and current forces. Wind speed and direction are measured by the wind sensor. The vessels response to wave and current forces is accurately calculated.

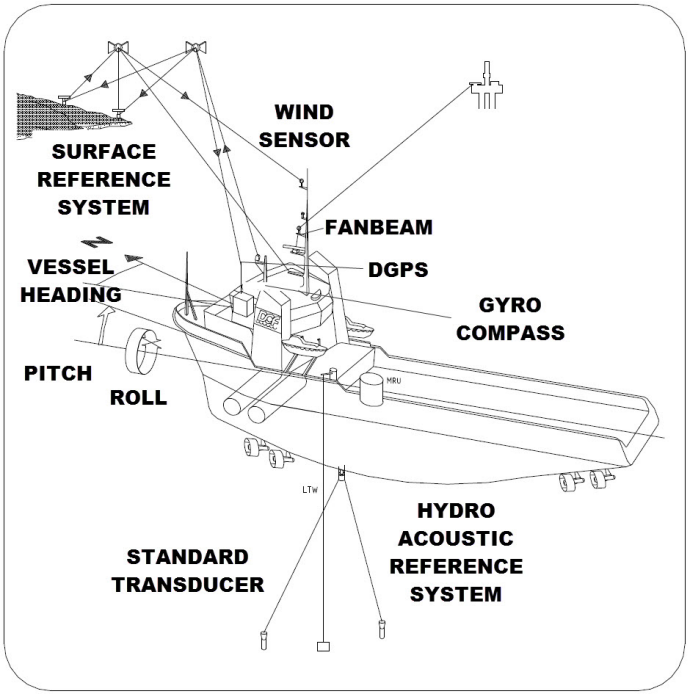

(b) The DP system controls the vessels motion in the three horizontal degrees of freedom - SURGE, SWAY and YAW. Vessel movements are measured by the Gyro compass and the reference systems.

Figure 2.2: Dynamic positioning system [2].

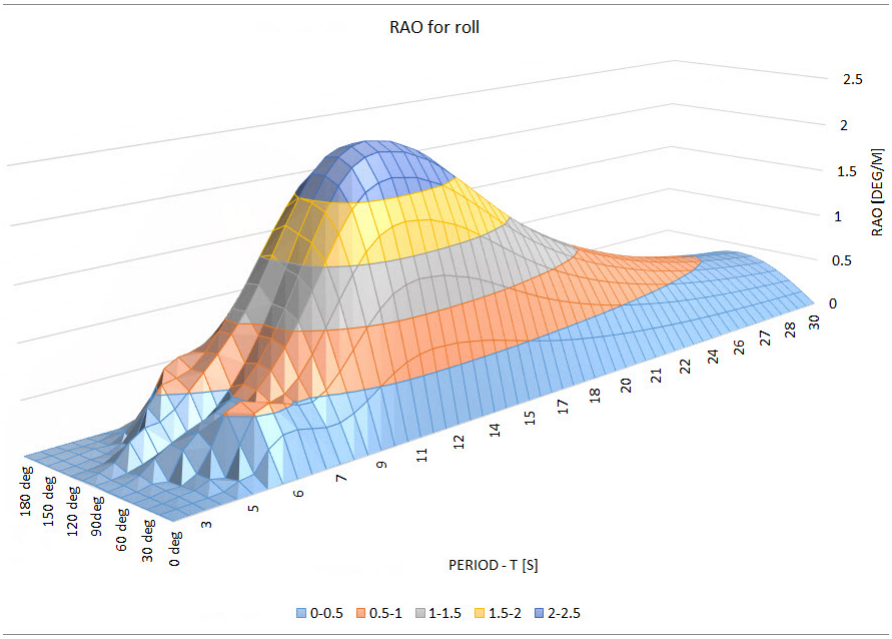

Figure 2.3: RAO for roll

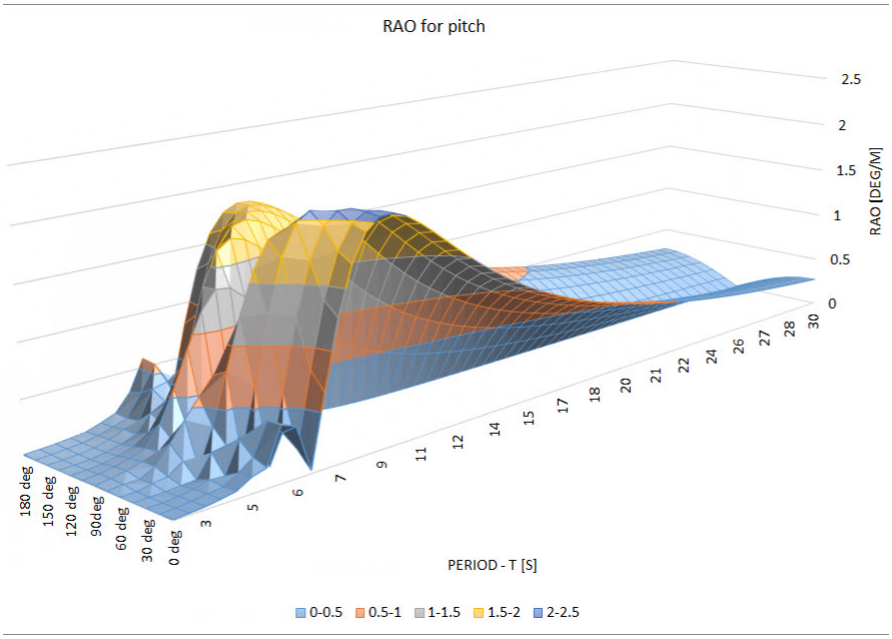

Figure 2.4: RAO for pitch

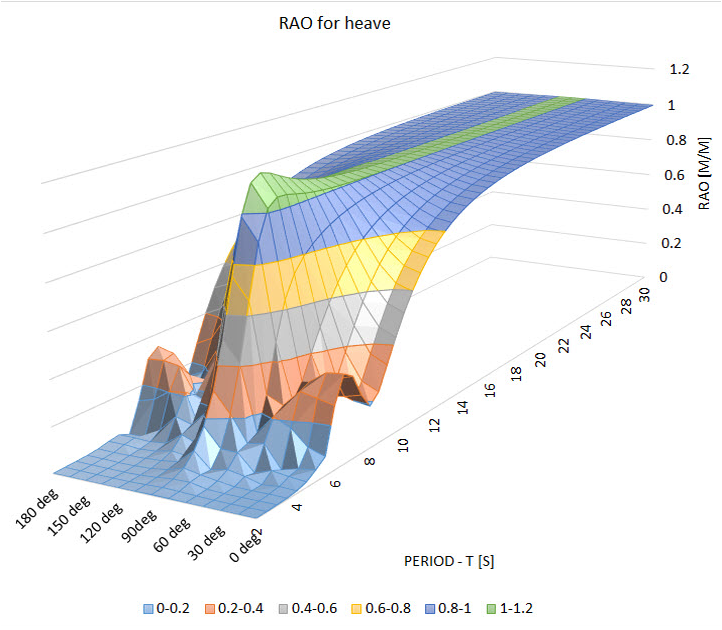

Figure 2.5: RAO for heave

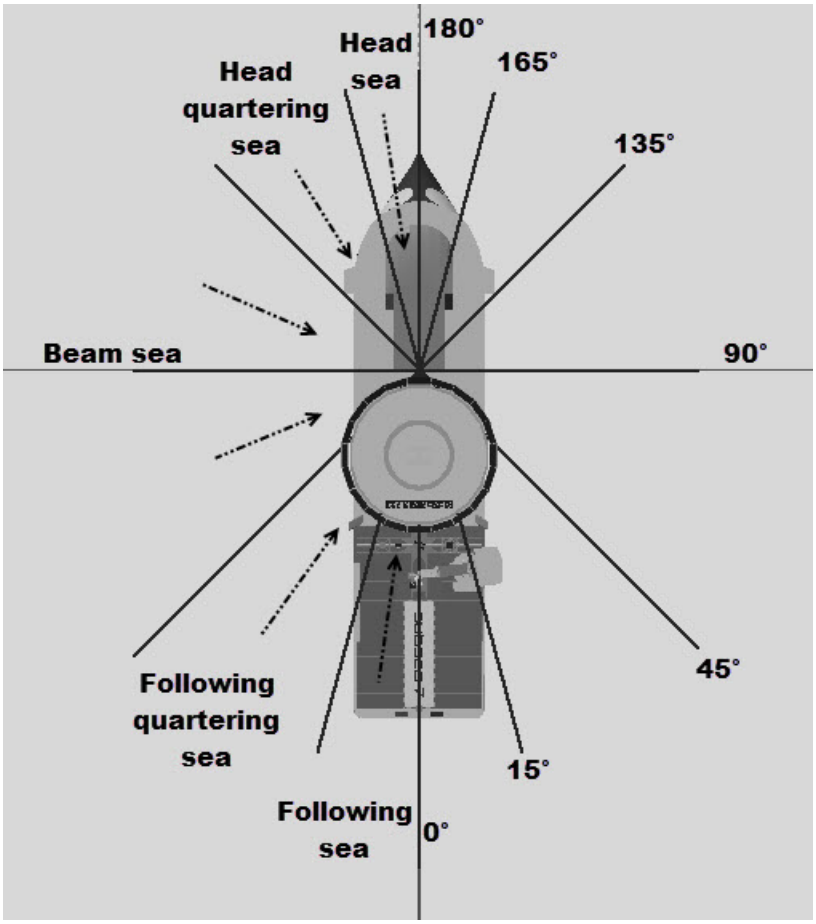

Figure 2.6: Wave direction definitions

2.3 Marine Operations

According to the DNV standard for Marine Operations, [5] a marine operation is:

> "Non-routine operation of a limited defined duration related to handling of object(s) and/or vessel(s) in the marine environment during temporary phases. In this context the marine environment is defined as construction sites, quay areas, inshore/offshore waters or subsea."

The standard also defines an object as:

> "The structure handled during the marine operation, typically a module, deck structure, jacket, GBS (Gravity Based Structure), subsea structures, risers, pipes, etc."

A routine operation (i.e. an automated factory assembly) is where all the phases of the operation is precisely known. The conditions are controlled so that the phases are only dependent on each other. It is also completely repeatable, meaning that the duration and the outcome of the operation will not vary.
In a non-routine operation, the varying conditions control the duration and outcome of the operation. A non-routine operation is therefore non-repeatable in the sense that the scope of operation may vary because of the uncertainties regarding the variable conditions.

There are many considerations to be made during the planning of a marine operation. The DNV standard, [5], states that:

> "Marine operations shall be planned according to safe and sound practice, and according to codes and standards."

And:

> "A marine operation shall be designed to bring an object from one defined safe condition to another."

The above mentioned standard for marine operations, [5], is a part of the VMO (Veritas Marine Operations) standards along with DNV-OS-H102 and DNV OS-H201 through DNV OS-H206. The objective of these standards is to:

> "... ensure that marine operations are performed within defined and recognized safety levels"

According to DNV [5], it is recommended that the following seven steps are followed when a marine operation is carried out:

1. Identify relevant and applicable regulations, rules, company specifications, codes and standards, both statutory and self-elected.
2. Identify physical limitations. This may involve pre-surveys of structures, local conditions and soil parameters.
3. Overall planning of operation i.e. evaluate operational concepts, available equipment, limitations, economic consequences, etc.
4. Develop a design basis describing environmental conditions and physical limitations applicable for the operation.
5. Develop design briefs describing activities planned in order to verify the operation, i.e. available tools, planned analysis including method and particulars, applicable codes, acceptance criteria, etc.
6. Carry out engineering and design analyses.
7. Develop operation procedures.

2.4 Lifting Operations

Lifting operations can, according to [8], be divided into two categories:

- Light lifts where the lifted object is very small compared to the crane vessel. The weight of the lifted object is less than 1-2% of the displacement tonnage of the crane vessel, typically less than a few hundred tons. In this case the motion characteristics of the vessel (at the crane tip) is not affected by the lifted object.
- Heavy lifts where the weight of the lifted object is more than 1-2% of the vessel displacement tonnage and typically more than 1000 tons. For such lifts the coupled dynamics of the vessel and the lifted object must be considered.

With a static load capacity of 70Te, the lifts executed with the MHS classify as light lifts. The motion of the MHS be determined directly from the wave induced rigid body motion of the vessel. The motion of the MHS can be determined using the vessel RAOs. The eigen period for horizontal motion of a lifted module is of particular interest since it has a direct effect on the reaction between the funnels of the module and the prong system on the cursor guide frame on the MHS The reaction between the module and the prongs is illustrated in fig. 2.7.

The eigen period for horizontal motion of a lifted object in air is given by [8]:

$$T_h = 2\pi\sqrt{\left(\frac{L}{G}\right)\left(\frac{M+0.33m_L L}{M+0.45m_L L}\right)} \tag{2.1}$$

where:

M = mass of lifted object $[kg]$

m_L = mass per unit length of hoisting line $\left[\frac{kg}{m}\right]$

L = length of hoisting line + distance to module CoG in z-direction $[m]$

g = acceleration of gravity $\left[\frac{m}{s^2}\right]$

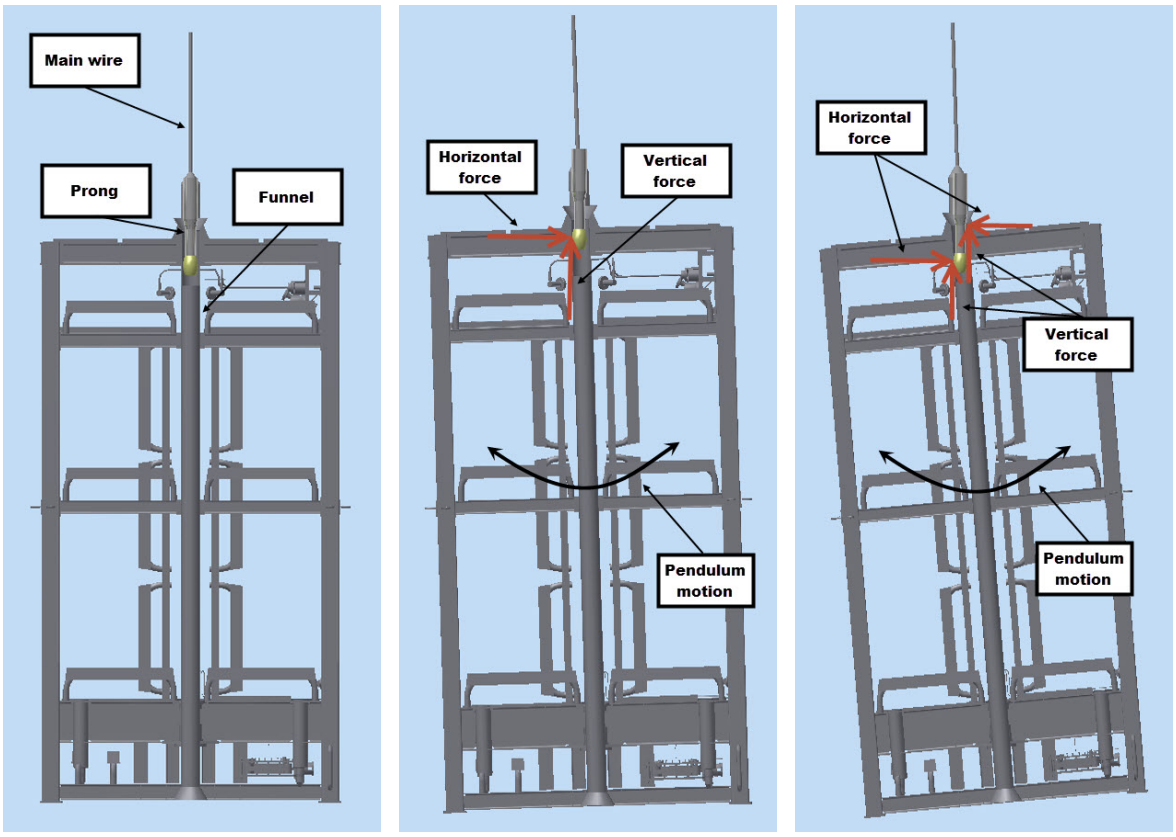

(a) Module in static equilibrium. Clearance in the prong-funnel couplings allow for some movement before contact. No forces are exerted on the MHS

(b) The pendulum motion of the module cause the funnels to make contact with the prongs, thus exerting a horizontal and vertical force on the MHS

(c) After initial contact, the module continue to rotate until the upper part of the funnels comes into contact with the prongs. At this point momentum is exerted on the MHS

Figure 2.7: Reaction forces acting on the prongs in rotational motion

When the mass of the hoisting line is less then the mass of the module, the mass of the the hoisting line can be neglected and eq. (2.1) reduces to:

$$T_h = 2\pi\sqrt{\frac{L}{G}} \tag{2.2}$$

An offshore lifting operation typically consists of the following four phases [8]

1. Lift off from deck and manoeuvring object clear of transportation vessel
2. Lowering through the wave zone

3. Further lowering down to sea bed
4. Positioning and landing

These phases and the recovery phase are described in detail in chapter 4.

2.5 Environmental Conditions

Environmental conditions are natural phenomena which contribute to structural stress and strain, impose operational limitations/restrictions or navigational considerations [5]. Phenomena of general importance are;

- Wind
- Waves
- Current
- Tide

In this thesis, only wave conditions will be described in detail as the other condition have little importance for the analysis conducted.

2.5.1 Wave Conditions

Wave conditions which are to be considered for structural design purposes, may be described either by deterministic design wave methods or by stochastic methods applying wave spectra [7].

Structures with significant dynamic response require stochastic modelling of the sea surface and its kinematics by time series. A sea state is specified by a wave frequency spectrum with a

given significant wave height, a representative frequency, a mean propagation direction and a spreading function. In applications the sea state is usually assumed to be a stationary random process. Three hours has been introduced as a standard time between registrations of sea states when measuring waves, but the period of stationariness can range from 30 minutes to 10 hours [7].

The wave conditions in a sea state can be divided into two classes: wind seas and swell. Wind seas are generated by local prevailing wind, while swell have no relationship to the local wind. Swells are longer period waves that were generated by the winds of distant weather systems [8].

2.5.2 Wave spectrum

Short term stationary irregular sea states may be described by a wave spectrum. A wave spectrum is a power spectral density function of the vertical surface displacement [7]. Two spectra are commonly used for wind seas; the Pierson-Moskowitz (PM) and JONSWAP spectra. The JONSWAP spectrum is most used as the PM spectrum is used for fully developed sea, while the JONSWAP spectrum extends the PM spectrum to include fetch limited sea, thus describing developing sea states.

The Pierson-Moskowitz spectrum $S_{PM}(\omega)$ is given by:

$$S_{PM}(\omega) = \frac{5}{16} \cdot H_S^2 \omega_P^3 \cdot \omega^{-5} exp\left(-\frac{5}{4}\left(\frac{\omega}{\omega_P}\right)^{-4}\right) \tag{2.3}$$

where:

H_S = Significant wave height $[m]$

$\omega_P = \frac{2\pi}{T_P}$ = Angular spectral peak frequency $[\frac{rad}{s}]$

$\omega = \frac{2\pi}{T}$ = Angular frequency $[\frac{rad}{s}]$

T_P = Peak period $[s]$

T = Period $[s]$

In DNV RP-C205 [7], the JONSWAP spectrum $S_j(\omega)$ is given by:

$$S_j(\omega) = A_\gamma S_{PM}(\omega)\gamma^{exp\left(-\frac{1}{2}\left(\frac{\omega-\omega_p}{\sigma\cdot\omega_p}\right)^2\right)} \tag{2.4}$$

The JONSWAP spectrum can also be written as a function of frequency f :

$$S_j(f) = \frac{5}{16}H_s^2 T_p^{-4} f^5 exp\left(-\frac{5}{4}T_p^{-4}f^{-4}\right)(1-0.287\ln\gamma)\gamma^{exp\left(-\frac{1}{2}\left(\frac{T_p f-1}{\sigma}\right)^2\right)} \tag{2.5}$$

where:

f = frequency $\left[\frac{1}{s}\right]$

γ = Non-dimensional peak shape parameter

σ = Spectral width parameter

$\sigma = \sigma_a$ for $\omega \leq \omega_p$ for eq. (2.3) or $t_p f < 1$ for eq. (2.4)

$\sigma = \sigma_b$ for $\omega > \omega_p$ for eq. (2.3) or $t_p f \geq 1$ for eq. (2.4)

$A_\gamma = 1 - 0.287\ln(\gamma)$ = Normalizing factor

Average values for the JONSWAP experiment data are $\gamma = 3.3$, $\sigma_a = 0.07$, $\sigma_b = 0.09$. For $\gamma = 1$ the JONSWAP spectrum reduces to the PM spectrum.

To describe the sea state were both wind sea and swell occur at the same time, the Torsethaugen spectrum is commonly used. The Torsethaugen spectrum is a two-peaked spectrum which is essentially two superimposed JONSWAP spectra [19]. The difference is that the high frequency tail of the Torsethaugen spectrum is assumed to be proportional to f^{-4} , while f^{-5} is used for the JONSWAP spectrum [11].

The Torsethaugen spectrum is defined as a sum of wind sea and swell and is given by:

$$S(f) = \sum_{j=1}^{2} E_j S_{nj}(f_{nj}) \tag{2.6}$$

$j = 1$ is for the primary sea system, and $j = 2$ is for the secondary sea system. Here:

$$f_{nj} = f T_{Pj}$$

$$E_j = \frac{1}{16} H_{Sj}^2 T_{Pj}$$

$$S_{nj}(f) = G_0 A_{\gamma j} \Gamma_{Sj} \gamma_{Fj}$$

For the simplified version of the spectrum it follows:

$\Gamma_{Sj} = f_{nj}^{-4} exp\left[- f_{nj}^{-4} \right]$ = Pierson-Moskowitz form of the wave spectrum

$G_0 = 3.26$ = Normalizing factor related to the Pierson-Moskowitz form

$\gamma_{F1} = \gamma^{exp\left[-\frac{1}{2\sigma^2} \left(f_{n1} - 1 \right)^2 \right]}$ = Peak enhancement function

$\gamma_{F2} = 1$ = Peak enhancement function

$\sigma = 0.07$ for $f_{nj} < 1$ and $\sigma = 0.09$ for $f_{nj} \geq 1$

$A_{\gamma 1} = \frac{1 + 1.1\left[\ln(\gamma) \right]^{1.19}}{\gamma}$ = Normalizing factor

$A_{\gamma 2} = 1$ = Normalizing factor

Common parameter:

$$T_f = 6.6 H_s^{\frac{1}{3}}$$

For wind dominated sea $\left(T_p \leq T_f \right)$

Primary peak:

$$H_{S1} = H_{Sw} = r_{pw} H_S$$

$$T_{P1} = T_{Pw} = T_P$$

$$\gamma = 35 \left[\frac{2\pi}{g} \frac{H_{Sw}}{T_P^2} \right]^{0.857}$$

Secondary peak:

$$H_{S2} = H_{Ssw} = \sqrt{1 - r_{pw}^2} H_S$$

$$T_{P2} = T_{Psw} = T_f + 2.0$$

$$\gamma = 1$$

$$r_{pw} = 0.7 + 0.3\exp\left(- \left(2 \frac{T_f - T_P}{T_f - 2\sqrt{H_s}} \right)^2 \right) = \text{Wind sea significant wave height ratio}$$

For swell dominated sea $\left(T_p > T_f\right)$
Primary peak:

$$H_{S1} = H_{Ssw} = r_{ps} H_S$$

$$T_{P1} = T_{Psw} = T_P$$

$$\gamma = 35 \left[\frac{2\pi}{g} \frac{H_S}{T_f^2} \right]^{0.857} \left(1 + 6 \frac{T_p - T_f}{25 - T_f} \right)$$

Secondary peak:

$$H_{S2} = H_{Sw} = \sqrt{1 - r_{ps}^2} H_S$$

$$T_{P2} = T_{Pw} = 6.6 H_{Sw}^{\frac{1}{3}}$$

$$\gamma = 1$$

$$r_{ps} = 0.6 + 0.4\exp\left(- \left(\frac{T_P - T_f}{0.3\left(25 - T_f\right)} \right)^2 \right) = \text{Swell significant wave height ratio}$$

The spreading function describes the spreading of the wind waves in the fetch zone [18] and is described as:

$$D\left(\theta - \theta_m\right) = Ccos^n\left(\theta - \theta_m\right) \text{ for } -\frac{\pi}{2} \leq \theta - \theta_m \leq \frac{\pi}{2} \tag{2.7}$$

where:

θ_m = Mean wave direction

θ = Wave direction

n = Spreading exponent. In absence of more detailed documentation, the exponent is taken to be the most unfavourable value between 2 and 10.

$$C = \frac{\Gamma\left(1+\frac{n}{2}\right)}{\sqrt{\pi}\Gamma\left(\frac{1}{2}+\frac{n}{2}\right)}$$

Γ = Gamma function

2.5.3 Loads and Load Effects

During a lifting operation different forces acts on the module and the vessel. According to DNV [8] the following forces should be taken into account when assessing the response of the module:

F_{line} = Force in hoisting line/cable

W_0 = Weight of module in air

F_B = Buoyancy force

F_C = Steady force due to current

F_I = Inertia force

F_{WD} = Wave damping force

F_D = Drag force

F_W = Wave excitation force

F_S = Slamming force

F_E = Water exit force

2.6 Metocean Data

When marine operations are planned, they are planned for specific fields. Metocean data is field specific data regarding environmental conditions. It is based on hindcast data. Metocean data is used to determine parameters such as probable H_S, Peak period (T_P), wave direction, current and wind.

Chapter 3

Module Handling System (MHS)

3.1 Chapter overview

This chapter introduces the Module Handling System (MHS) and describes the different steps of deployment and recovery.

3.2 MHS Tower

The MHS tower on Seven Viking is fully integrated in the hangar and designed to perform deployment and recovery operations in depths down to 2,000 meters. The MHS was designed to operate in sea states up to 5.0 m Hs and has a static capacity of 70 Te [9]. An illustration of the MHS tower is given in fig. 3.1. Six winches contribute to deploy and recover modules:

- Main Lift Winch (MLW), 70Te
- Auxiliary Lift Winch (ALW), 20Te
- 3 x Guide Wire Winch (GWW), 5Te

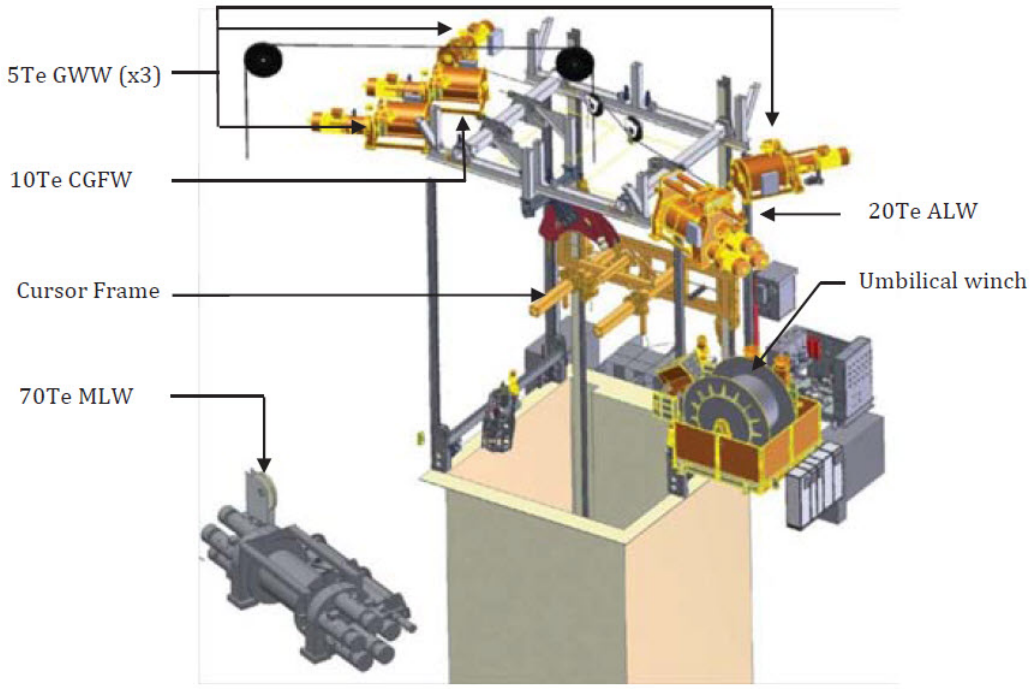

Figure 3.1: MHS Tower [12].

- Cursor Guide Frame Winch (CGFW), 10T

The cursor guide frame, fig. 3.2, is a system that follows the deployment/recovery from the top position in the hangar and down through the moonpool and vice versa. To do this, it utilizes its six sub-components:

- Cantilever system
- LWC (Swan neck)
- Prong system
- Cursor wagon
- Transverse adjustment system
- Cursor rails

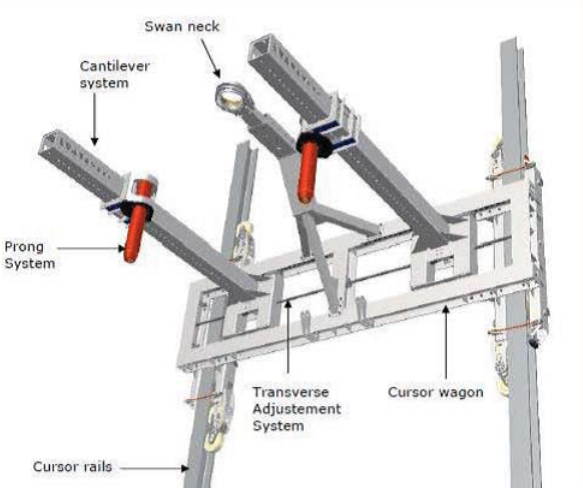

Figure 3.2: Cursor guide frame with sub-components [12]

The transverse adjustment system, cantilever system and the prong system can be configured to fit different modules and running tools. Together with the swan neck, the prong system is constructed to reduce the pendulum movements of modules hanging in the main winch wire.

3.3 Moonpool

The moonpool on Seven Viking is a standardized square moonpool of 7.2m x 7.2m, which is typical for IMR-vessels. An illustration of the moonpool is presented in fig. 3.3.

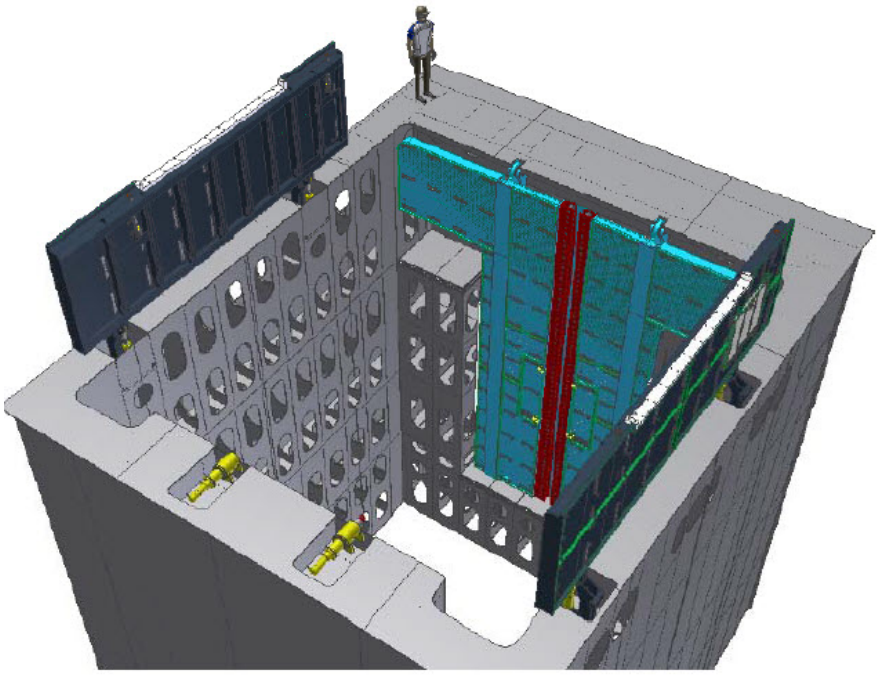

(a) Moonpool hatches in open position. Ready for deployment of modules

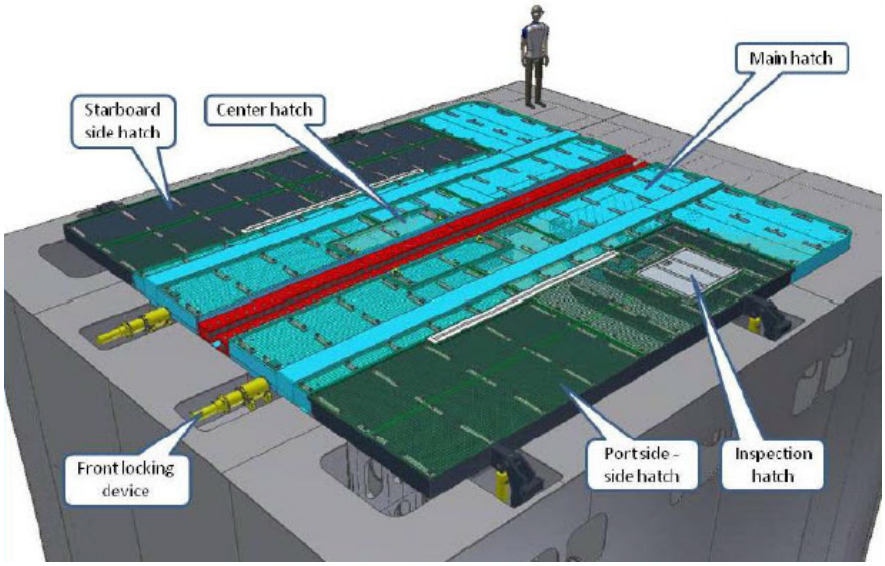

(b) Moonpool closed. Ready for skidding of modules.

Figure 3.3: Illustration of moonpool

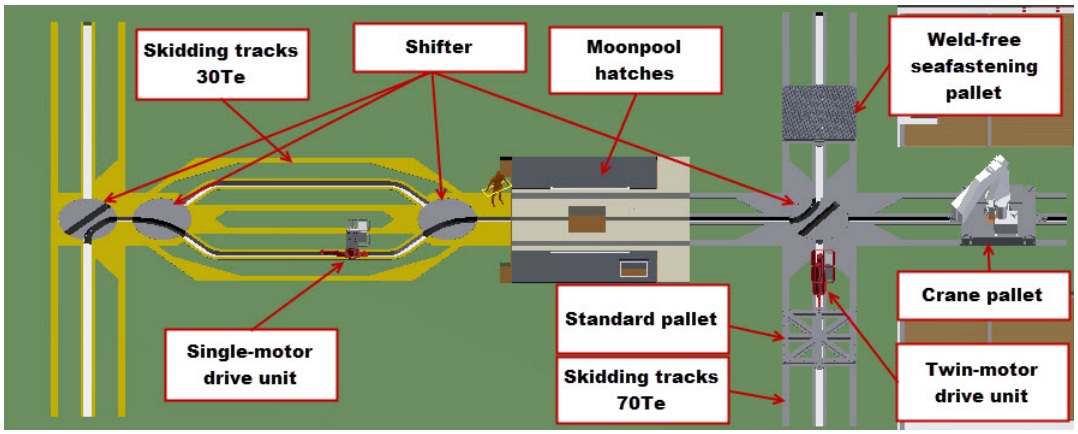

Figure 3.4: Skidding system with subcomponents

3.4 Skidding System

The skidding system allows for safe transportation of modules,Remote Operated Vehicles (ROVs), and other equipment under operating conditions and consists of the following components (see fig. 3.4):

- Skidding tracks
- Skidding pallets
- Drive units
- Shifters
- Crane pallet
- Moonpool hatches

The skidding track which consists of the skidding rails and the center rail, fig. 3.5, is a platform for the transportation of the skidding pallets. The centre rails function is to act as a rack in the Riggenbach rail system and to guide pallets and drive units around the skidding system. It is subjected to loads from the drive units and from the pallet's guiding wheels. The Riggenbach rail system is illustrated in fig. 3.6

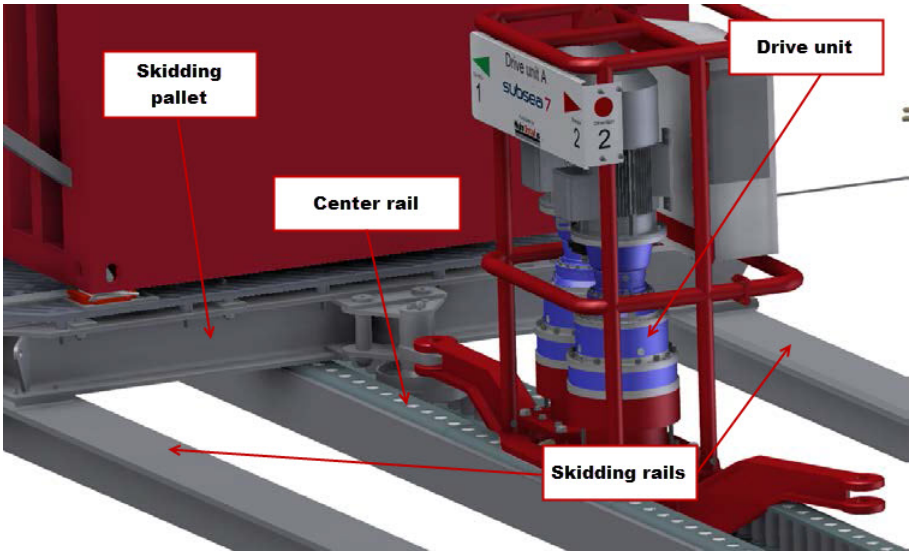

Figure 3.5: Skidding system setup, figure adapted from [17]

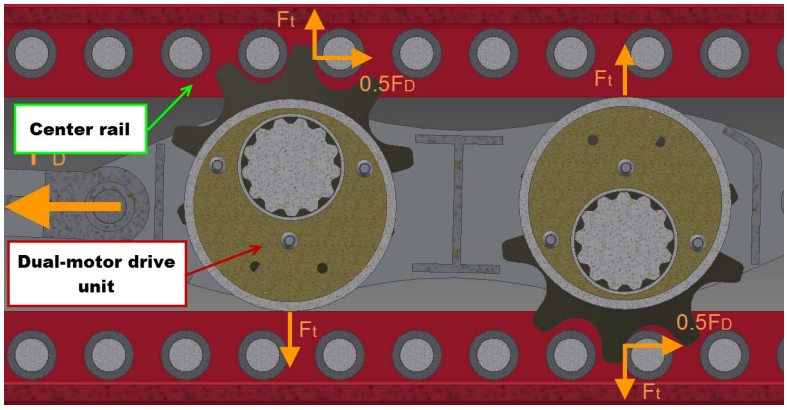

Figure 3.6: Riggenbach rail system [17]

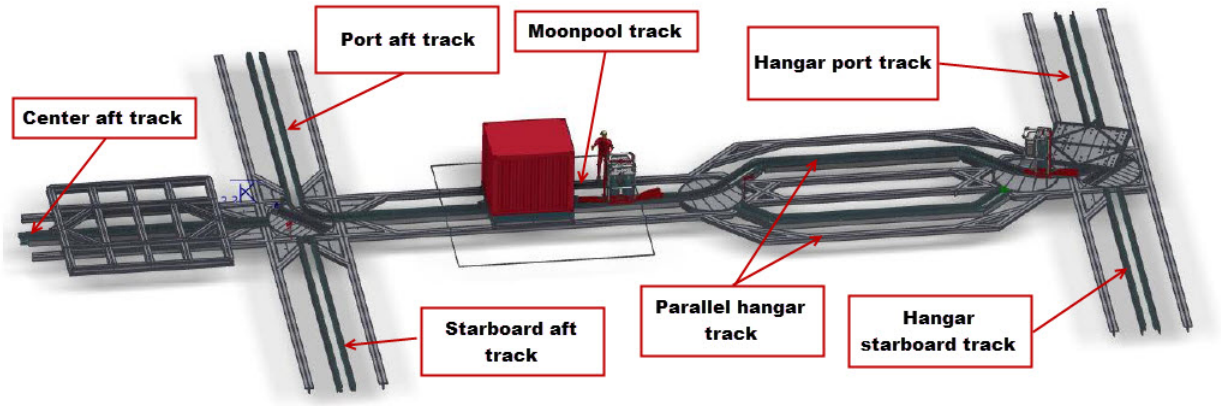

Figure 3.7: Skidding system overview adapted from [17]

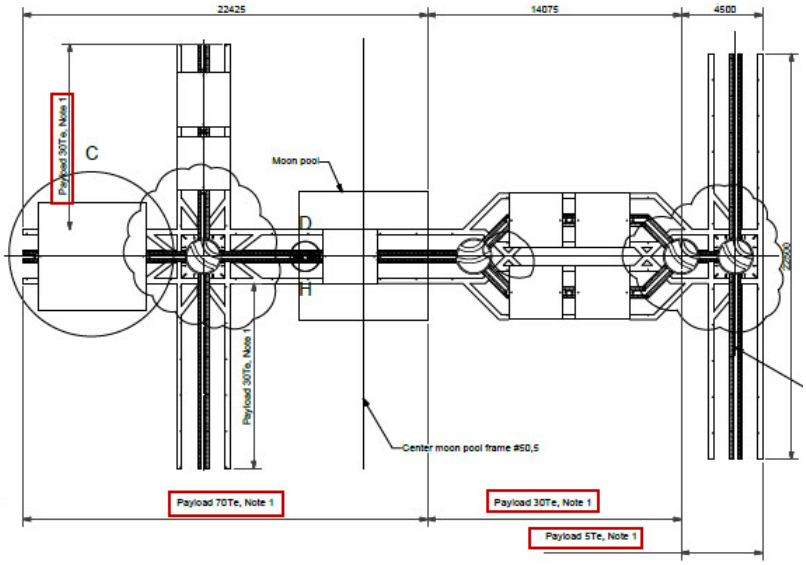

Figure 3.8: Original payload overview, adapted from [9]

The skidding tracks is positioned so that modules can be stored under transit and transported into the hangar before deployment. An overview of the tracks is displayed in fig. 3.7

The payload capacity of the skidding system is of major importance. Originally only the center track including the moonpool track was designed to have a payload capacity of 70Te, and the port and starboard aft track was designed with a payload capacity of 30Te. The original payload overview is displayed in fig. 3.8.

The hangar port-and starboard tracks have a payload capacity of 5Te. These tracks are only used for transportation of the Working Class ROVs (WROVs).

Figure 3.9: Single-motor drive unit [17]

Two drive units are used with the skidding system: a single-motor drive unit and a dual-motor drive unit displayed in fig. 3.9 and fig. 3.10.

Figure 3.10: Dual-motor drive unit [17]

The different tracks are connected with two different shifters. Two 4-way shifters, one aft and one in hangar(note that the hangar shifter only acts as a 3-way shifter as it connects three tracks), and two 2-way shifters also in the hangar. See fig. 3.11 for illustration.

The shifters together with the center rail section in near proximity of the shifter have been identified to be the most critical factors of the skidding system [10]. The critical position when the pallets are skidded is illustrated in fig. 3.12

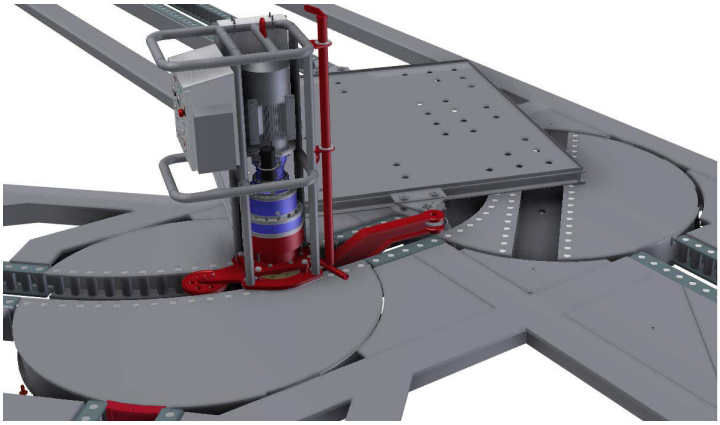

Figure 3.11: 4-way and 2-way shifter [17]

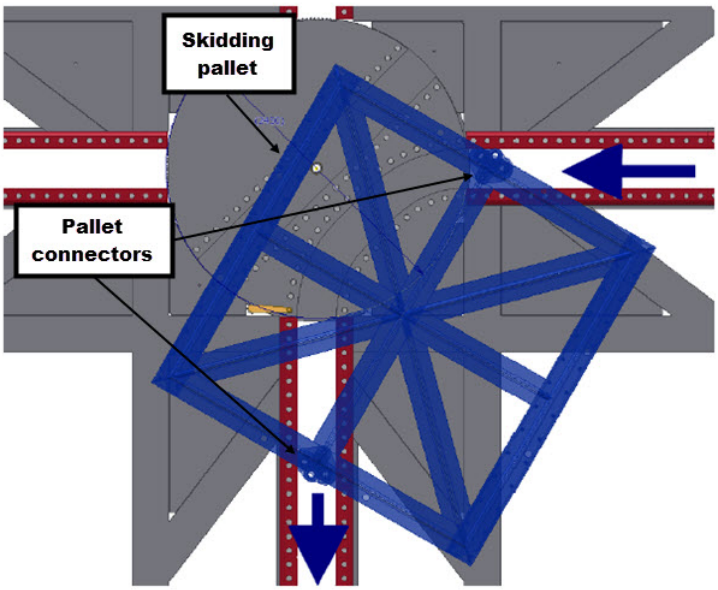

Figure 3.12: Critical position of pallet [10]

3.4.1 Friction test of the skidding system

As seen in fig. 3.8 the skiddding system capacity does not match the static capacity of the MHS tower of 70Te. During work with the GSC project a friction test was conducted. The conclusion from the test was that as long as distance between the connectors of the skidding pallets are not increased, the skidding tracks and shifters should be able to handle modules up to 70Te [10].

Chapter 4

Lifting operations

4.1 Chapter overview

This chapter describes the different phases of lifting operations and presents previous work with deployment and recovery of modules.

Phases of deployment and recovery

There are many considerations to be taken when deploying and recovering modules. The forces exerted on the system varies depending on the phases of the lift. The different phases are:

1. Lift of module to top of MHS
2. Deployment through moonpool
3. Lowering of module from vessel to subsea structrure
4. Docking of module on to subsea structure

5. Module entering moonpool and docking of module to cursor guide frame

4.2 Phase 1. Lift of module to top of MHS

The cursor guide frame is lowered to the top of the module. The height of lift depends on the height of the module as the module must have clearance to the moonpool hatches. See fig. 4.1 and fig. 3.3 for illustration.

The situation where the module hangs in the lift wire, coupled to the cursor guide frame, could have been treated as a regular sea-fastening problem. But the clearance between the module funnels and the prong system allows for some pendulum motion. The pendulum motion is the main concern during this phase. When the vessel motion aligns with the module motion, resonance will occur. The pendulum motion is governed by the horizontal eigen period of the module, given by eq. (2.2).
The eigen period for this situation will be approximately $5s$.

In figs. 2.3 and 2.4 one can see that for certain wave directions, the RAO's are significant and the periods may align with the eigen period of the module. Because of the nature of irregular waves, the period of the waves will vary and interference will occur when there is contact between the module and the prongs of the cursor guide frame. Since the winch of the main wire is not directly above the gyration point of the vessel, the vessel motion will also influence the motion of the module through the main wire.

4.2.1 Prong-funnel coupling

The cursor guide system restrain the lateral motion of the module. With the original prong design as illustrated in fig. 4.2, the module can move and rotate to a certain degree depending on the diameter of the funnel of the module and the penetration of the prongs into the funnels before the module exerts momentum force on the cursor guide system . The maximum relative

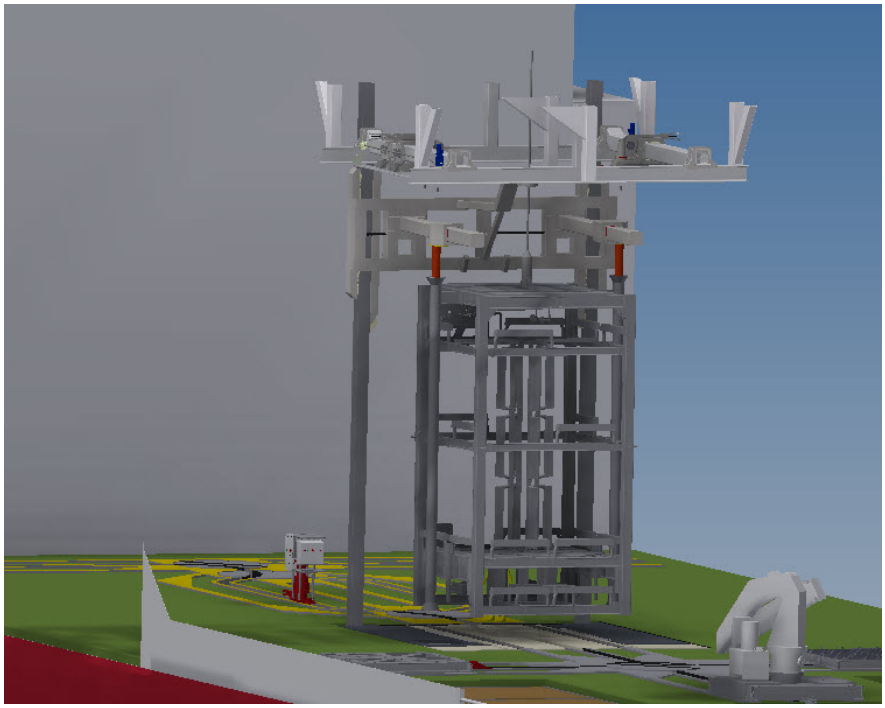

(a) Module lifted clear of moonpool hatches

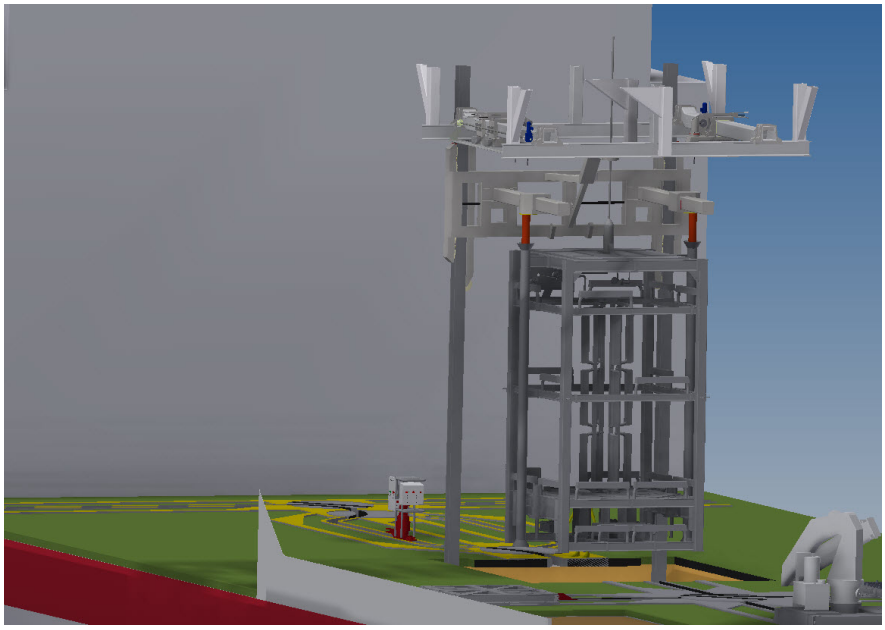

(b) Moonpool hatches opened. Note that the hatches are not illustrated.

Figure 4.1: Phase 1 - Lift of module

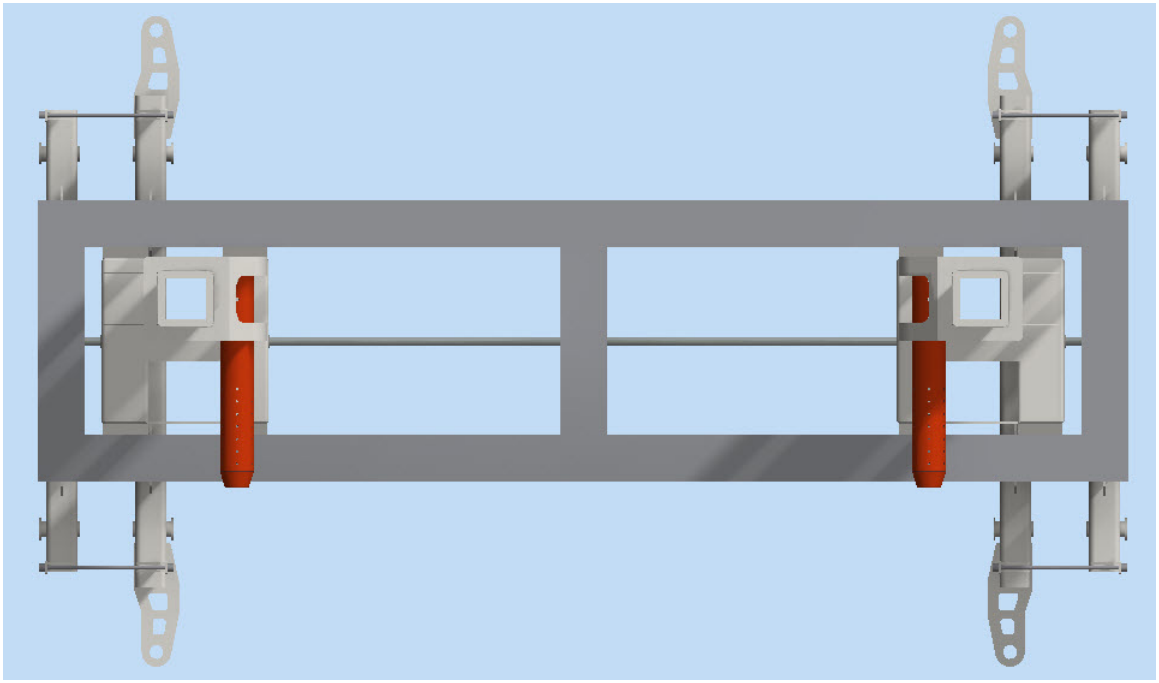

Figure 4.2: Cursor guide frame with the original prongs

rotation angles are presented in table 4.1 and an illustration is presented in fig. 4.3. When the relative rotation reaches the maximum angle, the structural capacity of the cursor guide system is challenged. The original design report [9] states the following limitations of the MHS:

- H_S of 5.0m
- Heading = ±15°
- Module CoG = 3.0m below the below the top of the funnels
- Module CoG at maximum 6.0m above main deck
- Module footprint = 6x6m

The new PILT prong design allows for greater angles of relative rotation before momentum is exerted on the MHS while still restricting the lateral movement. The PILT prongs are illustrated in fig. 4.4. The maximum relative rotation angles are presented in table 4.2 and an illustration is presented in fig. 4.5. The design sea state will for the case of the PILT prongs be when the

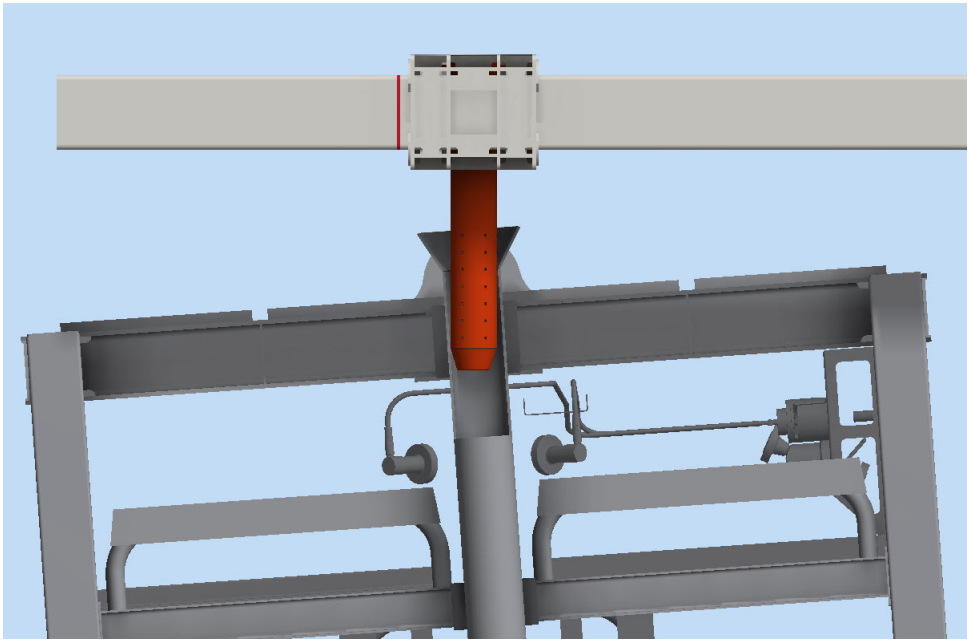

Figure 4.3: Prong inserted into module funnels. The figure illustrates when the module exerts moment force on the prongs.

Table 4.1: Original prong maximum relative rotation

Penetration of prong [m]	Max. Relative rotation [deg]
0.00	33.0
0.10	13.1
0.15	9.8
0.20	7.7
0.25	6.3
0.30	5.3
0.35	4.6
0.40	4.1
0.45	3.6
0.50	3.3
1.00	1.7

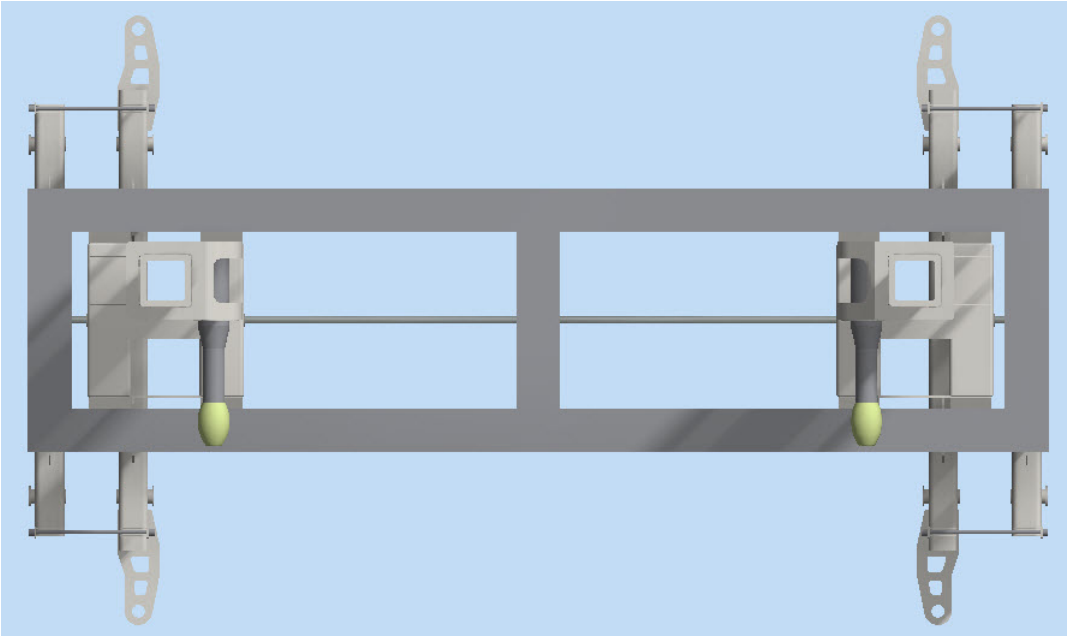

Figure 4.4: Cursor guide frame with the new PILT prongs

module exert moment force on the MHS for phase 1. One should note that when the module is lowered, the clearance between the module and the moonpoll walls may be the limiting factor. Whether it will be the limiting factor or not depends on the geometry of the module. When the footprint and height of the module exceeds a certain value, the tilt of the module relative to the cursor guide frame will cause an impact with the moonpool walls. Impact with the moonpool walls will occur before the maximum angle of tilt between the prongs and funnels is reached. An illustration showing the maximum tilt for a module with footprint $5385x4200mm$ and a height of $8354mm$ is shown in fig. 4.6

Table 4.2: PILT prong maximum relative rotation

Penetration of pilt [m]	Max. Relative rotation [deg]
0.00	33.0
0.10	24.3
0.15	19.2
0.20	15.6
0.25	13.1
0.30	11.2
0.35	9.8
0.40	8.7
0.45	7.8
0.50	7.0
1.00	3.6

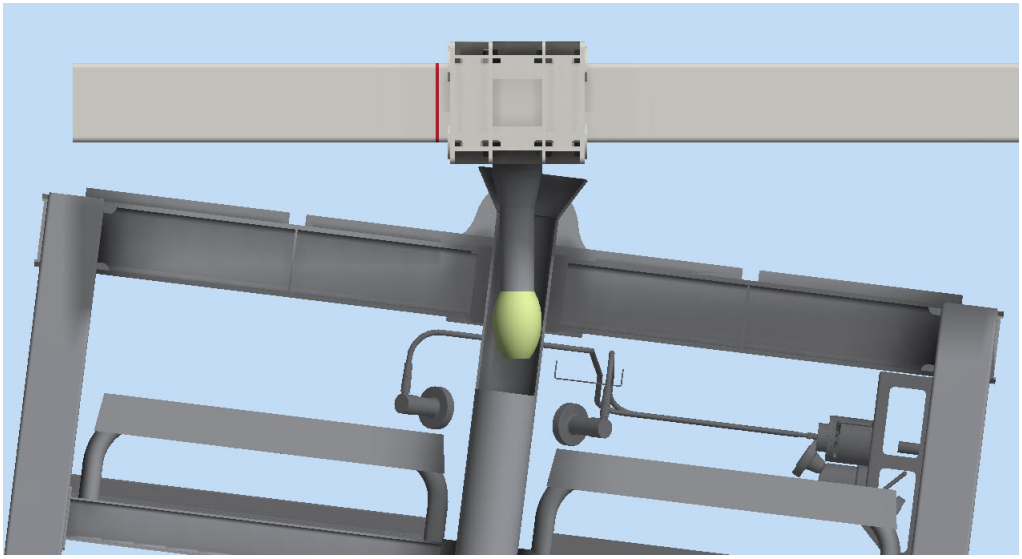

Figure 4.5: Prong inserted into module funnels. The figure illustrates when the module exerts moment force on the prongs

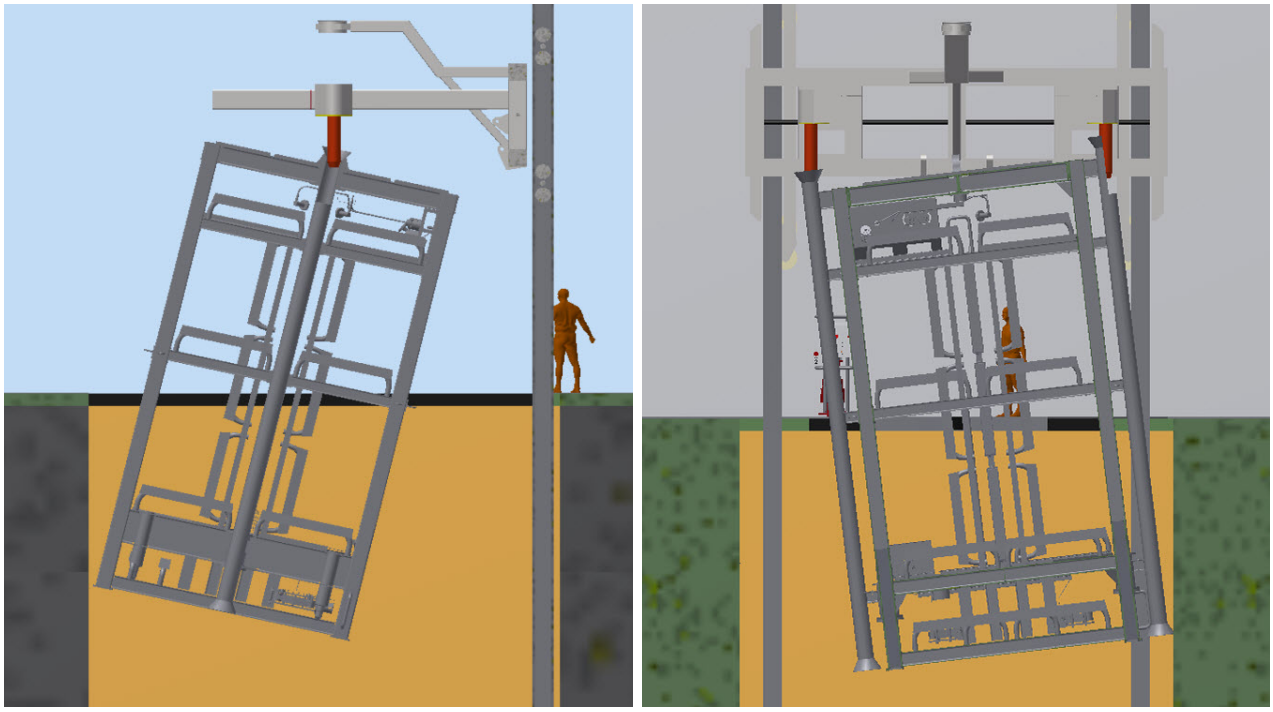

(a) Longitudinal tilt of module (b) Transversal tilt of module

Figure 4.6: Tilt of module in longitudinal and transversal direction

4.2.2 Effect of Guide wires

The relative rotation before the guide wires make impact with the funnels of a module is low, just under 2°.Guide wires can be used to reduce the horizontal motion and rotation of the module. Analysis performed by Næss,and illustrated in fig. 4.7, show that the effect of guide wires is minimal in transversal direction. They also show that in longitudinal direction, the effect is prominent and the guide wires will clearly reduce the relative motion [15].

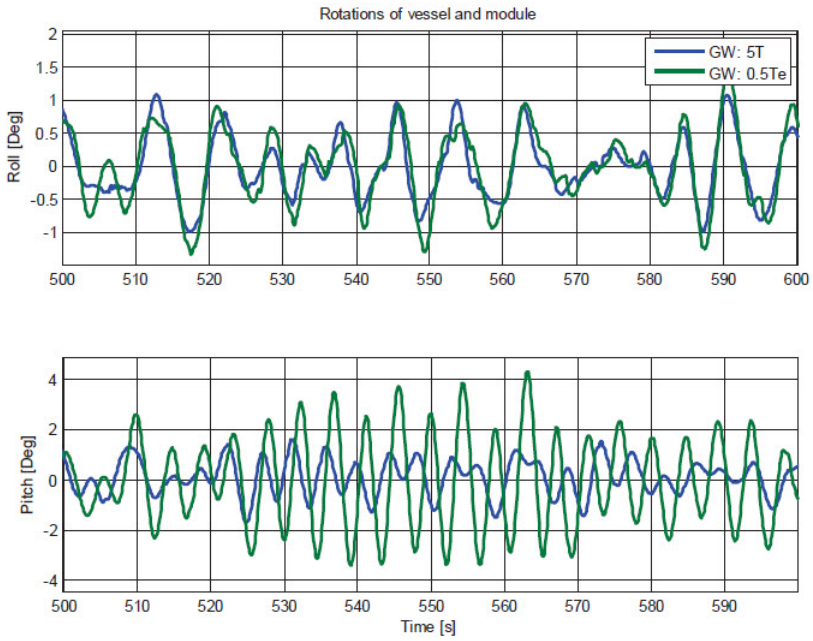

Figure 4.7: Effect of guide wires - Relative rotations [15]

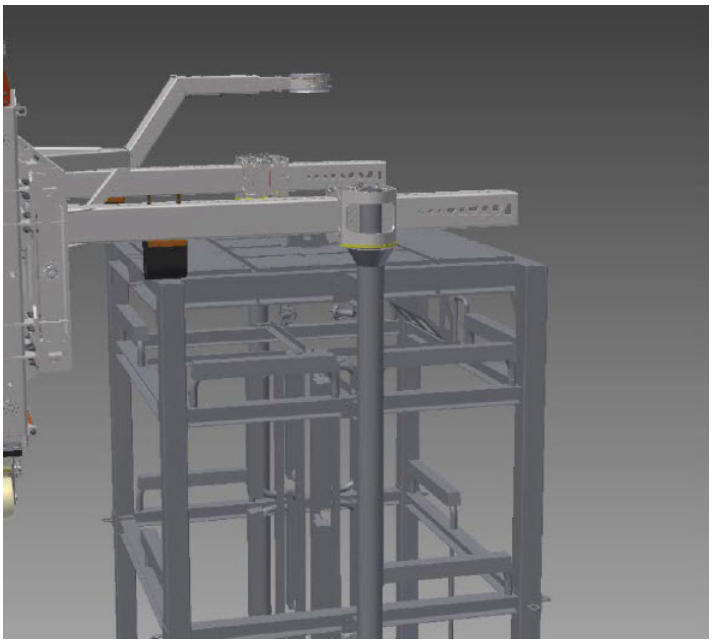

Figure 4.8: Cursor guide frame with bumpers [15]

4.2.3 Effect of bumper

The cursor guide frame can be modified with a bumper to reduce the tilting of the module as illustrated in fig. 4.8. The bumper is placed so that it disturb the resonance motion of the module and vessel. The result is illustrated in fig. 4.9 and clearly show reduced relative rotation in pitch [15].

The mass of the cursor guide frame is about $10Te$ and will be lifted if the uplift force exerted from the module to the bumpers is greater than weight of the cursor guide frame.
The stiffness of the bumpers in the simulations shown in fig. 4.9 is set to a level so that the force exerted on the cursor guide frame is about $5Te$. This will set a limit on how much the bumper can reduce the resonance of the system, but when the stiffness of the bumper is low, and the force transferred from the module is about $2Te$, the tilt motion in pitch will still be dramatically reduced [15].

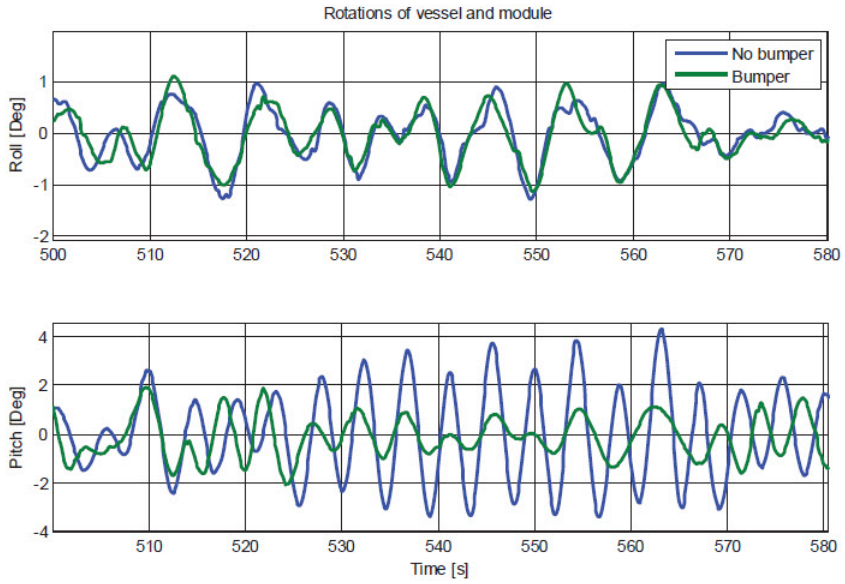

Figure 4.9: Effect of bumpers - Relative rotations [15]

4.3 Phase 2. Deployment through moonpool

In phase 2 the module is lowered into the moonpool. The cursor guide frame follow the module as it is lowered in order to restrict the module motion. See fig. 4.10 for illustration.

The phase of the operation where the module is inside the moonpool is challenging to model and analyse. The flow pattern inside a moonpool is complex and hard to model in analytical set-up [8]. And even if there has been some important developments regarding this issue in the latest years [10], it is still not possible to estimate the hydrodynamic forces on an object inside a moonpool analytically.

During the work with GSC, model testing was done by MARINTEK. The results of the testing was used to establish a comprehensive approach for estimating the expected forces in the lift line when a UTA is lowered through moonpool. The main principles for the mthodology for estimating dynamic force is presented in fig. 4.11. An illustration of the UTA is illustrated in fig. 4.12. The main assumption in the new methodology is that it is possible to describe the hydrodynamic force on the object inside the moonpool by applying a transfer function on the undisturbed relative piston mode water response. The basic setup for the methodology is illustrated in fig. 4.13

The response spectrum achieved combining the transfer function with a wave spectrum is in-line with the response spectrum established directly from the model tests as shown in fig. 4.14

By model testing of the UTA transfer functions between the hydrodynamic force and the relative piston mode water response for an empty moonpool (“undisturbed wave in moonpool”). and relative piston mode water response for the moonpool with the UTA inside (“actual wave in moonpool”) are established. The force transfer functions are shown in fig. 4.15.

The plots in fig. 4.15 show the transfer functions for three different positions of the UTA as shown in fig. 4.16 and three different levels of energy (excitation levels) in the relative piston

mode. The maximum and minimum observed hydrodynamic loads from model tests are illustrated in fig. 4.17. The discrepancies in the minimum observed load may be caused by surface breaking of the UTA in position #1 and #2.

Traditionally, the slamming force is assumed to be the governing load effect when an object is penetrating the surface. This is most probable not the case for the UTA inside the moonpool of Seven Viking. The slamming force is non-linear and will give a positive force on the UTA. Since the results from the model test show that the positive force amplitude is well predicted using linear theory, slamming seems not to play an important role in the overall load picture. A pragmatic approach in this setting is to use the test results from position #3 to estimatethe expected hydrodynamic loads. From the model tests one then know that the mathematic model used to estimate the forces reports reliable results for the UTA positioned in the moonpool inlet. The result from the model tests show that the forces may be under estimated, but not much. Hence, as long as the loads are not considered critical, one may still use the proposed methodology to estimate the most probable hydrodynamic loads on the UTA when recovered through the moonpool of Seven Viking [14].

For a operation of short duration, less than 30 minutes, the design loads for the process may be estimated by multiplying the standard deviation of the line tension response spectrum by 3.6 [8]. The resulting dynamic loads for different wave directions using the Torsethaugen and JONSWAP spectrum is shown in fig. 4.18

The Dynamic Amplification Factor (DAF) of the main lifting winch is 1.75. Even with a conservative approach where the buoyancy term of the UTA of $12Te$ is added, the maximum dynamic load in a realistic sea state will not be critical. For a realistic sea state the maximum dynamic load will be approximately $30Te$ and the minimum load will be approximately $20Te$. As the static capacity of the main winch is $70Te$ the maximum allowed dynamic load is $52.5Te$.

Even with this conservative approach the maximum and minimum loads in the lift wire is far from critical. Hence, based on the presented methodology one therefore may conclude that the phase of the operation where the module is inside the moonpool will not be critical [14].

In 2012, a study regarding the weather limitations for a module running tool was conducted. A running tool is a device which can install and recover small subsea modules such as Subsea Control Modules (SCMs) and Flow Control Modules (FCMs). An illustration of the running tool is illustrated in fig. 4.19. The vessel in the study was the IMR vessel Havila Subsea. The main conclusions of the study was [13]:

- The moonpool increases the vertical hydrodynamic loads on tool and is the governing load factor with respect to tension in lifting wires
- Launch and recovery of running tool in $H_S = 5.0m$ is technically feasible (design loads within capacities) but is operationally questionable due to vessel roll and pitch
- The results are representative for similar vessels (Seven Viking) and similar tool

Both the work with the UTA and the running tool show that the moonpool phase is not critical for realistic sea states, but this may not be representative for all modules and extensive testing and analysis of specific modules are required to decide the limitations for the specific case is needed. If a database with transfer functions for a wide range of objects and moonpools could be established, object forces will be easy to predict for any vessel where the moonpool responses are well documented [4].

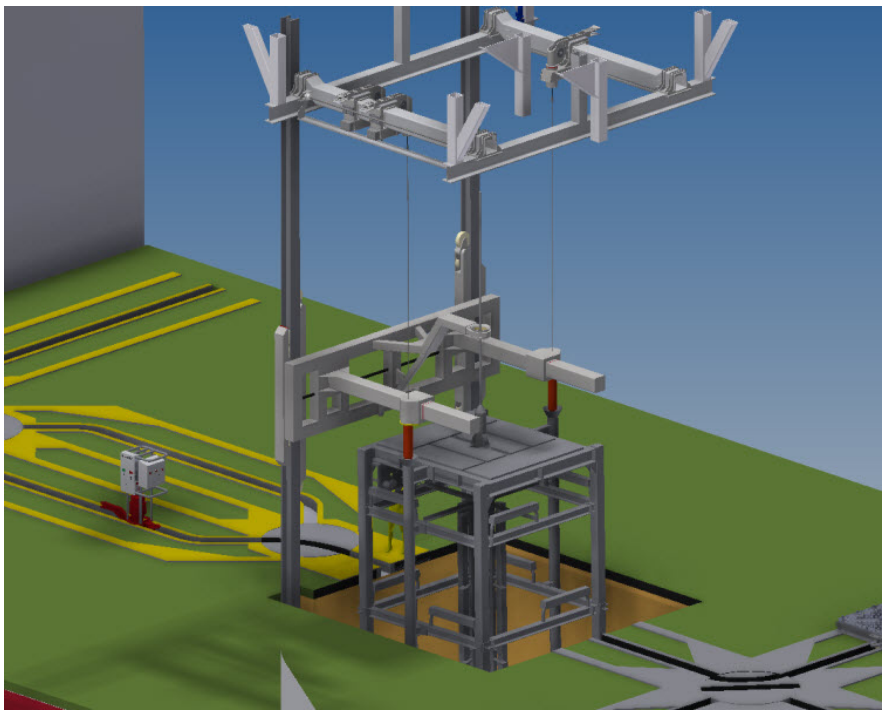

(a) Lowering of module into moonpool

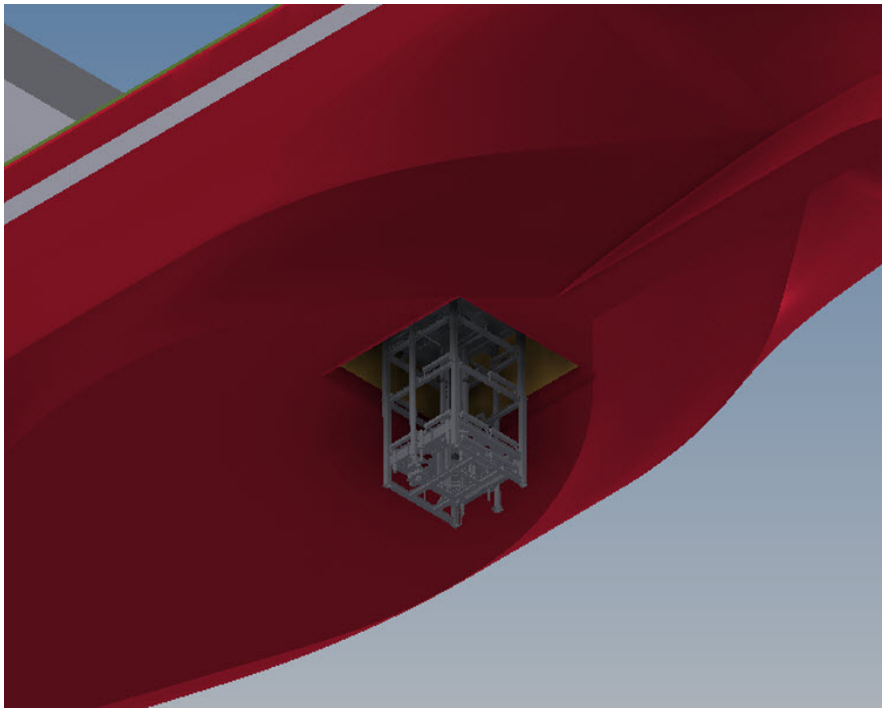

(b) Lowering of module through moonpool

Figure 4.10: Phase 2 - Deployment through moonpool.

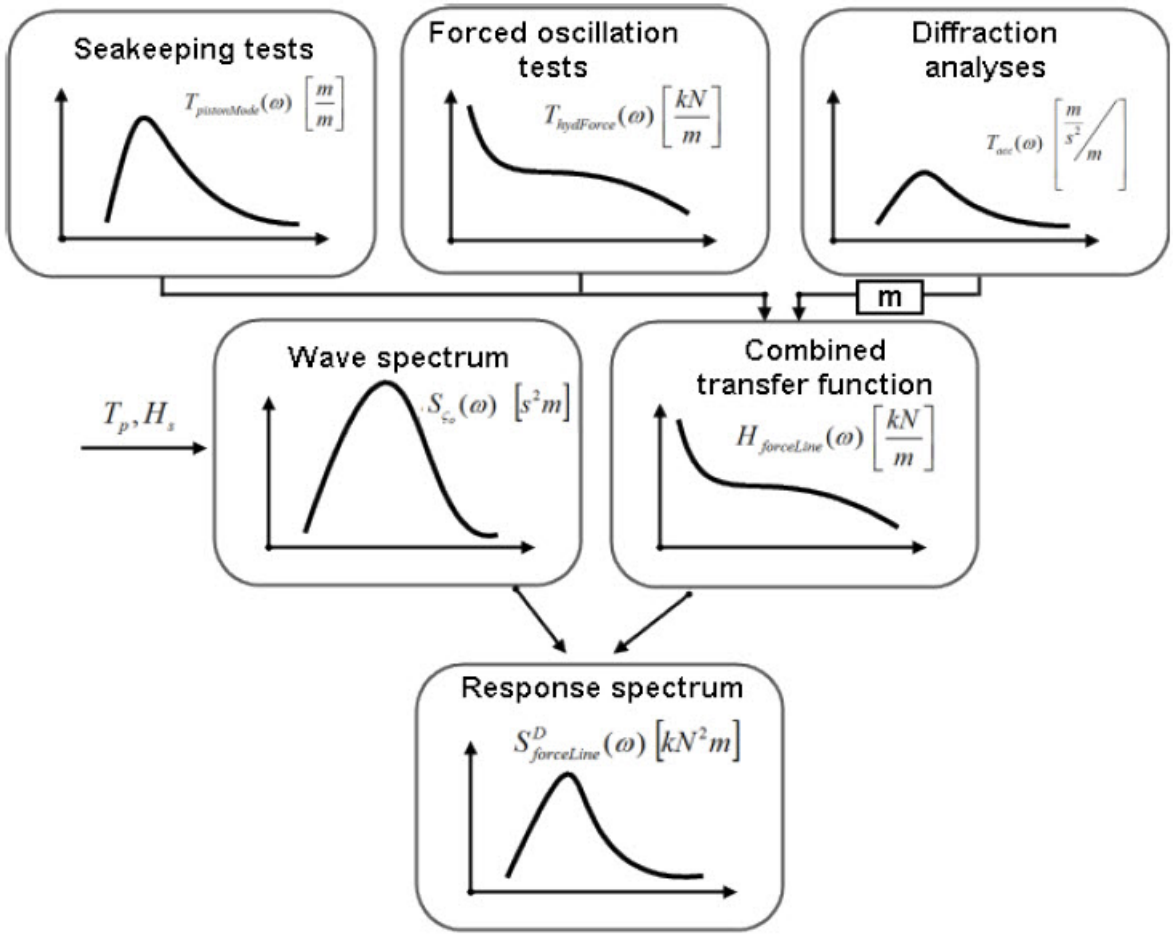

Figure 4.11: Main principles for methodology for estimating dynamic force [14]

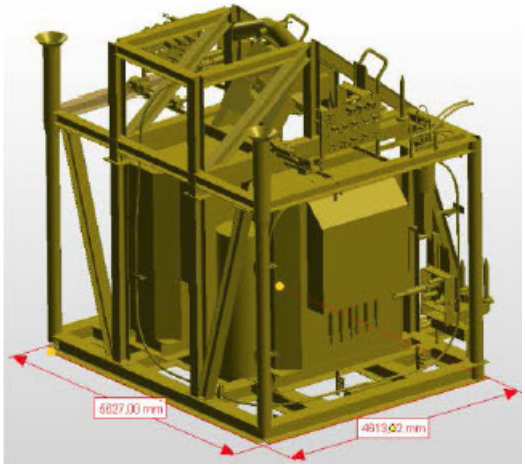

Figure 4.12: UTA with dimensions $5827x4919x5690mm$, flooded mass of $69Te$, and submerged weight of $56.6Te$ [14]

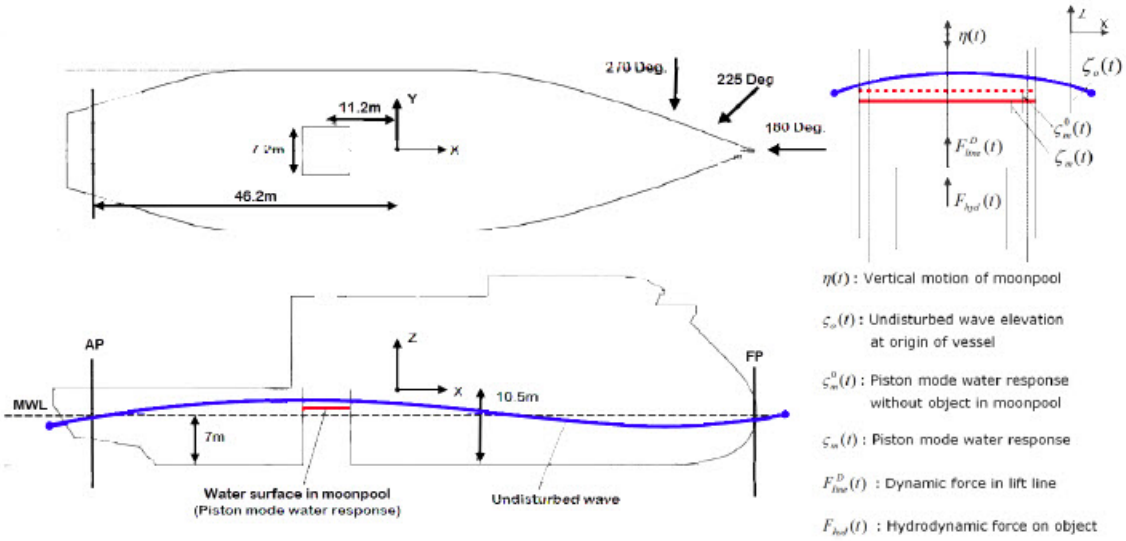

Figure 4.13: Basic principles in methodology for estimating forces inside moonpool [14]

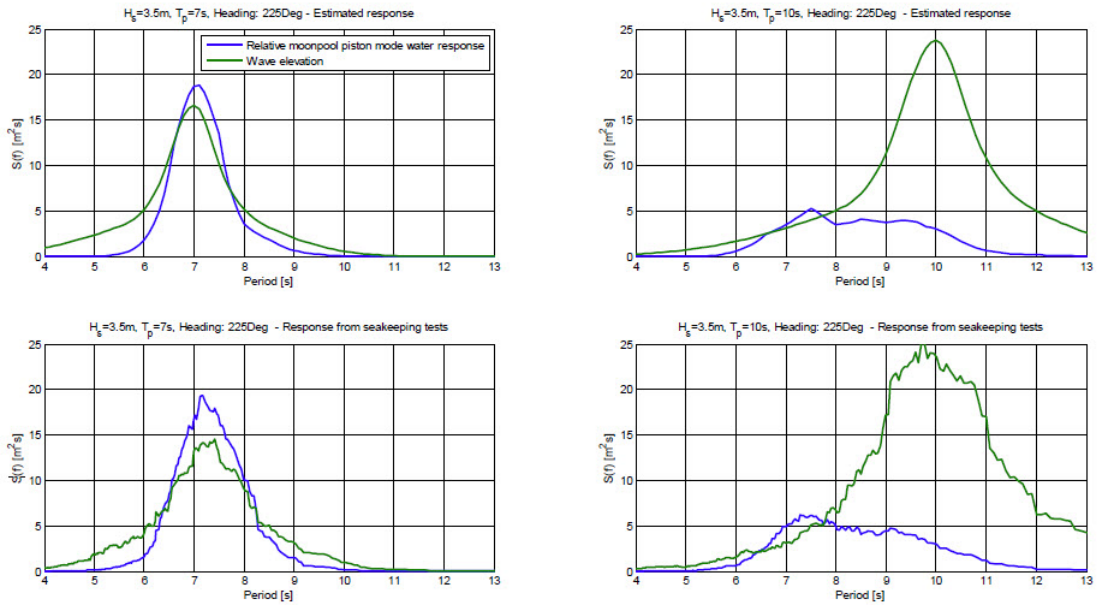

Figure 4.14: Verification of transfer function for relative piston mode water response [14]

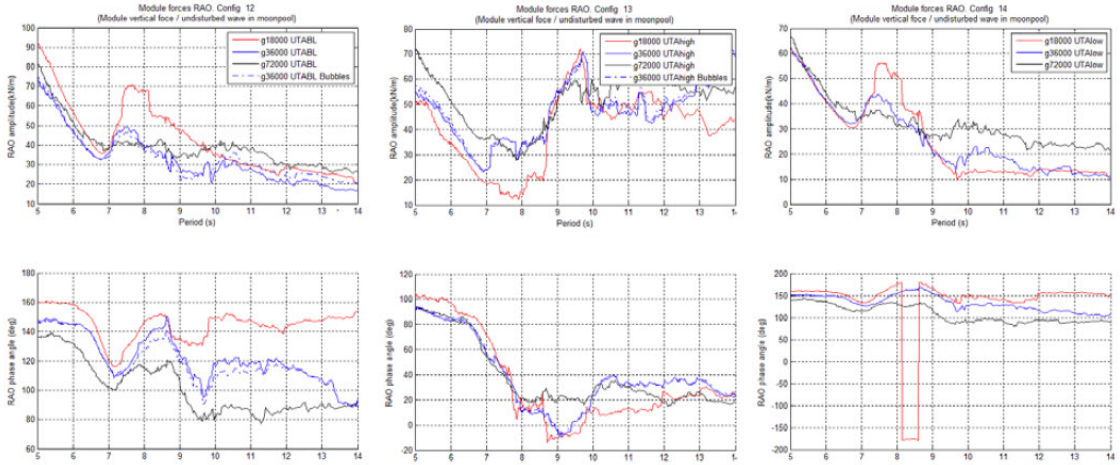

(a) Transfer function for hydrodynamic force - "Undisturbed wave in moonpool"

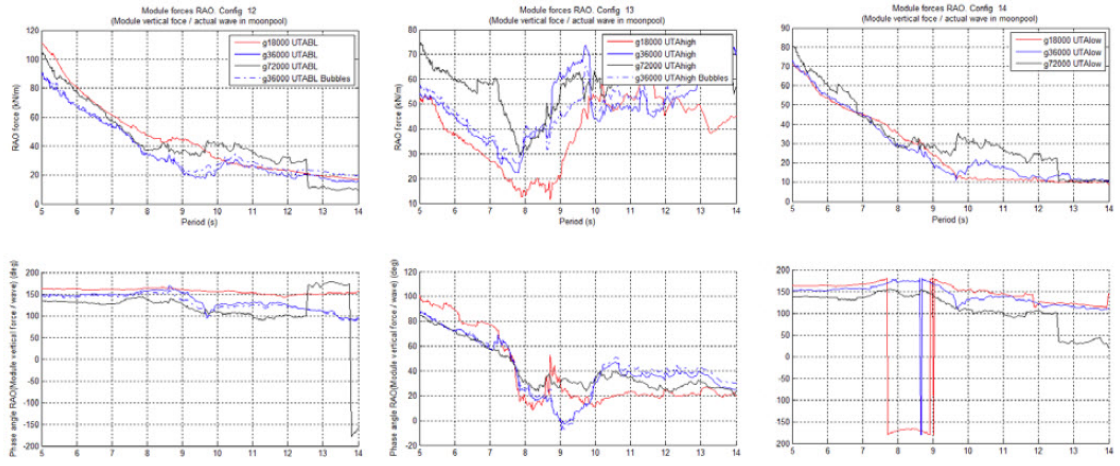

(b) Transfer function for hydrodynamic force – “Actual wave”

Figure 4.15: Force transfer functions for piston relative mode water response for three different positions in moonpool [14]

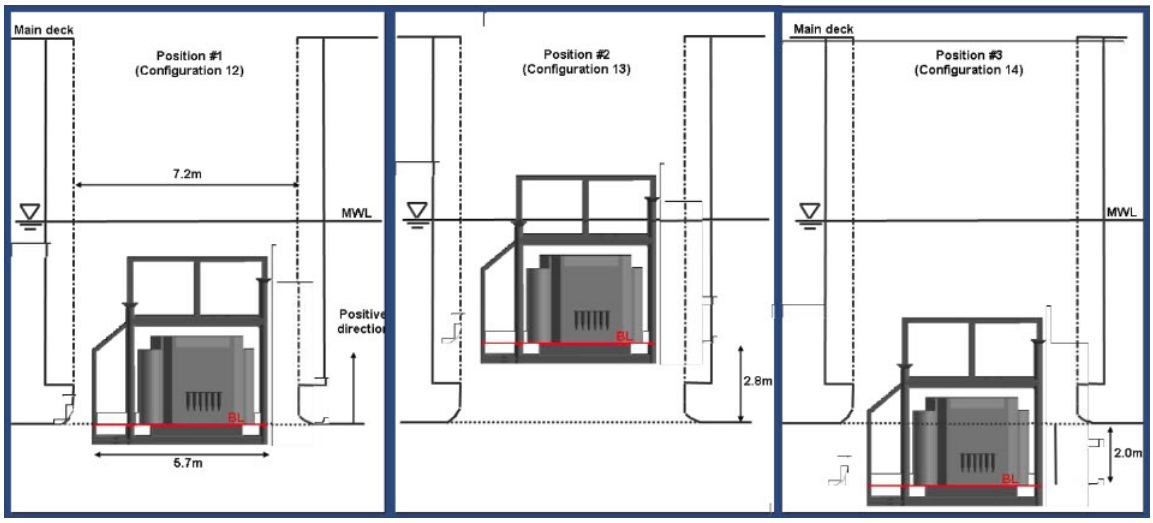

Figure 4.16: UTA positions of model test [14]

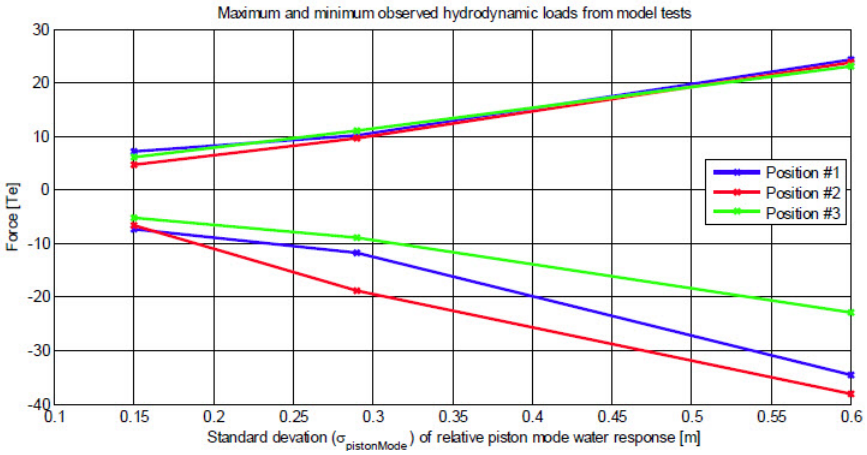

Figure 4.17: Maximum and minimum observed hydrodynamic loads from model tests [14]

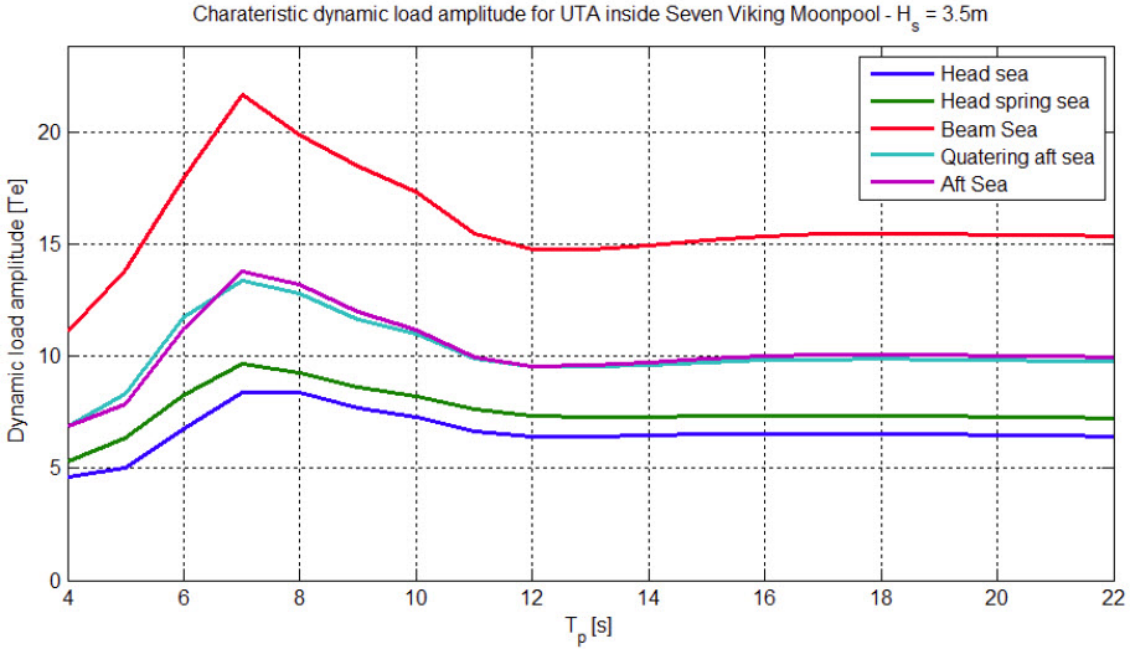

(a) Characteristic dynamic loads in main lift wire - Torsethaugen spectrum

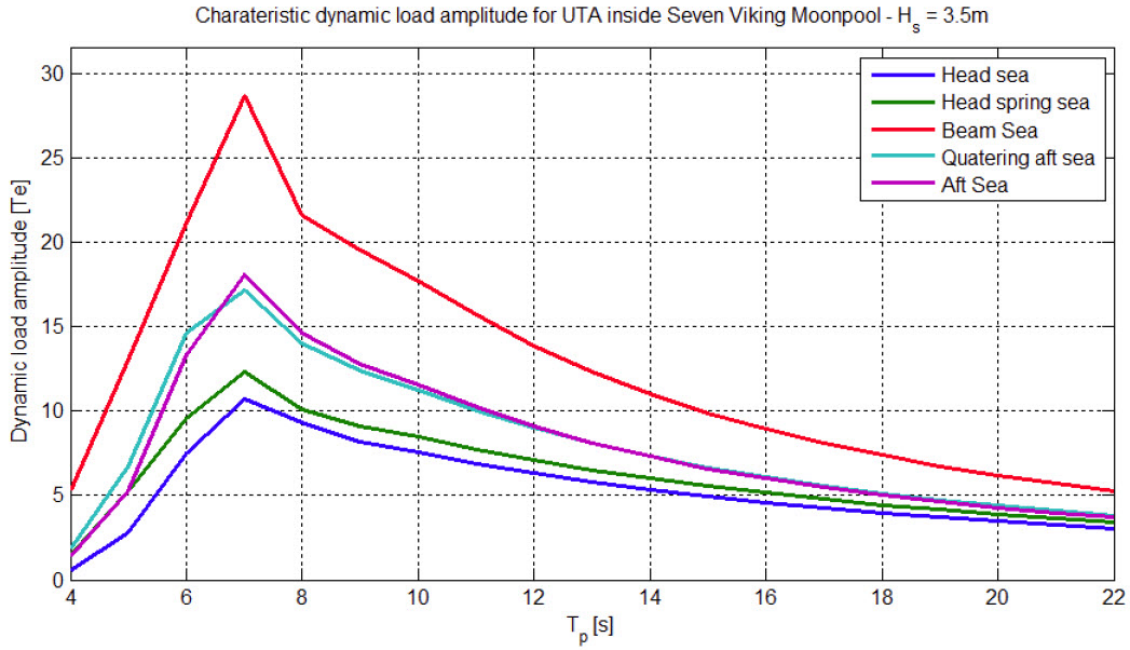

(b) Characteristic dynamic loads in main lift wire - JONSWAP

Figure 4.18: Characteristic dynamic loads for different wave directions. Note that head spring sea is 15° off head sea, quartering aft sea is following quartering sea and aft sea is following sea [14]

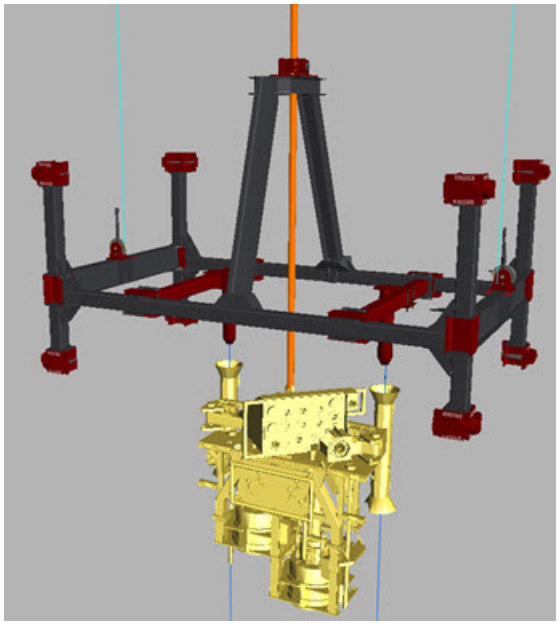

Figure 4.19: Running tool - Mass of running tool is 9.6Te [13]

4.4 Phase 3. Lowering of module from vessel to subsea structrure

The cursor guiding frame lowers to approximately $1m$ above the keel. When the module is lowered further, it is kept in position by the guide wires.

When the module leave the moonpool it is exposed to both vertical and horizontal wave forces. The horizontal wave forces and hydrodynamic parameters affecting the module is discussed in section 4.6 and the dynamic loads in the main lift wire is discussed in section 4.3 When module is realised from the prongs, the loads exerted on the Cursor guide frame (CGF) are small and combined with the issues discussed above this phase does not seem to be critical.

4.5 Phase 4. Docking of module on to subsea structure

The guide wires are fixed to the subsea structure by ROV's. The guide wires helps to guide the funnels on the module onto the guide posts of the subsea structure. See fig. 4.20 for illustration. The guide wires are pulled in tension as the module is docked. The hydrodynamic forces could potentially cause the module to drift off. When the module is lowered, the hydrodynamic forces acts against the module which may in turn cause an increase in tension in the guide wires. The hydrodynamic forces are not critical in this phase as the forces with depth.

The vertical movements of the module may cause impact loads with the subsea structure. The main lift winch is equipped with an Active Heave Compensator (AHC) that reduce the vertical motion (heave) caused by the vessel motion. The AHC is minimum to compensate for 95% of the heave motion or vertical position should only deviate $\pm 10cm$. The maximum heave motion characteristics of the AHC is $\pm 4.5m$, $1.9m/s$ and $1m/s^2$. The possible impact loads affect the funnels and the subsea structure, which both must be designed to withstand the loads. As the AHC reduce the vertical motion, this phase is not critical.

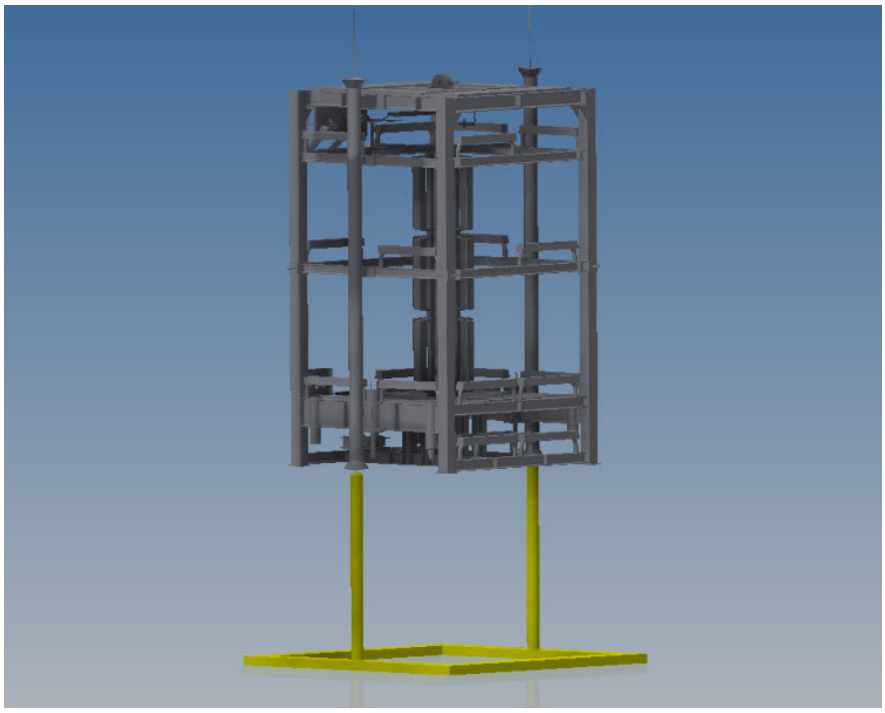

(a) Docking of module on to subsea structure.

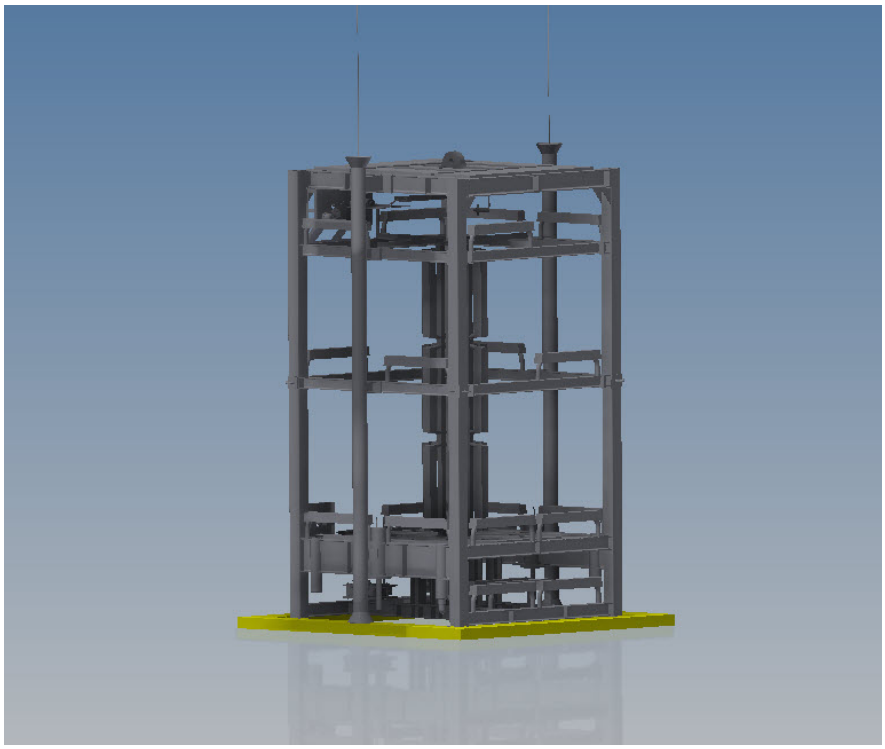

(b) Module fully docked on to subsea structure.

Figure 4.20: Phase 4 - Docking of module on to subsea structure.

4.6 Phase 5. Module entering moonpool and docking of module to cursor guide frame

Recovery of module. Guiding of module by guide wires until docking of prongs into module funnels. Hydrodynamic forces are small/negligible compared to the response of the module caused by the vessel motions. Pendulum motion of module.

The results presented in this section is based on [14] and [15]. The main conclusions of the reports are:

1. The critical issue for the entry phase is the clearance between the forward moonpool wall and the top of the forward funnels on the UTA
2. The vertical position of the Hook Cursor is an important parameter when it comes to the clearance
3. The wave kinematics is not an important issue for the clearance. The relative motion between the module and the moonpool is mainly governed by the wave induced motion of the vessel
4. It is hard to estimate the wave induced motion of the vessel due to the uncertainties involved when modelling the sea state
5. The operation can be carried out in sea states with Hs in the range of $2-3m$ depending on the sea state parameters
6. The dynamic tension in the lift wire will not be the governing case as long as a DAF of 1.3 is incorporated in the design.

The size of the UTA makes clearance between it and the moonpool walls a critical issue. For modules with a larger footprint larger than that of the UTA the sea state where recovery operations can be conducted would most likely have to be reduced compared to the UTA sea state limits.

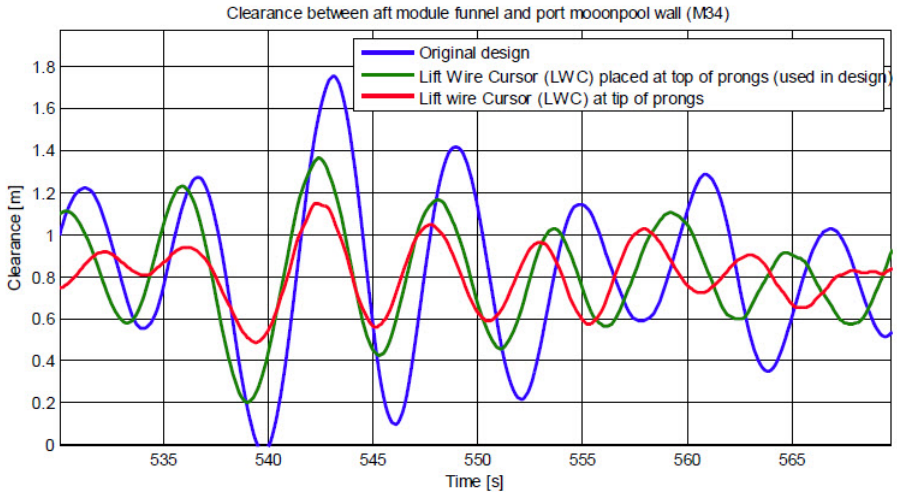

Figure 4.21: Clearance between aft module funnel and port moonpool wall [14]

4.6.1 Effect of vertical position of LWC

The vertical position of the LWC ("swan neck") influence the motion behaviour of the module. By lowering the LWC, the clearance to the moonpool walls increase [14]. In fig. 4.21 the effect is shown.

4.6.2 Effect of wave kinematics

The wave kinematics seems to be of minor importance for the clearance. This can be seen from fig. 4.22

4.6.3 Effect of hydrodynamic properties

The plots in fig. 4.23 show that the effect of hydrodynamic properties is minimal.

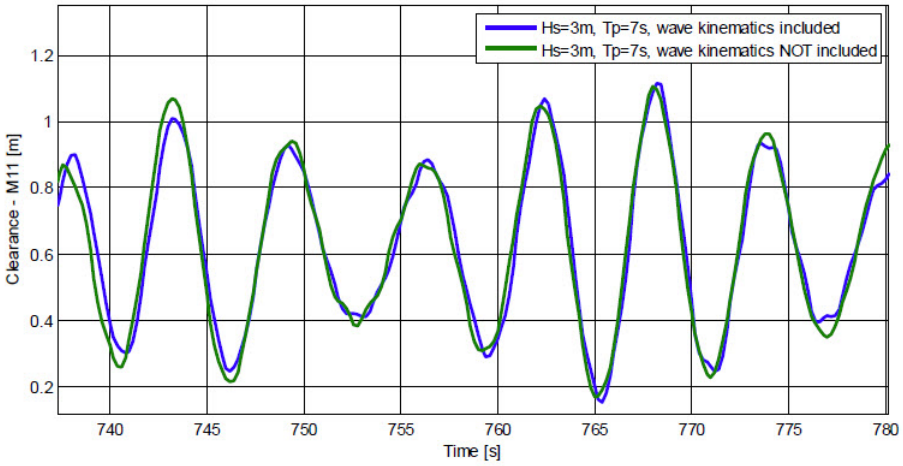

Figure 4.22: Effect of wave kinematics on clearance [14]

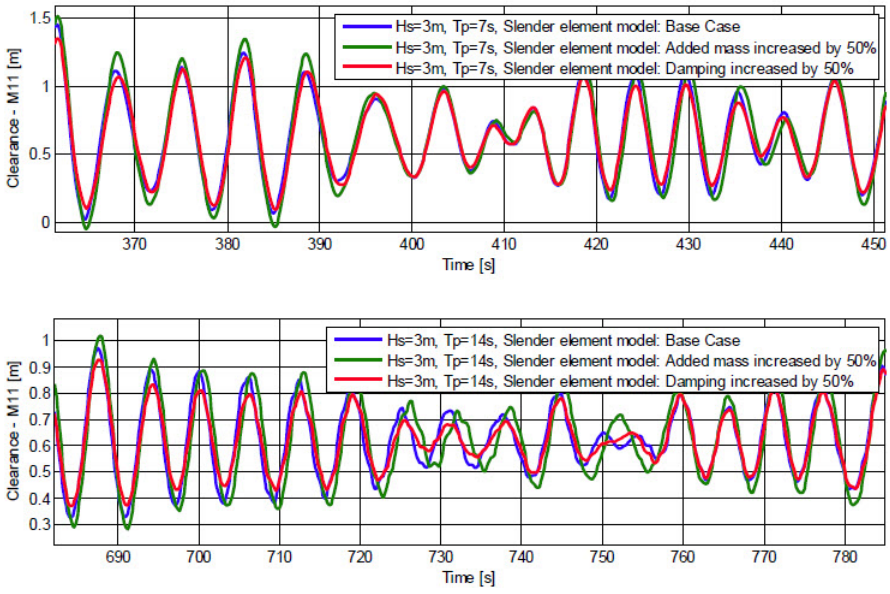

Figure 4.23: Effect of hydrodynamic properties on clearance [14]

Chapter 5

SIMO

5.1 Chapter overview

This chapter give an introduction to SIMO and describe how the simulation model is set up.

5.2 Introduction to SIMO

SIMO is a time domain simulation program for simulation of motions and station-keeping behavior of complex systems of floating vessels and suspended loads [3] . It is developed by Marintek and performs both static and dynamic analysis. The results from the program are presented as time traces, statistics and spectral analysis of all forces and motions of all bodies in the analyzed system. Interactive simulations are possible by using the program SimVis, which visualizes the simulations. Essential features of SIMO are:

- Flexible modelling of multibody systems.
- Non-linear time domain simulation of wave-frequency as well as low-frequency forces.

SIMO	INPMOD	File system for communication between modules	Input generation and presentation, interface to external sources of data
	STAMOD		Read input data, static analyses, define initial condition
	DYNMOD		Dynamic analyses, generation of time series
	OUTMOD		Post-processing of time series
	S2XMOD		Export of time series
	PLOMOD		Plotting module, common with RIFLEX

Figure 5.1: SIMO layout [1].

- Environmental forces due to wind, waves and current.
- Passive and active control forces.
- Interactive or batch simulation.

5.3 Program layout

The program system consists of five programs or modules communicating by a file system as shown in fig. 5.1.

A complete dynamic analysis must include run of the modules STAMOD, DYNMOD and OUTMOD.
The purpose of INPMOD is to transport data from other sources (for example results from diffraction analyses) into the SIMO input file, and to present such data. This module was not used during this thesis.
The purpose of the STAMOD is to define the initial condition for the dynamic simulation. The description of the system to be simulated is read from a file, SYSFIL. Selection of different environmental conditions can be done. A static equilibrium position may be calculated with or without average environmental forces applied. The initial conditions are written to the file

INIFIL for use by DYNMOD.
The purpose of DYNMOD is to calculate responses in the time domain. Before starting time integration of the equation of motion, the various simulation techniques must be initialized. The purpose of OUTMOD is to read time series files generated in the DYNMOD module, generate print and plot of time series and statistical parameters.
In this thesis OUTMOD was used to generate prints of the results obtained in the analyzes and Matlab was used to process and plot the results. S2XMOD and PLOMOD was not used and will not be further explained.

5.4 SIMO model

The SIMO model is a simplified model with multiple bodies. Body 1 is the vessel Seven Viking and Body 2 is the module. To simplify the model, the cursor system is modelled as a docking cone coupling consisting of a docking cone and a guide pin, where the pin is fixed to the vessel. The docking cone represents the guide funnel on the module and the guide pin represents the prong/PILT. The whole cursor frame could have been modelled, but by assigning the stiffness of the cursor system to the prong-funnel coupling one avoids adding complexity to the model.

To model the main winch, a coupling point is modelled as fixed to the vessel and defined as a coupling winch. Variables such as max acceleration/velocity, wire length on drum and number of winch runs of the main winch can be specified. This will not be done in this thesis as the main focus is the scenario where the module is in top position before deployment. The main winch wire is modelled as a simple wire coupled between the winch and the module.

Guide wires have been modelled as simple wire coupling from the tip of the guide pins to a dummy subsea structure. The guide wires have no function in the setup used in this thesis , but do not influence the analyses performed. They are a part of the operational setup and are therefore not removed.

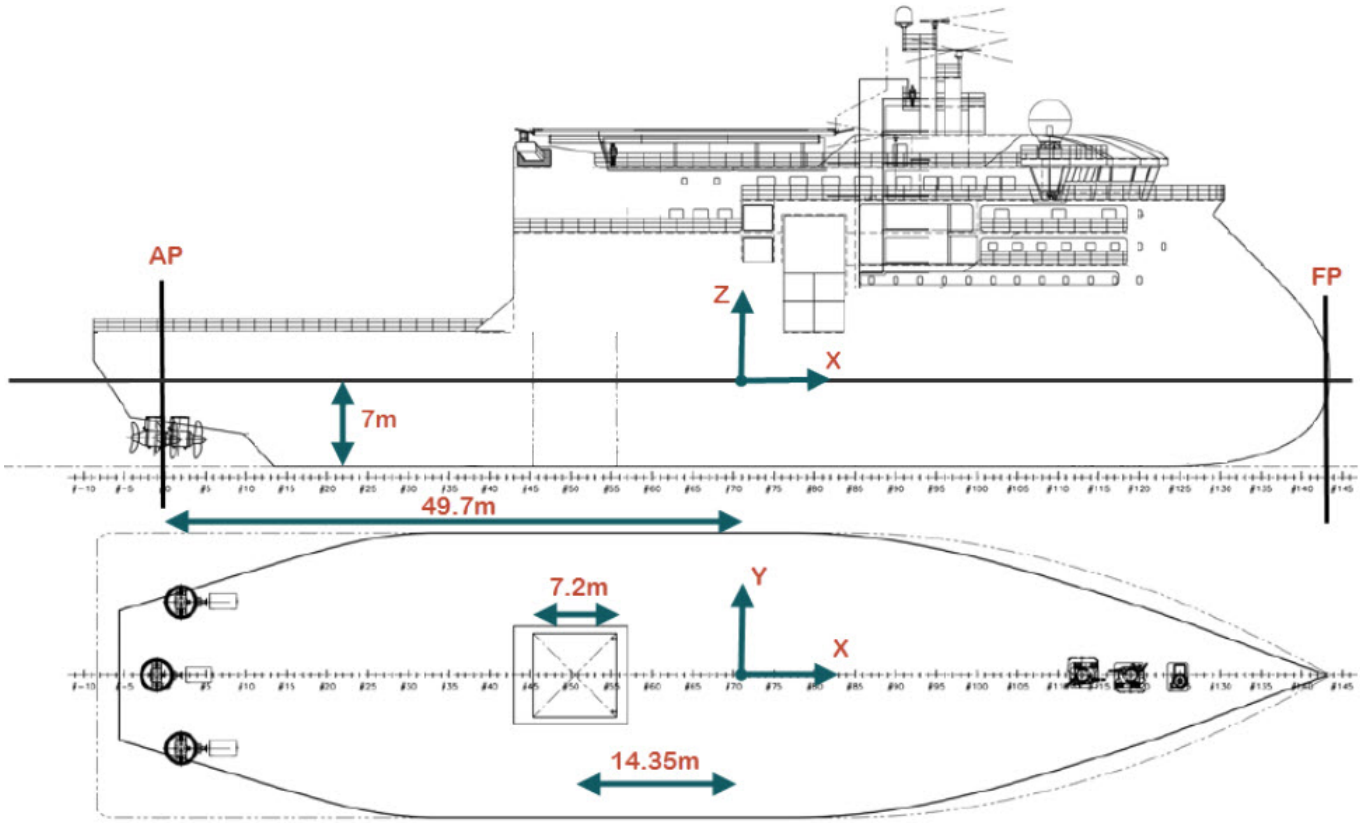

Figure 5.2: Coordinate system of vessel model [14].

5.4.1 Vessel model

The coordinate system of the SIMO vessel model is shown in fig. 5.2.

In order to establish the hydrodynamic SIMO model the following approach has been applied:

1. The hydrodynamic properties are established using WADAM (HydroD).
2. A preliminary SIMO model is generated by reading the result file from WADAM.
3. A mooring system is attached to the vessel model in order to model the effect of the DP-system.
4. The GM-value and non-linear damping in roll is adjusted in order to achieve a SIMOmodel with a representative response in roll.
5. The short term statistic properties for the SIMO model in roll and pitch is verified.

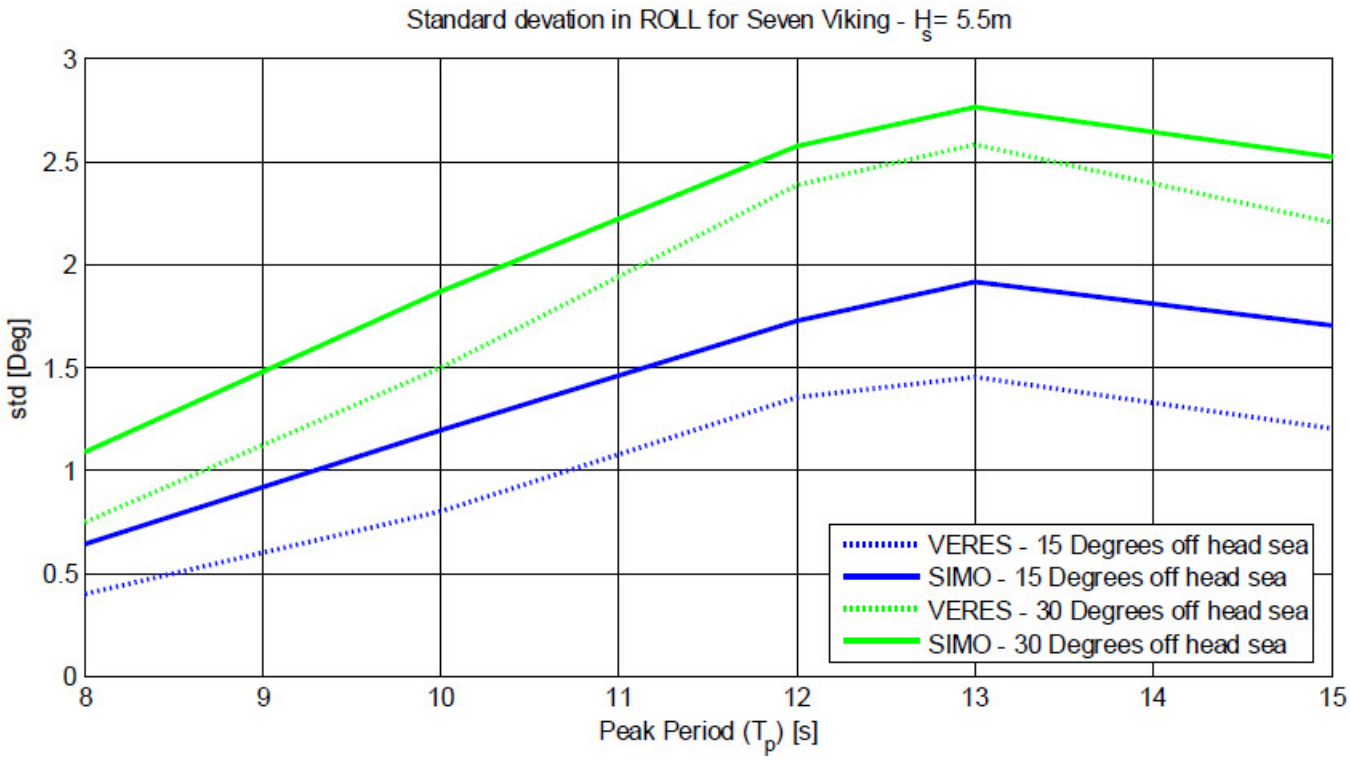

Figure 5.3: Verification of SIMO vessel model – short time statistics [14].

To verify the SIMO model with the actual roll and pitch, short term statistics for the roll from SIMO analyses with duration 3-hour have been compared to results reported by ULSTEIN. The comparison in roll is illustrated in fig. 5.3.

As shown in fig. 5.3 the SIMO model is slightly on the conservative side for 15 and 30 degrees off head sea. This is however not the case for beam sea. A comparison between the calibrated SIMO model roll RAO's and the results obtained from ULSTEIN show that SIMO under predicts the RAO in beam sea. The comparison is illustrated in fig. 5.4

Since the damping in SIMO is implemented as a quadratic damping term, the RAO will vary with the amplitude of the waves that is used to establish the RAO. Waves with larger amplitudes will result in lower RAO's.

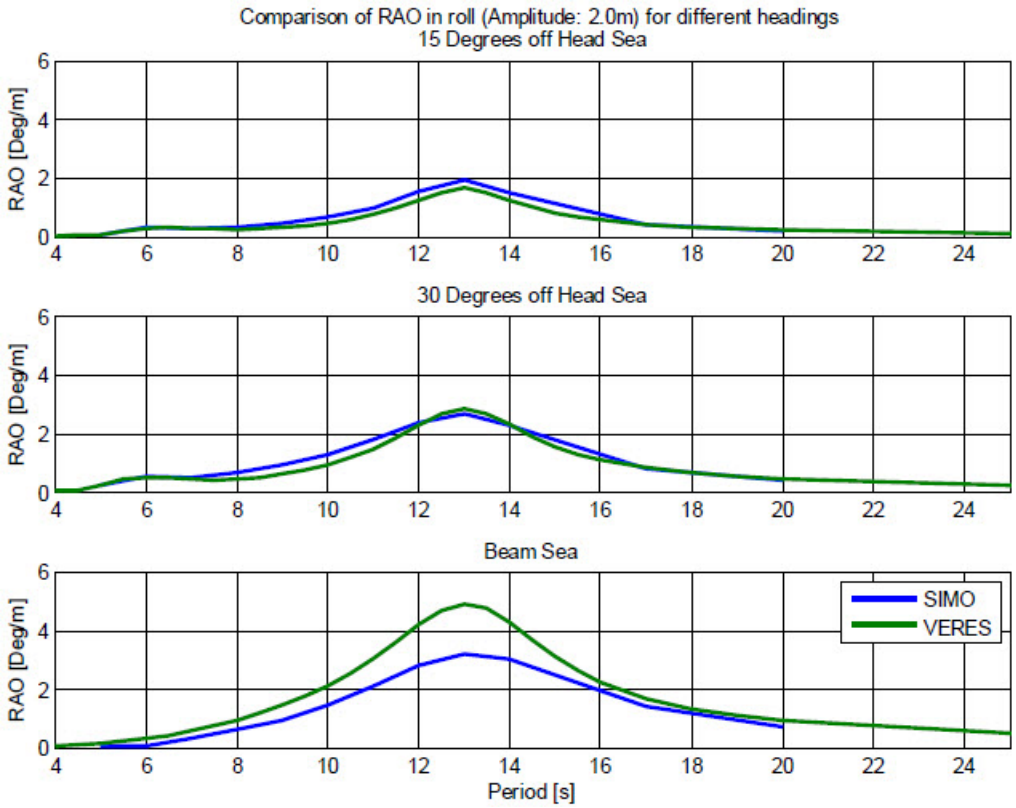

Figure 5.4: Comparison of RAO in roll [14].

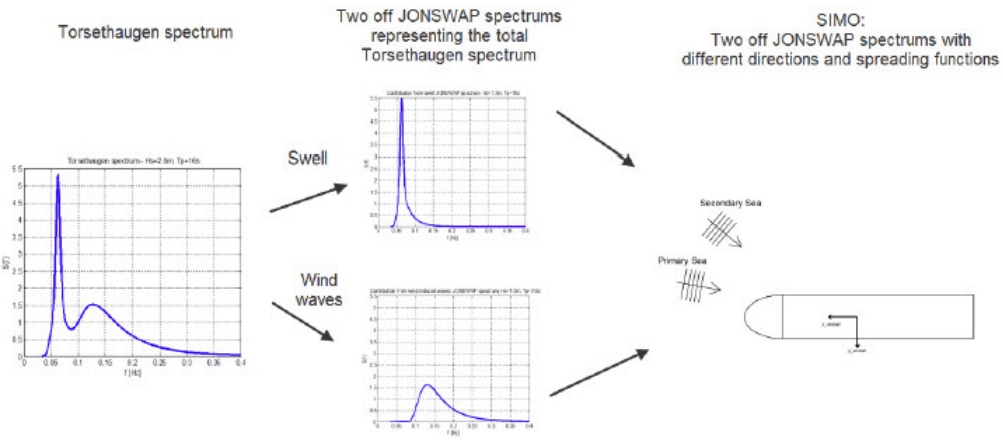

Figure 5.5: Two-peaked JONSWAP spectrum implemented in SIMO [16].

5.5 Seastate model

SIMO has incorporated several different sea state spectra to model irregular sea states. In this thesis the JONSWAP spectrum is mainly used. The Torsethaugen spectrum has also been used, but only to illustrate the effect of unidirectional sea waves and swell. To account for different direction of sea waves and swell, two-peaked JONSWAP specta are used. An illustration showing how this is implemented in SIMO is shown in fig. 5.5. A comparison of the Torsethaugen spectrum and two-peaked JONSWAP spectrum is illustrated in fig. 5.6. From the comparison one can see that there is some difference between the two spectra, but that the two-peaked JONSWAP spectrum is slightly more conservative.

5.6 Realisation of irregular sea

SIMO have several methods of generating realisations (time series) of irregular sea. The time series are generated by superposition of harmonic components with uniformly distributed phases by means of pre-generation by the Fast Fourier transform (FFT)[3]. Separate realisations of a sea-state can be achieved by changing the seed in SIMO. In this thesis every simulation is run 20 times, with random seed numbers. Scripts in Matlab are used to make

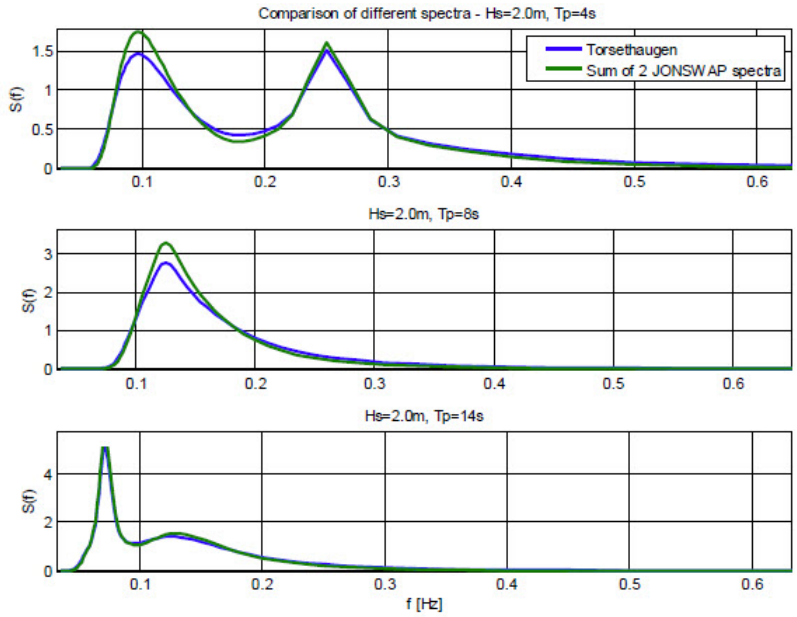

Figure 5.6: Comparison of Torsethaugen and two-peaked JONSWAP spectrum [16].

SIMO batches. Batches are pre-defined scripts that automates the process of giving inputs to SIMO.

5.7 MHS

In SIMO the MHS tower is modelled as a docking cone coupling. The docking cone coupling is a force model that represents the prong-funnel coupling. The docking cone coupling is modelled as attached to the vessel in order to simplify the model and making the results easier to interpret compared to modelling the MHS tower and all its sub-components.

In fig. 5.7 the principles used to model each prong-funnel connection is illustrated. As indicated in the figure, three docking cone coupling elements are used to represent the effect of one prong-funnel connection. The red colour indicates when the couplings are active. One should also notice that the force model includes the effect of friction in the axial direction of the connection.

In fig. 5.7 the docking cone elements are represented by the notation P1, P11 and P111. For the

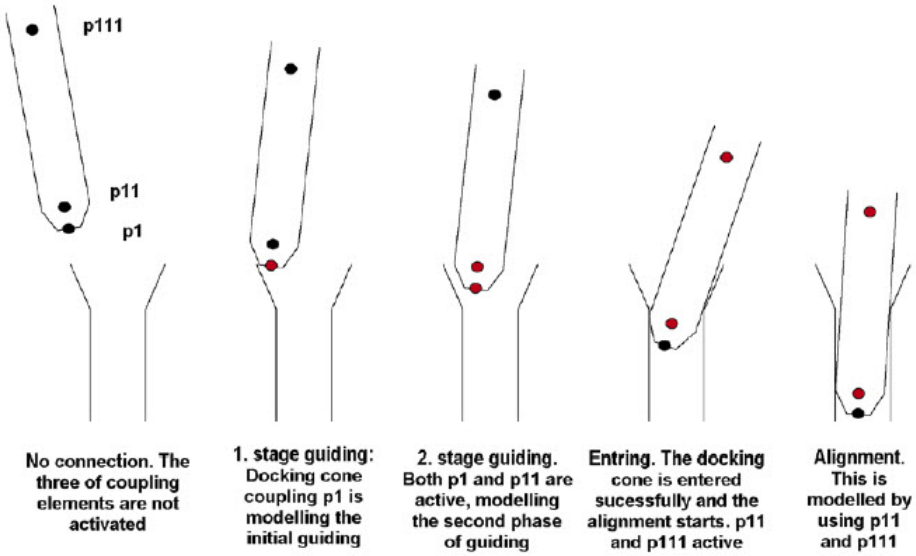

Figure 5.7: Prong-funnel coupling – Principles – red colour indicates active element [14]

situation where the module is hanging in air from the top of the MHS tower the module will be docked. In this situation, P1 will not be active as it cannot come into contact with the funnels. P11 will be active when lower part of the prong is in contact with the funnel. P111 will be active when the upper part of the prong is contact with the funnel and when both P11 and P111 are active, moment will be exerted on the prong.

The stiffness of the cursor guide frame could be set to a high value to prevent rotation over the maximum value, but the cursor guide frame is made of structural steel and will deflect when large loads are applied to the prongs. The stiffness in the model is calculated using the software Ansys and will be made available in the new MHS design report. An illustration of the Ansys model is presented in fig. 5.8.

With the stiffness value obtained from structural analysis in Ansys, one will see relative rotation over the theoretical maximum value.

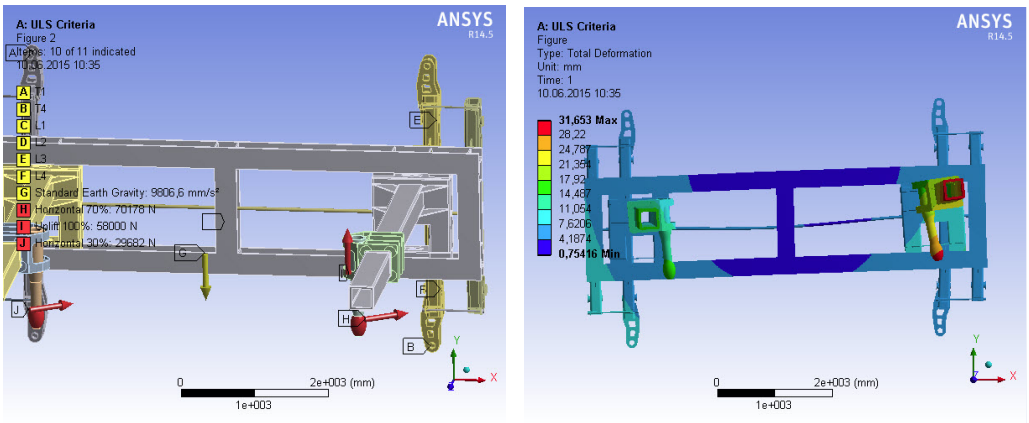

(a) Forces acting on the cursor guide frame - Ansys model

(b) Total deformation with loads fram (a) applied - Ansys model

Figure 5.8: Structural analysis to determine stiffness - Ansys model

5.8 Module

In the original file the module is modelled using slender elements to be able to capture the hydrodynamic response. In the scenario of having the module hanging inside the hangar from the top of the MHS, the hydrodynamic properties are redundant. The properties that are of importance is the weight, mass moment of inertia and the CoG of the module. These properties are assigned to the slender element model. Using this method the attributes and behaviour of the module can be changed to suit modules of different weight, geometry and CoG.

A dummy model has been set up in Mathcad to calculate the different properties. The standard dummy model, see fig. 5.9 for illustration, has the dimensions:
Width: W = 4200 mm
Breadth: B = 4200 mm
Height: H = 8500 mm
The global position is set at the center top of the module where the main wire will be connected. This yields a CoG of -4.25 meters in z-direction.

To change the CoG and moment of inertia the height of the dummy module is changed. See fig. 5.10 for illustration. The global position remains the same.

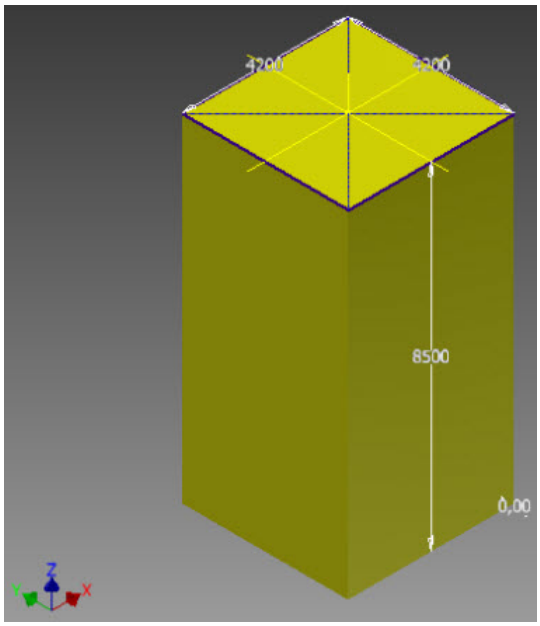

Figure 5.9: Dummy module.

With the mass of the module being the governing parameter together with the dimensions, it is straightforward to calculate the mass moment of inertia and the position of the CoG. The mass moment of inertia is found by using the parallel axis theorem:

$$I = I_{CoG} + md^2 \tag{5.1}$$

Where I_{CoG} is the mass moment of inertia of the module about the center of gravity:

$$I_{CoG} = \frac{1}{12}mk^2 \tag{5.2}$$

where:

m = Mass of the module [kg]

k = Radius of gyration of the module [m]

d = Radius of gyration of the module from the global position [m]

The input needed for the SIMO system file is:CoG for x, y and z directions, I_{xx}, I_{xy}, I_{yy}, I_{yz}, I_{xz}

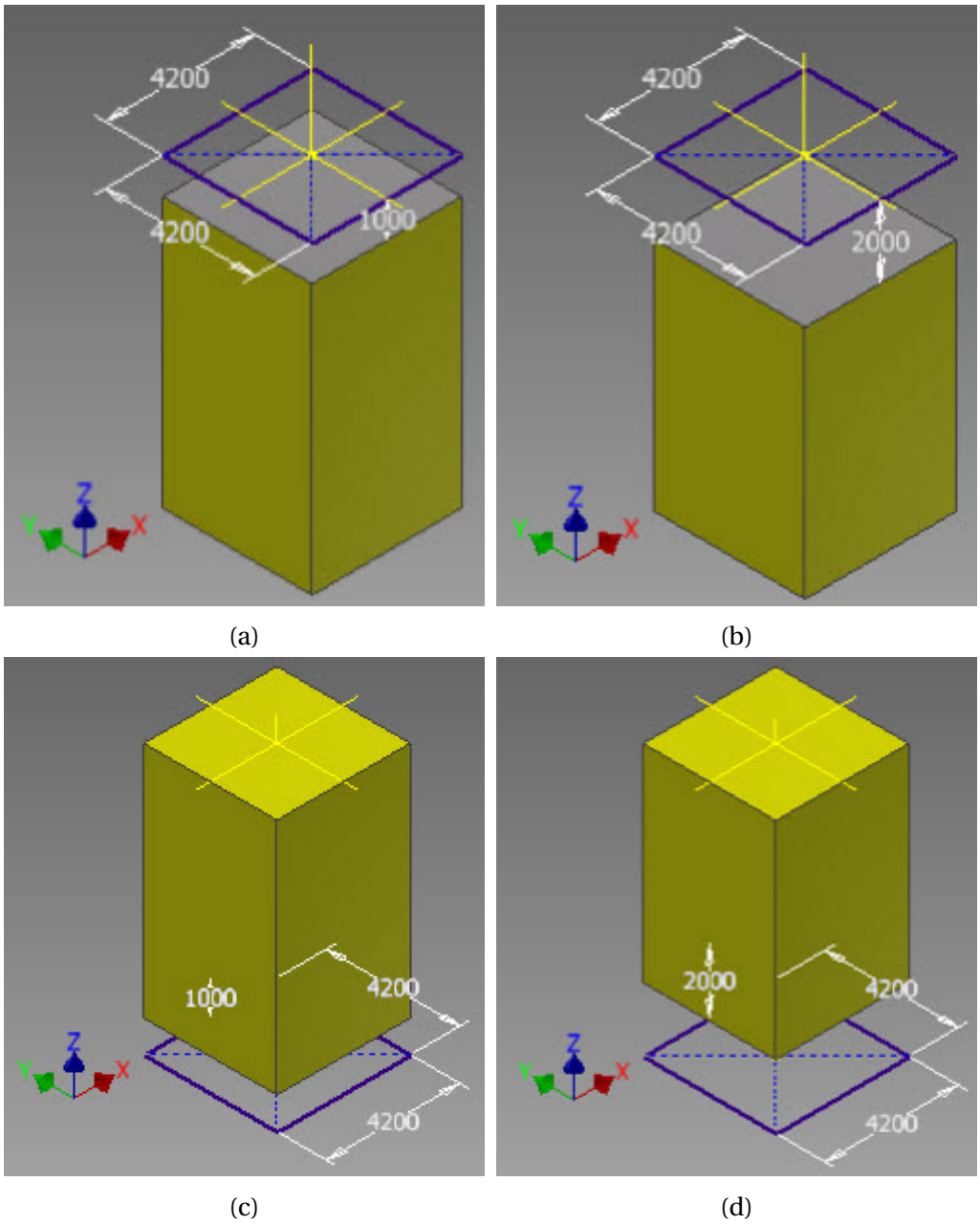

(a) (b)

(c) (d)

Figure 5.10: Dummy modules with different extrusion to alter CoG.

and I_{zz}:

$$CoG_z = h_c + \frac{h}{2} \tag{5.3}$$

where:

h_c = height if the extrusion [m]. Positive when CoG is to be lowered,see fig. 5.10 (a) and (b),

and negative when the CoG is to be raised, see fig. 5.10 (c) and (d)

h = Altered height of the dummy module [m]

CoG_x and $CoG_y = 0m$ because of the symmetry of the module.

$$I_{xx} = \frac{1}{12} m(W^2 + h^2) + m \cdot CoG_z^2 \tag{5.4}$$

$$I_{yy} = \frac{1}{12} m(B^2 + h^2) + m \cdot CoG_z^2 \tag{5.5}$$

$$I_{zz} = \frac{1}{12} m(W^2 + B^2) \tag{5.6}$$

Because of the symmetry of the module I_{xy}, I_{yz} and I_{xz} equal 0.

Chapter 6

Sensitivity analysis

6.1 Chapter overview

This chapter presents and discuss the results of the sensitivity analysis.

6.2 Analysis setup

The objective of this thesis was not to look into deployment and recovery of modules in specific sites/fields, but general deployment and recovery to find the general sea state were modules can be safely deployed and recovered. A sensitivity analysis of different sea states have been carried out to achieve this objective. The variable parameters was the significant wave height H_S, peak period T_P and wave direction. Analysing every variation of these three parameters would take a significant amount of time. It was therefore decided to analyse significant wave height from $1.0m$ to $5.0m$ and peak period from $5.0s$ to $14.0s$. The wave direction was analysed for a specific significant wave height and peak period.

To simplify the analysis, notation to the different sea states are given. For a sea state with

$H_S = 3.0m$, $T_P = 9.0s$ and a wave direction of 165° relative to the vessels keel (see fig. 2.6 for definitions of wave directions) the notation becomes: H30T09H2. Table 6.1, table 6.2 and table 6.3 show the different notation used. One should note that the vessel can keep a desirable heading and H1 and H2 (180° and 165° are reaalistic wave directions during lifting operations with Seven Viking.

Table 6.1: Significant wave height notation

H_S $[m]$	Notation
1.0	H10
2.0	H20
3.0	H30
4.0	H40
5.0	H50

Table 6.2: Peak period notation

T_P $[s]$	Notation
5.0	T05
6.0	T06
7.0	T07
8.0	T08
9.0	T09
10.0	T10
11.0	T11
12.0	T12
13.0	T13
14.0	T14

Table 6.3: Wave direction notation

Wave direction $[Deg]$	Notation
180	H1
165	H2
150	H3
135	H4
90	H5
45	H6
30	H7
15	H8
0	H9

6.3 Sensitivity analysis introduction

The objective of this thesis was to find the design sea state. That is, the sea state where the module deployment or recovery cannot be executed. First of all, since the response of the module is expected to be dependent on the vessel motion, the vessel response to different sea states are examined. The RAOs of the vessel are examined. Since the module pendulum motion is of primary interest and caused by the roll and pitch of the vessel, the RAOs for the respective motions are examined. All RAOs are given in appendix B. From fig. B.1 one can see that the largest roll response occurs in beam sea with a period T around $11.5s$ and from fig. B.2 one can sea that the largest pitch response occurs in head sea with a period T around $9.5s$. This will only give an indication of the response of the vessel, and the response of the module will vary because of the horizontal eigen frequency. To avoid momentum acting on the prongs the relative rotation between the prongs of the cursor guide frame and the funnels of the module must be kept under 7° when the penetration of the funnels are $0.5m$ The relative rotation is the rotation of the module relative to the rotation of the vessel.

6.4 Extreme value estimation

To avoid momentum acting on the MHS, the maximum relative rotation of the sensitivity analysis should be examined. If the maximum relative rotation exceeds the design relative rotation, the prong will experience momentum forces. Three methods of estimating the extreme value for the relative rotation will be presented and compared in this section.

1. Four times standard deviation method.
2. Weibull extreme value.
3. Gumbel extreme value.

The first method can be a reasonable approach if the data is Rayleigh distributed. In table 6.4 the results from 20 realisations are presented. The results show that 4x Standard deviations (STDs) of the relative rotation can be a reasonable approach since the smallest 4 STD is at least 100 % of the global observed maxima. The results also show that using the maxima of one realisation may give a liberal result. This method can however give non-conservative results if the standard deviation is small. From table 6.5 one can see that the smallest 4 x STD is only 70 % of the largest observed global maxima.

The Weibull distribution can be used to estimate extreme values of time series. In this thesis Matlab is used to calculate the parameters and the distribution. To if the data follows a Weibull distribution, a probability plot is made plotting the Weibull fit against the data from the time series. Plotting the continuous data against the Weibull fit reveals that the data deviates from the fit for small and large values of relative rotation. One can remove small peaks closer than $1s$, to remove "noise" from the data. When doing this, only the peaks are registered. This is a manipulation of the data, but since the maxima is of main interest, this should not have a great effect on the extreme value. The two different probability plots are illustrated in fig. 6.1. The plots reveal that when only peaks are used, the data keeps it linearity for greater values of relative rotation, and the 90 percentile is more conservative for peaks compared to continuous

Table 6.4: 20 realisations of time series for H30T08H1 showing relative rotation in pitch. The smallest 4std is at least 100 % of the global observed maxima.

Realisation	4*std	Max loc [deg]	Max glob [deg]	4std/glob	4std/loc	Loc/glob
1	10.3	8.3	9.9	1.0	1.2	0.8
2	10.1	6.8	9.9	1.0	1.5	0.7
3	10.8	7.7	9.9	1.1	1.4	0.8
4	9.6	8.1	9.9	1.0	1.2	0.8
5	12.8	8.8	9.9	1.3	1.5	0.9
6	11.0	8.4	9.9	1.1	1.3	0.9
7	12.5	9.6	9.9	1.3	1.3	1.0
8	12.7	8.7	9.9	1.3	1.4	0.9
9	10.8	7.6	9.9	1.1	1.4	0.8
10	11.7	8.8	9.9	1.2	1.3	0.9
11	11.5	9.0	9.9	1.2	1.3	0.9
12	11.0	8.2	9.9	1.1	1.3	0.8
13	9.9	9.1	9.9	1.0	1.1	0.9
14	12.6	9.9	9.9	1.3	1.3	1.0
15	11.7	9.3	9.9	1.2	1.3	0.9
16	12.3	7.7	9.9	1.2	1.6	0.8
17	12.3	8.4	9.9	1.2	1.5	0.9
18	10.3	7.7	9.9	1.0	1.3	0.8
19	10.2	8.8	9.9	1.0	1.2	0.9
20	11.6	7.9	9.9	1.2	1.5	0.8

Table 6.5: 20 realisations of time series for H30T08H1 showing relative rotation in roll. The smallest 4std is only 70 % of the global observed maxima.

Realisation	4*std	Max loc [deg]	Max glob [deg]	4std/glob	4std/loc	Loc/glob
1	5.0	5.0	6.1	0.8	1.0	0.8
2	5.0	5.1	6.1	0.8	1.0	0.8
3	4.9	5.1	6.1	0.8	1.0	0.8
4	5.0	4.4	6.1	0.8	1.1	0.7
5	4.7	4.8	6.1	0.8	1.0	0.8
6	5.3	4.3	6.1	0.9	1.2	0.7
7	5.1	5.0	6.1	0.8	1.0	0.8
8	4.5	4.2	6.1	0.7	1.1	0.7
9	5.1	5.5	6.1	0.8	0.9	0.9
10	4.6	4.2	6.1	0.8	1.1	0.7
11	4.9	4.2	6.1	0.8	1.2	0.7
12	4.9	4.5	6.1	0.8	1.1	0.7
13	4.9	5.5	6.1	0.8	0.9	0.9
14	4.9	4.8	6.1	0.8	1.0	0.8
15	4.9	4.4	6.1	0.8	1.1	0.7
16	4.7	4.5	6.1	0.8	1.0	0.7
17	5.0	6.1	6.1	0.8	0.8	1.0
18	5.1	4.4	6.1	0.8	1.2	0.7
19	4.6	4.4	6.1	0.8	1.0	0.7
20	4.9	5.6	6.1	0.8	0.9	0.9

data. It should also be noted that for values over the 90 percentile, the Weibull distribution does not seem to fit the data.

The situation is the same for relative rotation in roll as seen in fig. 6.2. But the peak data follows the Weibull fit even for values over the 90 percentile.
To estimate the extreme value for data presumed to follow a Weibull distribution the formula for the Weibull cumulative distribution function is given:

$$F(X)_{27min} = \left(1 - exp\left\{-\left(\frac{X}{\alpha}\right)^{\beta}\right\}\right)^{n_{27min}} \tag{6.1}$$

Solving for X:

$$X = \left\{\left[-log\left(1 - F(X)_{27min}^{\frac{1}{n_{27min}}}\right)^{\frac{1}{\beta}}\right]\alpha\right\} \tag{6.2}$$

where:

X = Relative rotation [deg]

α = Scale parameter

β = Shape parameter

n_{27min} = number of crossing for a duration of 27 min

The scale and shape parameters α and β are the maximum likelihood estimates of the parameters of the Weibull distribution given the values in the time series data.

Realisation 8 from tables 6.4 and 6.5 is used to estimate the extreme values of relative rotation in roll and pitch. The Weibull cumulative distribution plot for relative rotation in roll and pitch

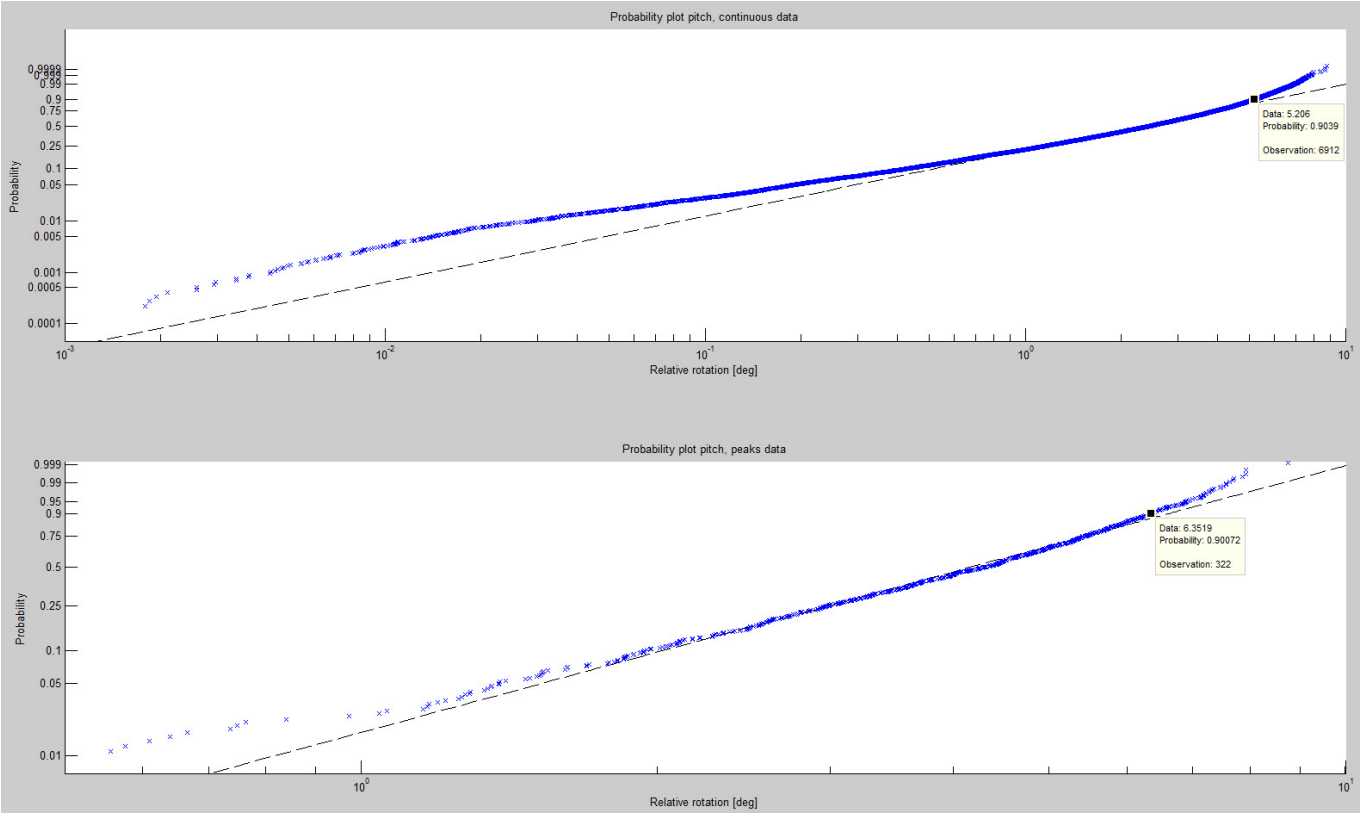

Figure 6.1: Probability plot of continuous data and peaks from data for relative rotation in pitch. The probability plot show that the peaks selection follow the Weibull fit better than the continuous data

is illustrated in fig. 6.3 and show that the 90 percentile for the relative rotation in roll and pitch is 4.6° and 10.2° respectively.

In order to use the Gumbel distribution (or extreme value distribution) several realisations have to be run. The maxima of each of the realisations is then used to estimated the parameters for the distribution, and the maxima data are then plotted with the Gumbel distribution to check for fit. The equation for the Gumbel distribution is given by:

$$F(X_{max}) = exp\left[-exp\left(-\frac{X-\mu}{\sigma}\right)\right] \tag{6.3}$$

solving for X:

$$X = ln\{-ln[1-F(X_{max})]\}\sigma + \mu \tag{6.4}$$

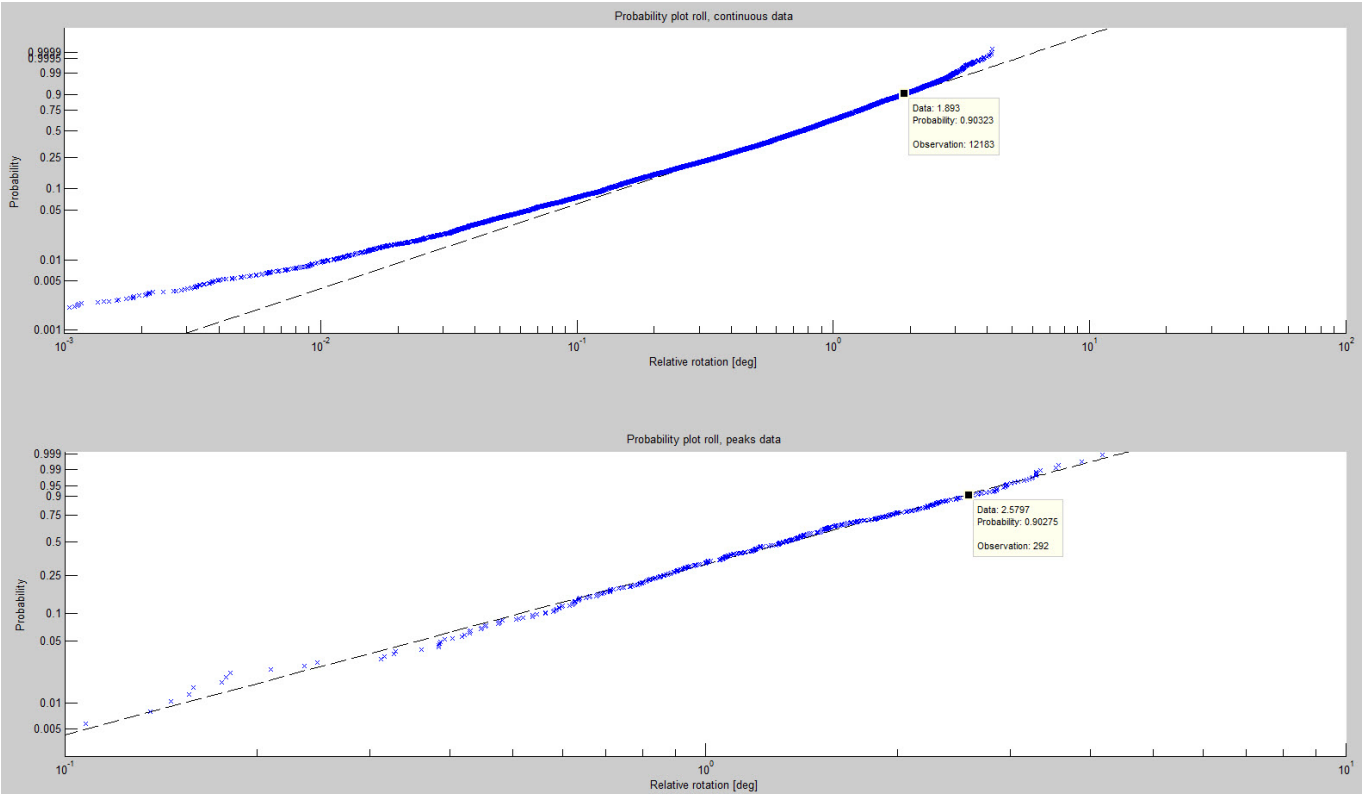

Figure 6.2: Probability plot of continuous data and peaks from data for relative rotation in roll. The probability plot show that the peaks selection follow the Weibull fit better than the continuous data

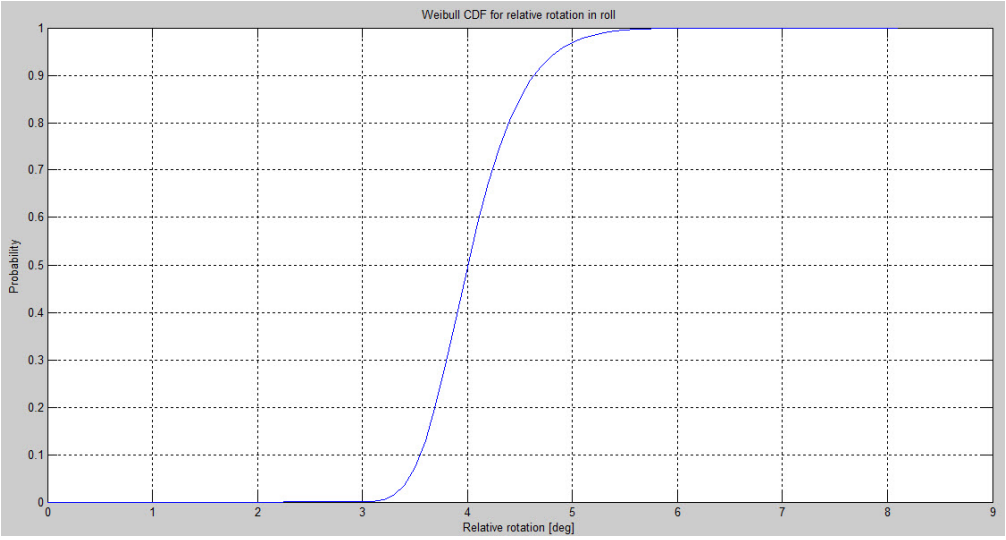

(a) Weibull CDF for relative rotation in roll.

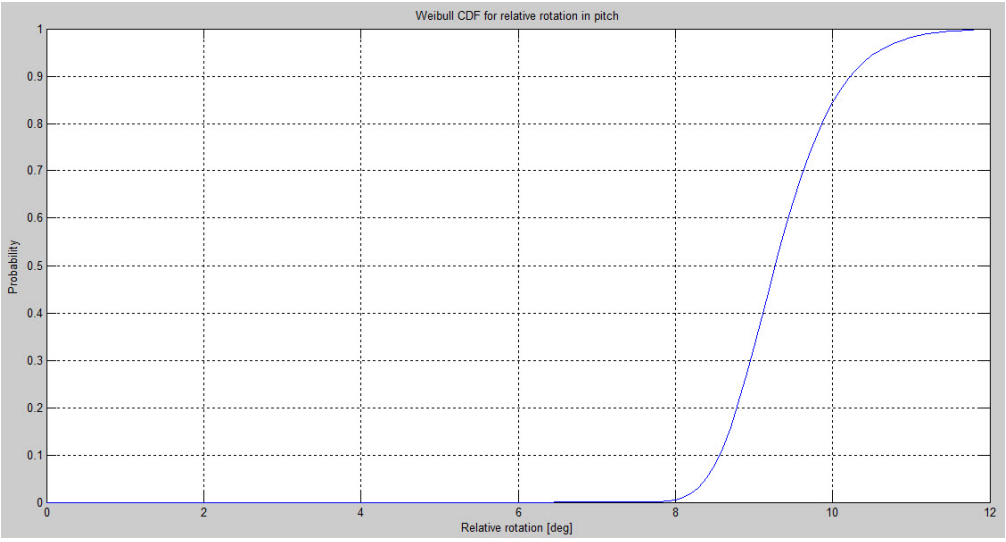

(b) Weibull CDF for relative rotation in pitch.

Figure 6.3: Weibull CDF of relative rotation in pitch and roll for H30T08H1. The plots show that the 90 percentile for roll and pitch is 4.6° and 10.2° respectively

The Gumbel CDF for the same sea state as the 4· standard deviation and the Weibul extreme value estimation methods is presented in fig. 6.4. The plots show that the 90 percentile for roll and pitch is 5.5° and 9.4° respectively. A comparison of the three methods is presented in table 6.6. Based on the results, the Gumbel method of estimating the extreme value was chosen. Both the extreme values for 4 times the standard deviation and the Weibull estimate in roll is non-conservative compared to the Gumbell estimated. It should be noted that the results presented in table 6.6 is for the realisation where the 4· standard deviation is at a minimum.

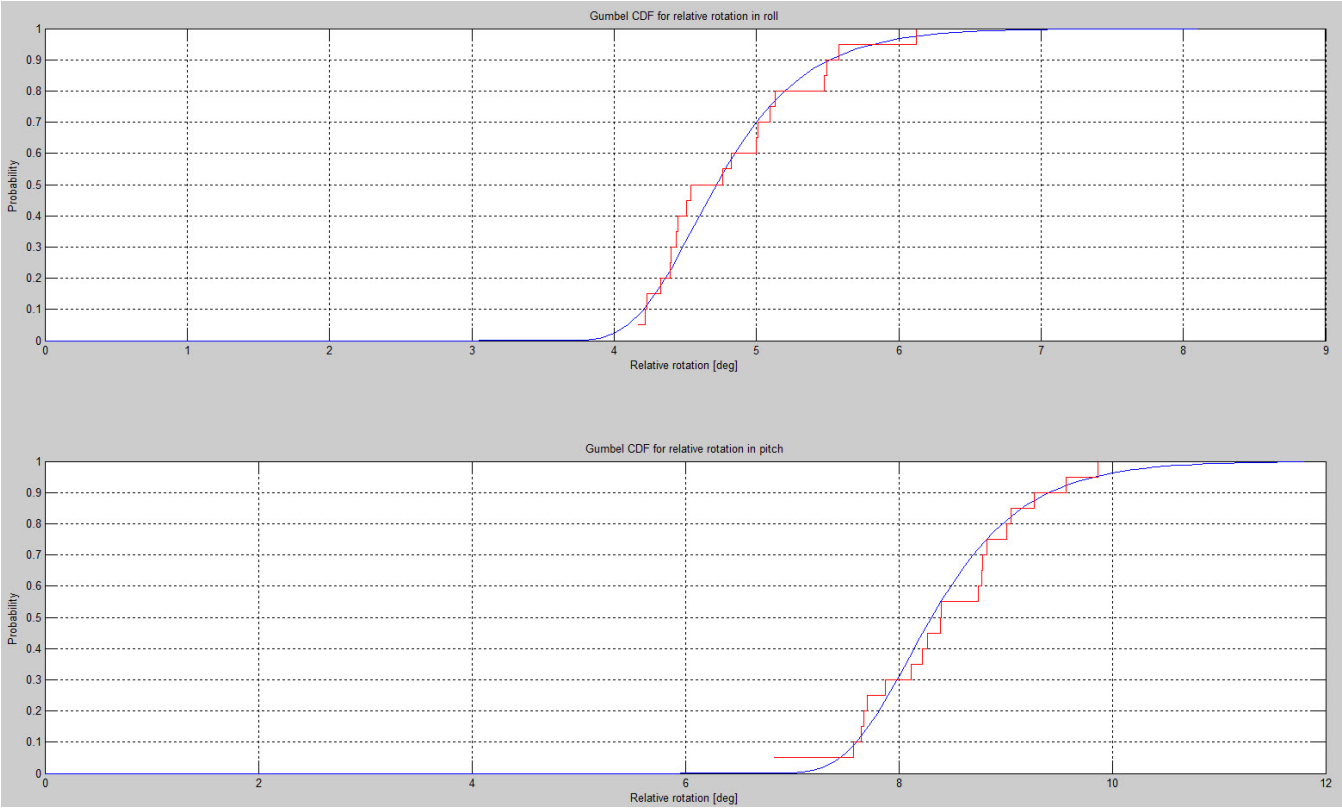

Figure 6.4: Gumbel CDF of relative rotation in pitch and roll for H30T08H1. The plots show that the 90 percentile for roll and pitch is 5.5° and 9.4° respectively

But by doing analysis with only one realisation, one may achieve the least conservative result.

Table 6.6: Extreme value estimation of relative rotation, H30T08H1

Extreme value estimation of relative rotation				
	Roll	/max obs	Pitch	/max obs
4*std	4.5	0.7	9.6	1.0
Weibull	4.6	0.8	10.2	1.0
Gumbell	5.5	0.9	9.4	1.0
Max obs	6.1		9.9	

A duration test was also performed to examined the effect of increased duration in relative rotation. Three different durations were; test 1: $1638s = 27.3min = 0.46h$; test 2: $3277s = 54.6min = 0.91h$ and test 3: $6554s = 109.3min = 1.8h$. The sea state of the test was H20T08H2.

The Gumbel extreme value distribution is used to estimate the maximum relative rotation. The results are presented in table 6.7.

Table 6.7: Duration test. Pitch and roll is the relative rotation

Duration	Pitch	Deviation	Roll	Deviation
1638	5.1		5.0	
3277	5.2	1.6 %	5.14	3.0 %
6554	5.5	7.7 %	5.23	4.9 %

From table 6.7 one can see that there are some deviation in relative rotation. Taking the duration of the actual phase of operation into consideration, which is expected to be approximately $15min$, the setup with a duration of $1638s$ should be adequate, especially when one use 20 realisations.

The difference between the durations for a single realisation is illustrated in fig. 6.5. From the figure it is possible to see that fluctuations in the relative rotation is similar for the three durations.

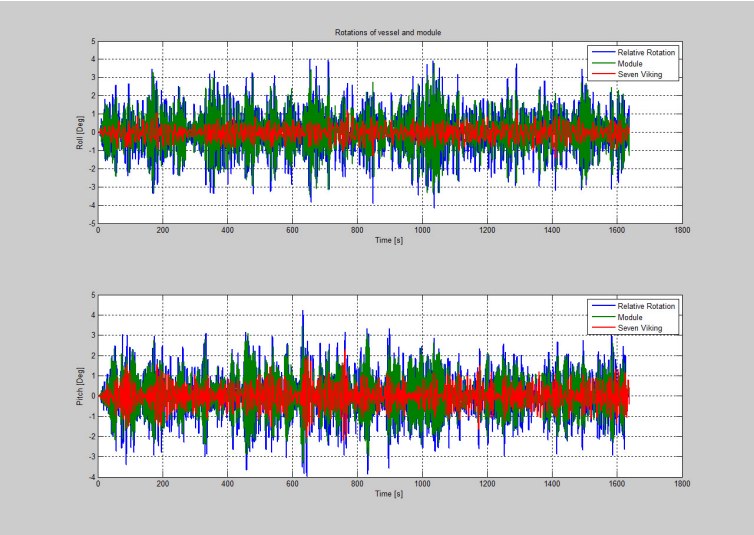

(a) Duration = 1638s

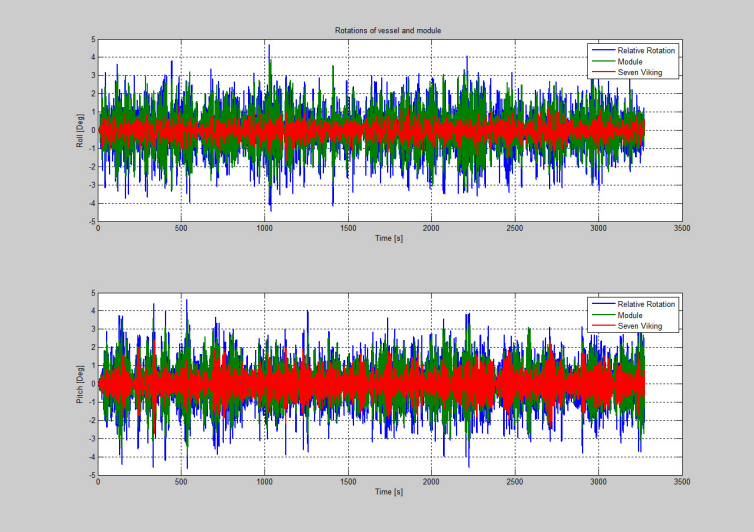

(b) Duration = 3277s

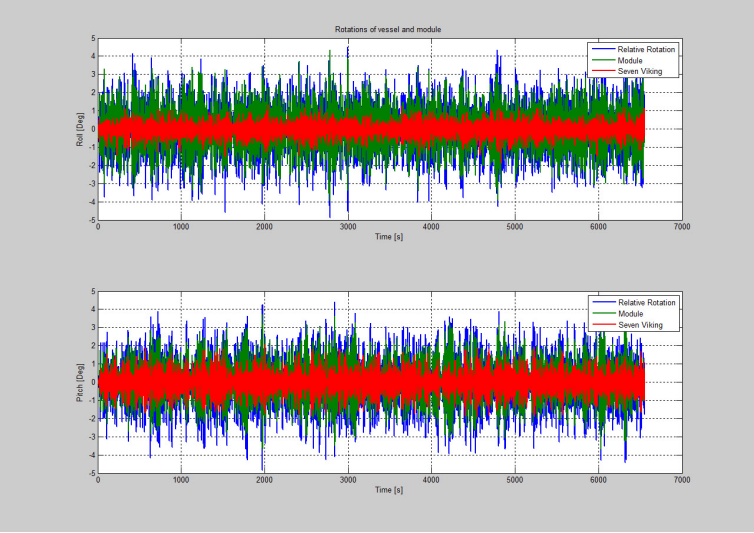

(c) Duration = 6554s

Figure 6.5: Times series for different durations

6.4.1 Effect of wave spreading

The exponent n in the spreading function given by fig. 6.6 should by taken as the value between $2-10$ which give the most conservative result. Figure 6.6 show that the relative rotation decrease when the spreading exponent increase. One should that the plot only show the effect for exponents in the range of $2-5$. This have not been done for every sea state analysed, and the exponent is therefore set to 2 for every simulation conducted in this sensitivity analysis.

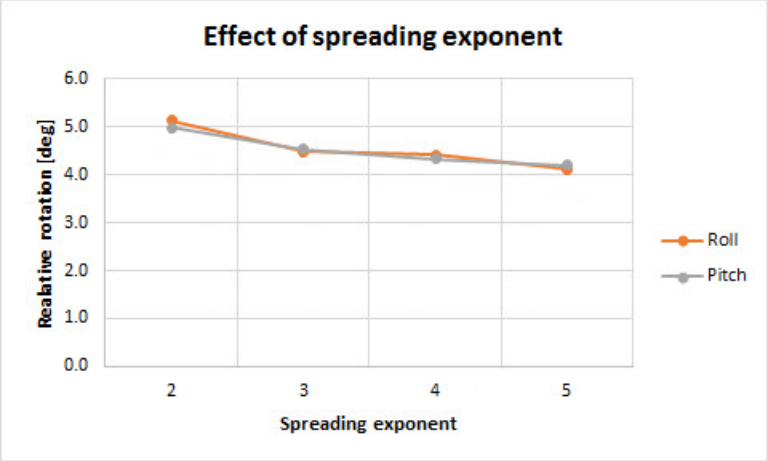

Figure 6.6: Effect of spreading exponent - H20T08H2

6.5 Comparison of sea states

To find the critical sea state where the module does not exert moment on the cursor prong frame, an analysis was done of the different sea states ranging from $1m$ to $6m$ H_S and $5s$ to $15s$ T_P. The wave direction used is $15deg$ off head sea. It must be noted that the results presented in this section are based on the simulations where the stiffness of the prong-funnel couplings is set to an unrealistically large value. The stiffness of the couplings will be discussed later in this chapter. The results can still be used to show the trends of the relative rotation of the module in different sea states, but because of the stiffness the values for relative rotation will be less than in a realistic scenario. It must also be noted that the values for relative rotation it based on single realisations, that a time series for each situation. The Weibull function was chosen to

estimate the extreme values.

The comparison is illustrated in figs. 6.7 and 6.8 and from the results one can see that a peak in relative rotation in pitch occurs when the period is about $7-8s$. The relative rotation seem to be greater for $7s$ periods when the wave height is over $3m$, and $8s$ periods give the largest values for $0-2.5m$ and second largest for larger wave heights. For roll, it seems that the relative rotation increase with both increasing wave height and period but for wave height larger than $2.5m$ and periods over $10s$ the relative rotation seem to flatten out.

To give a conservative look on the sensitivity analysis, and reduce the number of simulations to be made, a period of $8s$ and $14s$ is mostly used. The range of wave heights will vary from $1-5m$

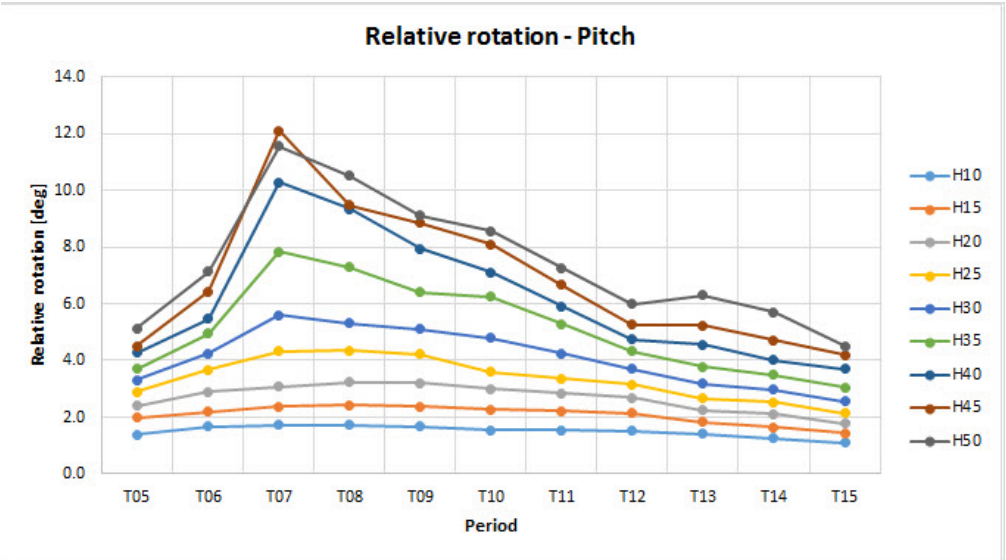

(a) Relative rotation in pitch for different wave heights. The plot show that a peak occurs when the period is $7-8s$

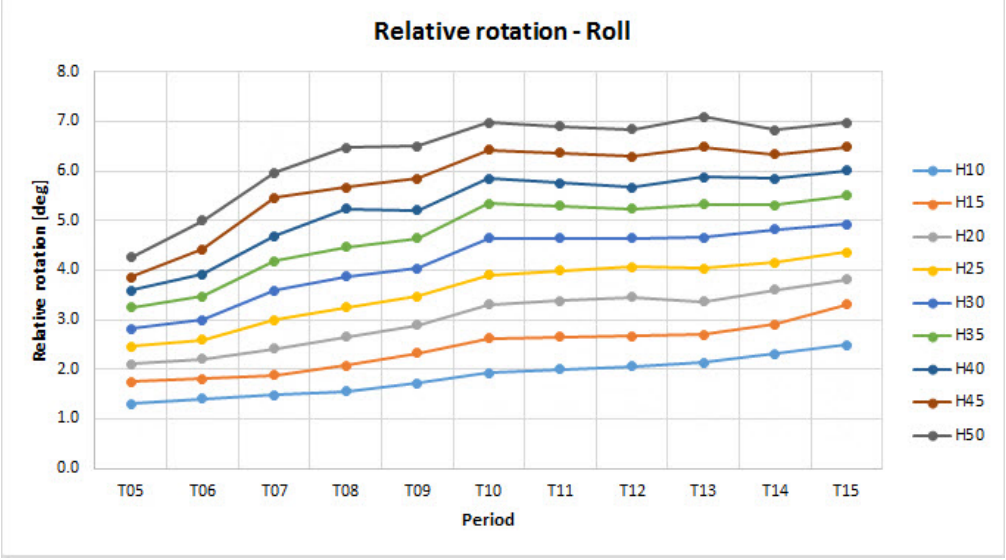

(b) Relative rotation in roll for different wave heights. The plot show that a the relative rotation increase slightly with increasing periods

Figure 6.7: Relative rotation in roll and pitch for different wave heights. A peak in relative rotation in pitch seem to occur when the period is $7-8s$ and the relative rotation in roll seem to increase slightly when the period increase

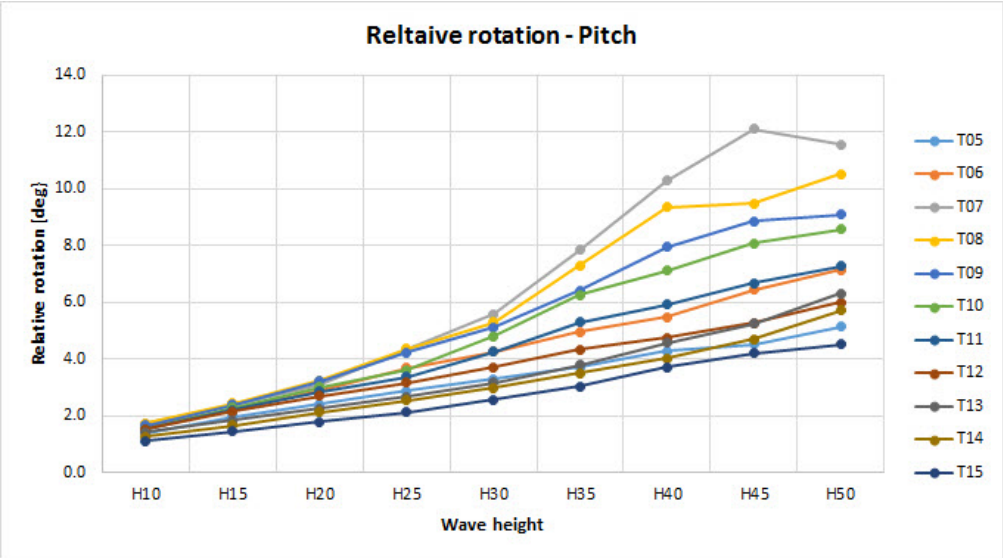

(a) Relative rotation in pitch for different periods. The plot show that the largest relative rotation occurs when the period is $7-8s$

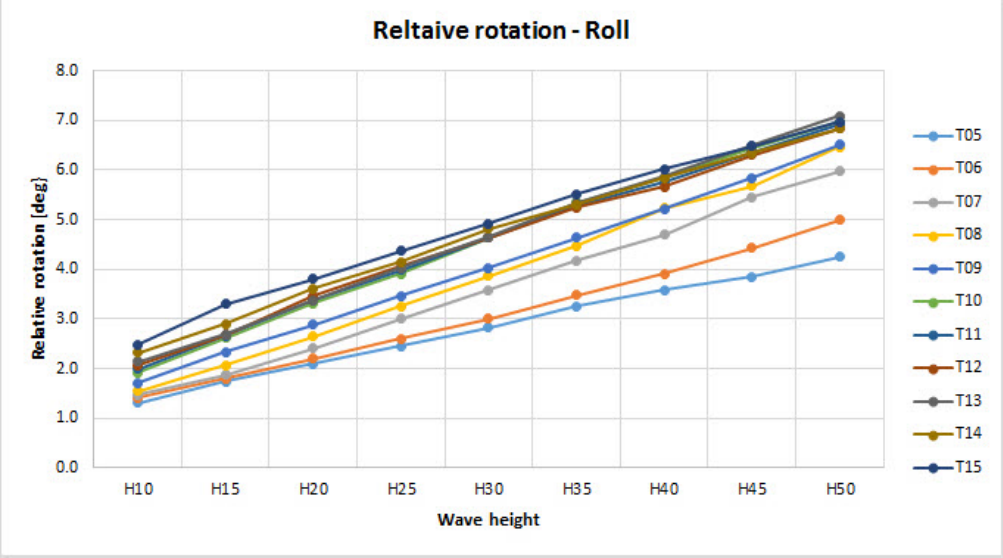

(b) Relative rotation in roll for different periods. The plot show that the relative rotation increase with increasing wave heights and that the relative rotation deviates little for periods between $10-15s$

Figure 6.8: Relative rotation in roll and pitch for different periods. T07 and T08 seem to yield the largest relative rotation in pitch and the relative rotation in roll seem to increase with increasing wave heights and that the relative rotation deviates little for periods between $10-15s$

6.6 Comparison of original prongs and PILT

The difference between the OP and the new PILT design is explained in section 4.2. In this section the two prong systems are analyzed using the same sea states. The purpose is to see what the effect of the new PILT design will have on the relative rotation. In fig. 6.9 the two designs are compared. The effect of the PILT seem to be minimal in roll, but significant in pitch. One should also note that the relative rotation in pitch does not seem to change significantly with varying wave directions.

The use of the anti-roll tanks might be a reasonable explanation to this trend. The pitch motion would normally not be significant,but when the anti-roll tanks compensates for the roll motion, the pitch motion increases and is thus affecting the motion of the module.

The setup of prongs also seem to affect the relative rotation. Since the prongs are positioned in line with the roll motion, they seem to disturb the resonance effect of the system. This can be explained by the force acting between the prong and funnels and the radius of gyration.

The resonance effect will be further discussed in the next section.

The purpose of the PILT is to allow for a larger relative rotation before momentum force is exerted on the cursor guide frame. This will increase the sea state in which modules can be deployed with the use of the PILT design.

From fig. 6.10 one can see that the OP experiences more incidents of momentum on the prongs than what is the case for the PILT because of the larger maximum tilt value.

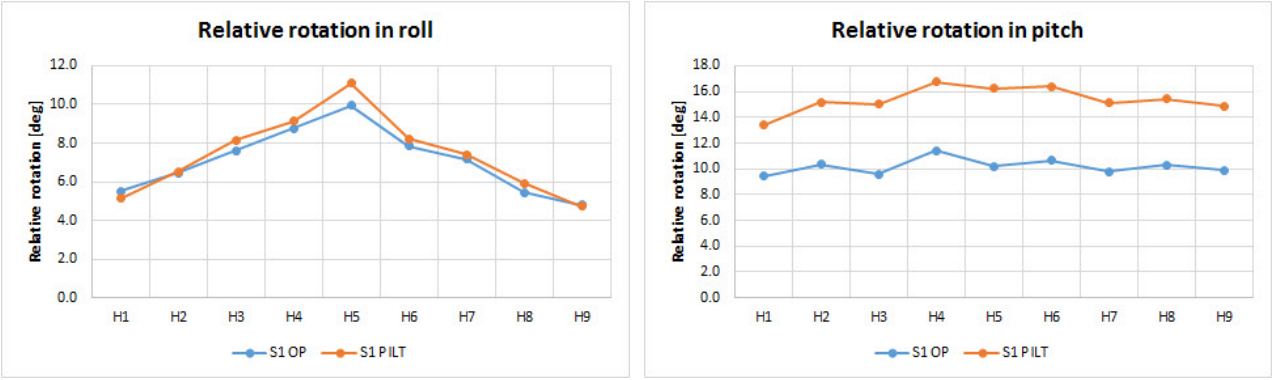

(a) Comparison of OP and PILT in roll

(b) Comparison of OP and PILT in pitch

Figure 6.9: Comparison of OP and PILT in roll and pitch for seastate H30T08. The x-axis show the different wave directions. The results show that the effect of the PILT is minimal in roll, but significant in pitch

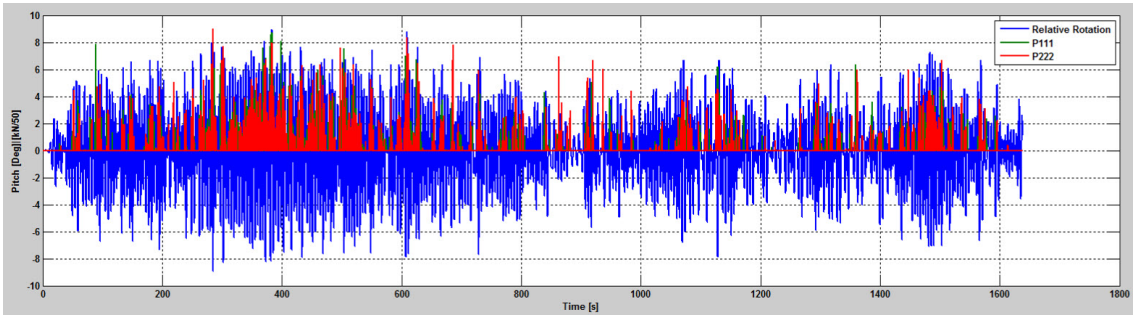

(a) Time series of OP in pitch

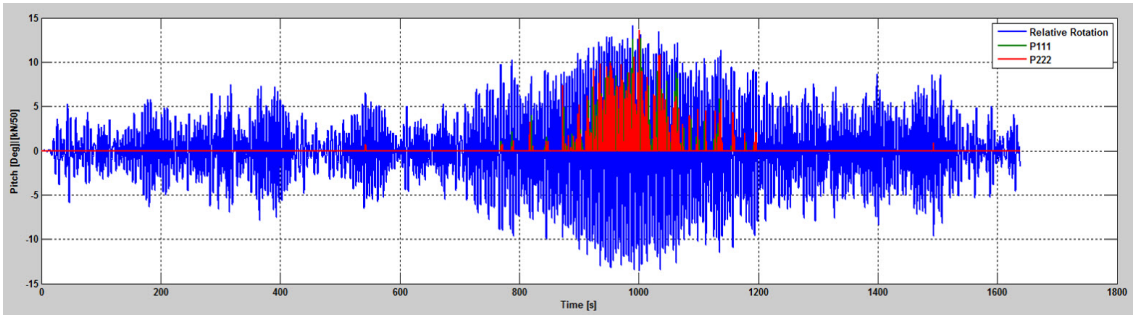

(b) Time series of PILT in pitch

Figure 6.10: Comparison of OP and PILT in pitch for seastate H30T08H5. P111 and P222 show the force acting on the prongs when moment is taken by the prongs

6.6.1 Stiffness of cursor guide frame

One should note that the relative rotation in fig. 6.9 exceeds the maximum tilt value. The loads acting on the CGF cause deflection the relative rotation can therefore exceed the thoretical value. Figure 6.11 show that for unrealistic values of stiffness (stiff coupling) in the CGF the relative rotation is significantly lower compared to realistic stiffness (flexible coupling).

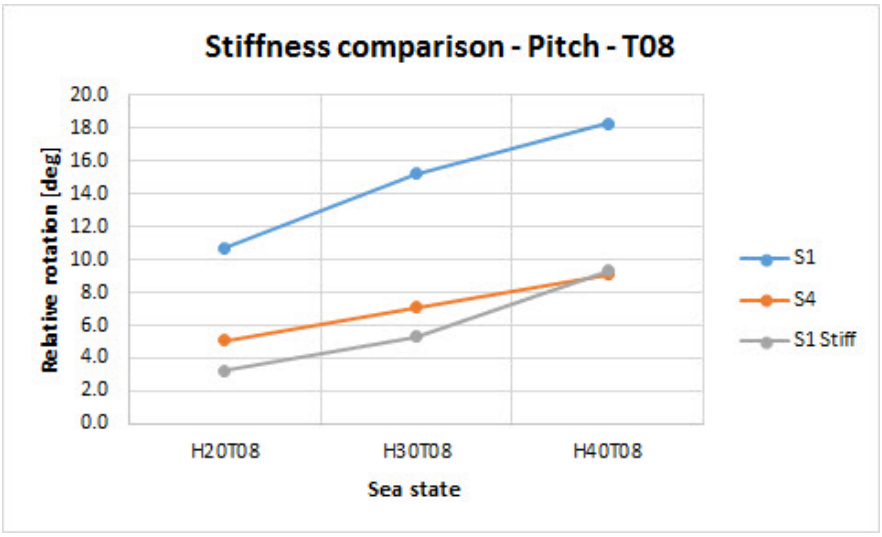

(a) Stiffness comparison in pitch

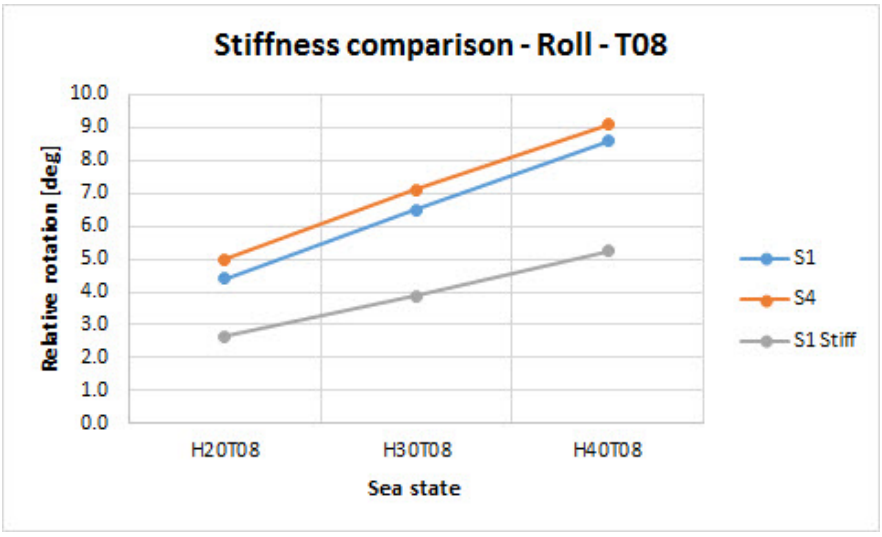

(b) Stiffness comparison in pitch

Figure 6.11: Effect of stiffness in the CGF - The relative rotation when stiffness is unrealistic high is significantly lower compared realistic values of stiffness.

6.7 Cursor configuration

The CGF allows for different configurations of the prong system. The prongs can be put in different positions along the cantilever beam. Since the module motion seem to react most to pitch motion, it is reason to believe that by placing the prong and funnels closer to the cursor wagon the vertical force between the prong and funnel may disturb the resonance motion of the module because if the moment created. To test this, six different prong/funnel configurations were analysed. The different setups are shown in fig. 6.12.

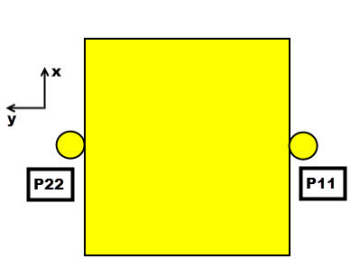

(a) Setup 1, prong-funnels in middle position. This is the current setup on Seven Viking

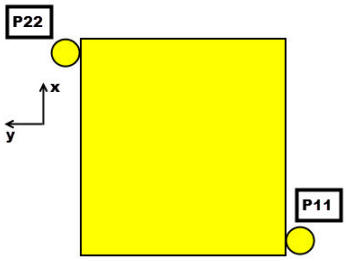

(b) Setup 2, prong-funnels in diagonal position.

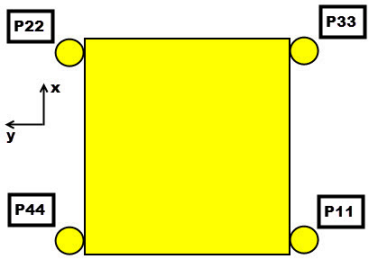

(c) Setup 3, prong-funnels in each corner.

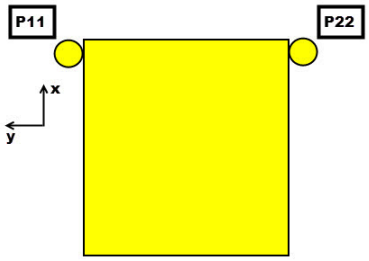

(d) Setup 4, prong-funnels in front position.

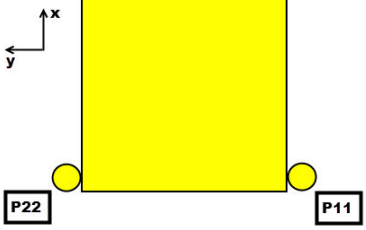

(e) Setup 5, prong-funnels in aft position.

Figure 6.12: Prong and funnel setup. Positive x-axis points toward the cursor guide frame

The analysis results are presented in tables 6.8 and 6.9 and clearly show that setup 1 yields the least favourable results for pitch motion. They also show that relative rotation in roll is most favourable when using setup 1.

The results in tables 6.8 and 6.9 show that setup 4 yields the most favourable results, especially

Table 6.8: Prong configuration test, sea state: H20T08H2.

Setup	Pitch [Deg]	Deviation	Roll [Deg]	Deviation
1	10.8		4.2	
2	7.5	-31 %	5.8	38 %
3	4.8	-56 %	4.5	7 %
4	5.1	-53 %	5.0	17 %
5	4.8	-55 %	4.7	10 %

Table 6.9: Prong configuration test, sea state: H50T08H2.

Setup	Pitch [Deg]	Deviation	Roll [Deg]	Deviation
1	20.7		11.1	
2	18.0	-13 %	16.1	46 %
3	12.3	-40 %	9.5	-14 %
4	12.8	-38 %	12.8	16 %
5	12.5	-40 %	11.9	8 %

since rotation in pitch is the most important parameter in the wave heading analysed. To explain the difference between the setup 1 and setup 4, one have to look at what happens during the time series analysis. The motion may appear to be much more efficiently dampened in setup 4 than in setup 1. When the prong collides with the funnel, the motion of the module will increase or decrease depending on what direction it is heading at the moment of collision and on the vessel motion.

To examine this phenomenon one have to look at the time series analysis for the specific realisations. In figs. 6.13 and 6.14 the difference between setup 1 and 4 is shown. One can clearly see that the relative rotation in setup 4 is far less than in setup 1. One should keep in mind that the two analysis does not use the same realisations, but as seen in figs. 6.13 and 6.14 the vessel motions are similar, although they appear in different intervals.

Disruption of resonance seem to occur both for setup 1 in roll and for setup 4 in roll and pitch. For setup 1 in pitch, the vertical force from the prong-funnel coupling will not exert a moment on the module because the radius of gyration is zero. A sketch of the different situations is presented in fig. 6.15. A plausible theory is that the vertical force from the prong-funnel couplings exerts moment on the module because of the radius of gyration and reduce the

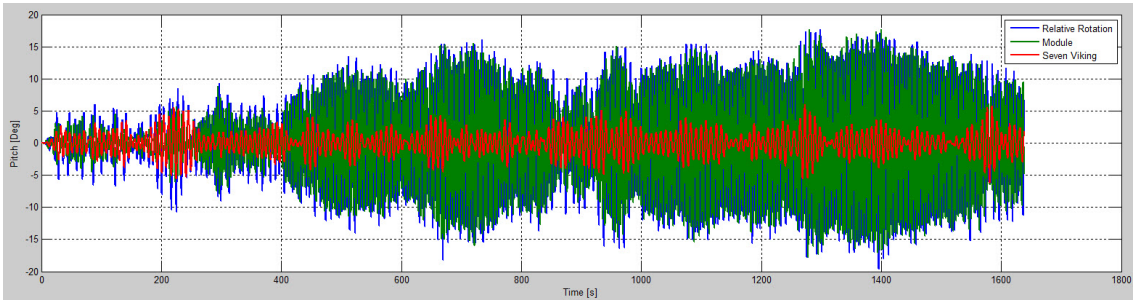

(a) Setup 1 - Pitch.

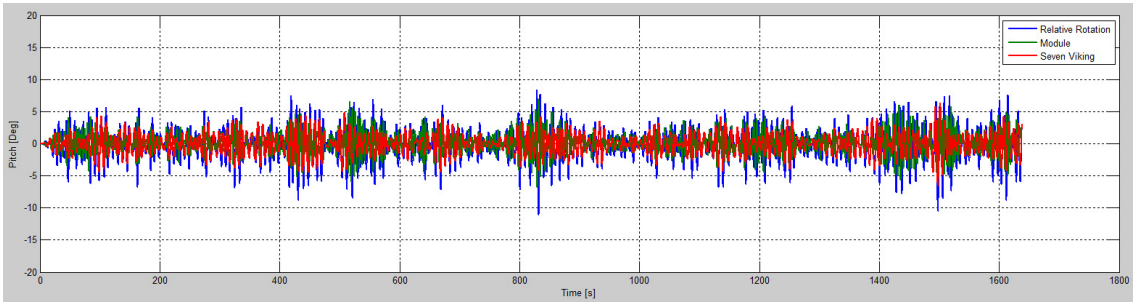

(b) Setup 4 - Pitch.

Figure 6.13: Time series showing vessel, module and relative rotation for setup 1 and 4, sea state: H50T08H2 - Resonance occurs in setup 1

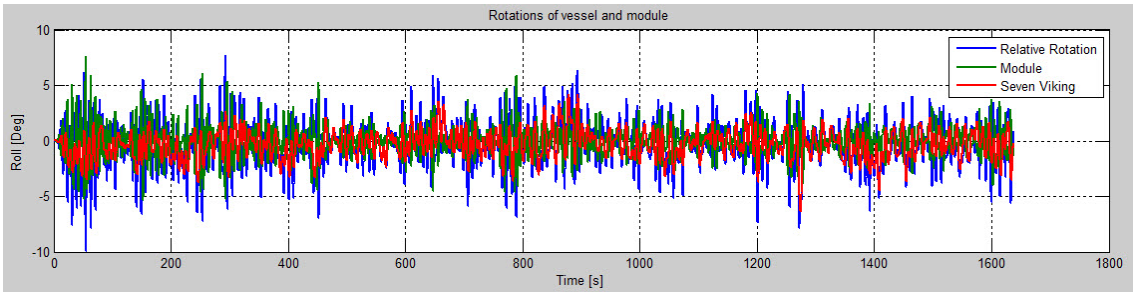

(a) Setup 1 - Roll.

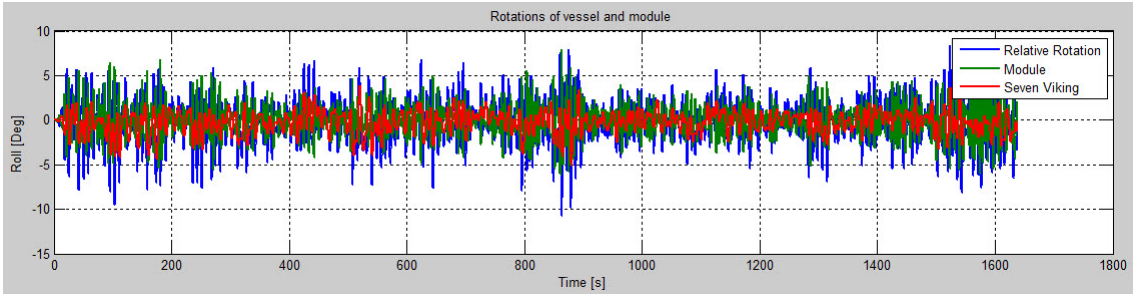

(b) Setup 4 - Roll.

Figure 6.14: Time series showing vessel, module and relative rotation for setup 1 and 4, sea state: H50T08H2 - No resonance

rotational motion of the module and disturb the resonance of the system. One should note that the vertical force will change direction depending on the motion of the module.

6.7.1 Loads on prong-funnel coupling

It was originally planned to examine the structural integrity of the MHS with a focus on the cursor guide frame in the thesis, but as this would be a thesis in it self. Some of the structural aspects have still been examined, especially the force on the prong-funnel connection. The forces exerted from the SIMO will be dependent on the stiffness of the couplings . The maximum loads exerted on the couplings only last for approximately $1s$ and should be treated as impulse loads. Analysis of the loads on the couplings can however give an indication of the advantages and disadvantages of choosing a different setup. A comparison of the forces acting on the couplings is shown in tables 6.10 and 6.11.

Table 6.10: Forces acting on prong-funnel couplings in sea state H20T08H2. The table show the deviation in percent compared to setup 1. Setup 2-5 show a reduction in force. * The results for setup 3 show the average force acting on the couplings on the same cantilever beam

Setup	Force P11 [kN]	Deviation	Force P22 [kN]	Deviation
1	86		85	
2	53	-38 %	60	-29 %
3	75*	-13 %*	74*	-13 %*
4	72	-17 %	50	-41 %
5	58	-33 %	48	-44 %

Table 6.11: Forces acting on prong-funnel couplings in sea state H50T08H2. The table show the deviation in percent compared to setup 1. Setup 4-5 show a reduction in force, while setup 2-3 show an increase in force. * The results for setup 3 show the average force acting on the couplings on the same cantilever beam

Setup	Force P11 [kN]	Deviation	Force P22 [kN]	Deviation
1	248		252	
2	249	1 %	259	3 %
3	258*	4 %*	268*	6 %*
4	179	-28 %	124	-51 %
5	157	-36 %	137	-46 %

From the results in tables 6.10 and 6.11 one can see that setup 4 and 5 give an reduction in forces acting on the couplings. In setup 5 the distance to the prongs on the cantilever beams are greater compared to setup 4, this will result in a greater momentum in the cursor guide frame. In addition to show less force than setup 1, setup 4 will produce less moment due to the shorter distance to the prongs.

The distribution of forces on the prongs can also be of interest for further structural analysis and is shown in table 6.12

Table 6.12: Distribution of forces on the prong-funnel couplings

Setup	P11 [kN]	P11	P22 [kN]	P22	P33 [kN]	P33	P44 [kN]	P44
1		0.5		0.5				
2		0.5		0.5				
3		0.3		0.3		0.2		0.2
4		0.6		0.4				
5		0.5		0.5				

6.7.2 Effect of vertical forces

A test was carried out in order to examine the effect of the vertical forces of the prong-funnel couplings. In this test the friction of the the coupling was set to zero, thus eliminating the vertical force. This is of course a simplification, since the prong and funnel will not always be positioned parallel to each other, and by setting the friction to zero the horizontal force will also be influenced. The result of the test is presented in table 6.13

Table 6.13: Effect of vertical forces on the prong-funnel couplings for setup 1 and 4 in sea state H20T08H2

S1 No friction		S1		S4 No friction		S4	
Roll	Pitch	Roll	Pitch	Roll	Pitch	Roll	Pitch
26.9	22.3	4.2	10.8	22.1	22.5	5.0	5.1

By examining the time series for setup 1 and 2 without friction, one can see that the system seem to be governed by constructive and destructive interference without any significant

forced damping by the force from the prong-funnel couplings. While for the the test with friction, the system seem to be dampened to a much greater extent, disturbing and reducing the module motion. This is illustrated in figs. 6.16 and 6.17

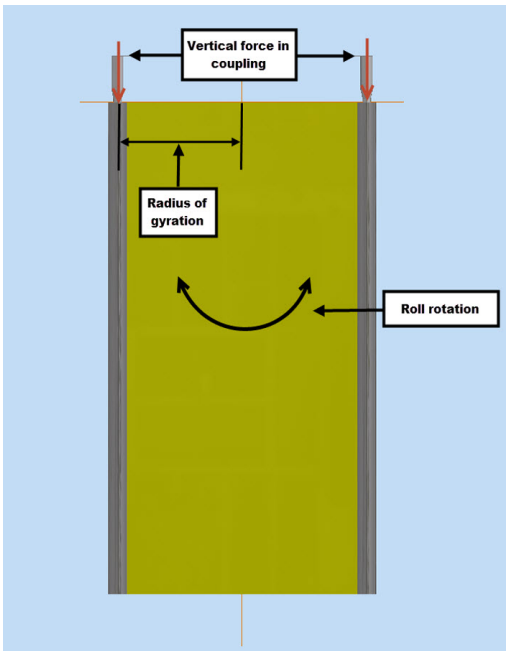

(a) Setup 1 roll

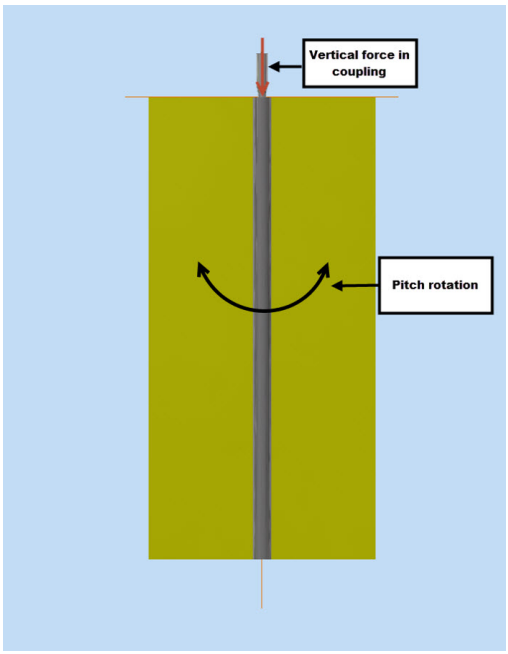

(b) Setup 1 pitch

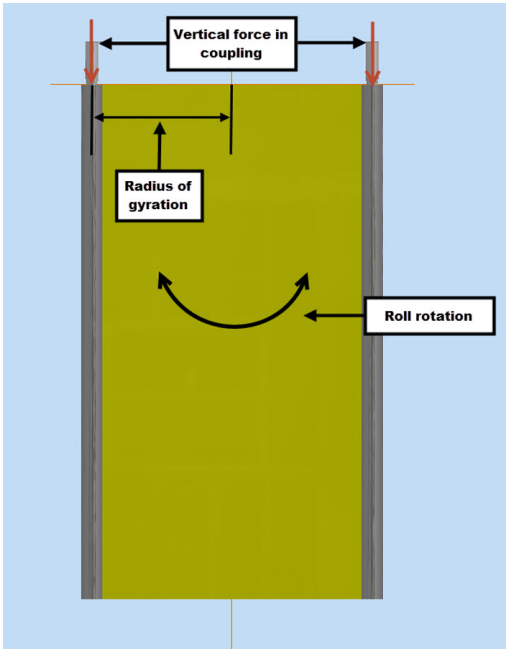

(c) Setup 4 roll

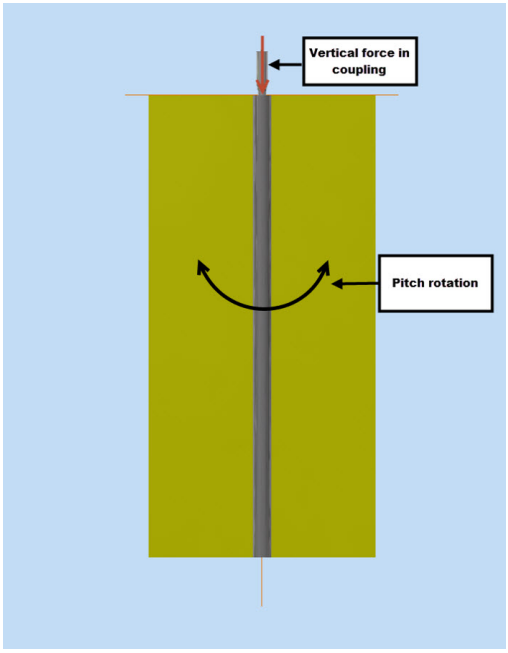

(d) Setup 4 pitch

Figure 6.15: Setup 1 and 4 - Forces and rotation acting on the module

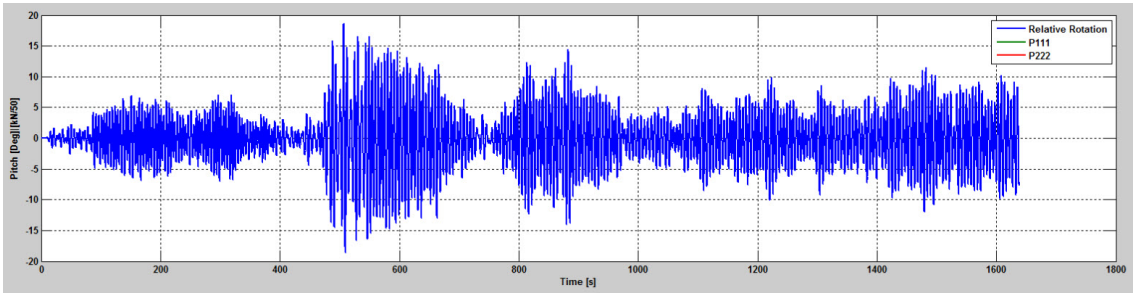

(a) Setup 1 pitch

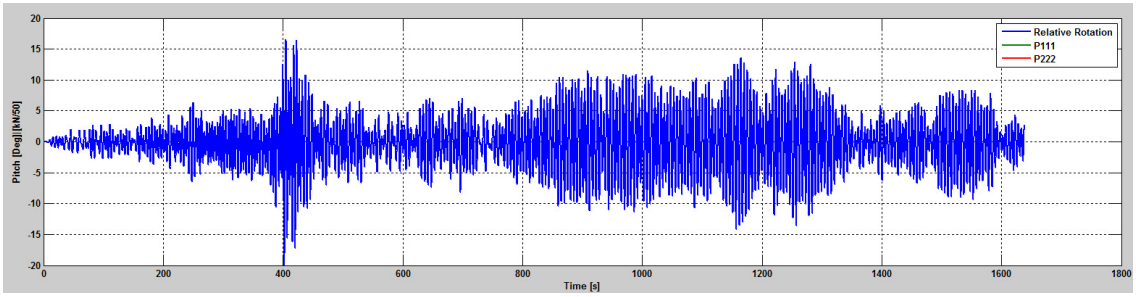

(b) Setup 4 pitch

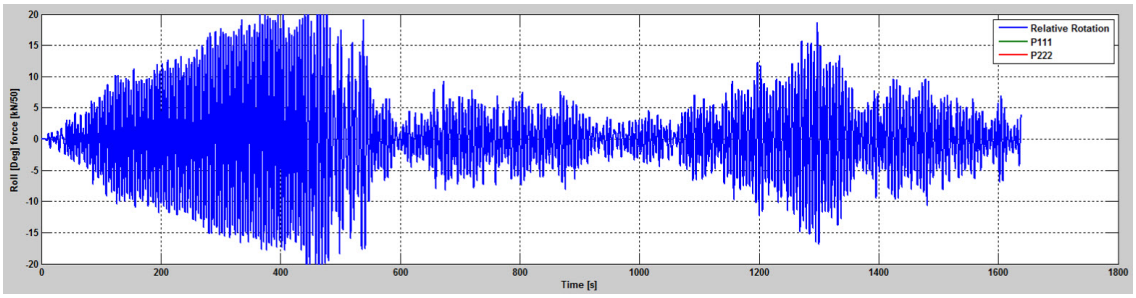

(c) Setup 1 roll

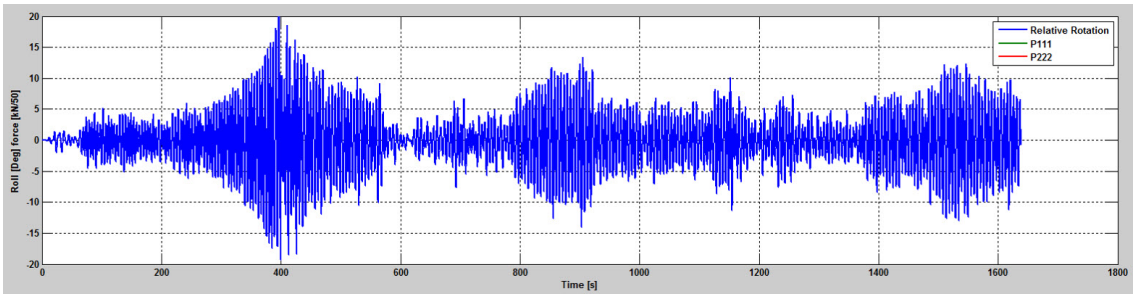

(d) Setup 4 roll

Figure 6.16: Test of couplings without friction. Without friction the rotation seem to be governed by constructive and destructive interference of the vessel and module motion without any forced damping from the coupling force

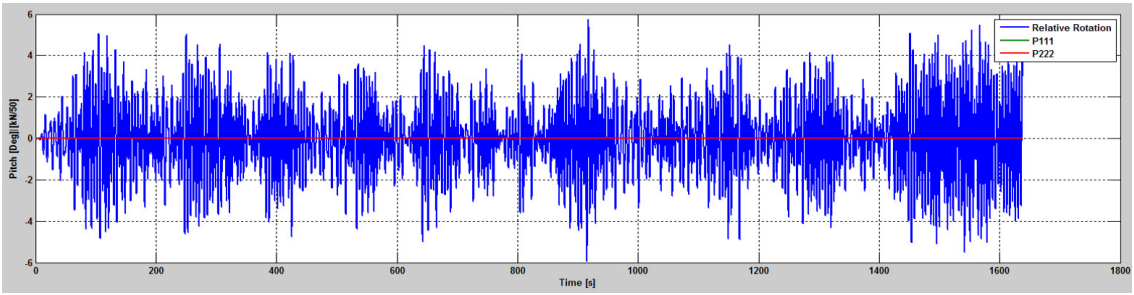

(a) Setup 1 pitch

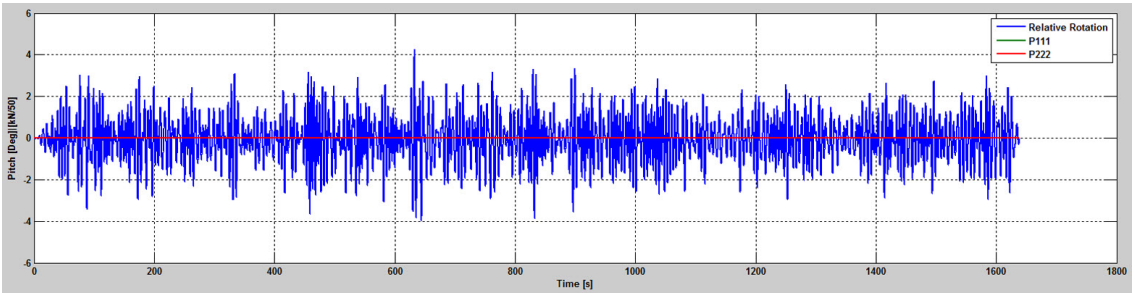

(b) Setup 4 pitch

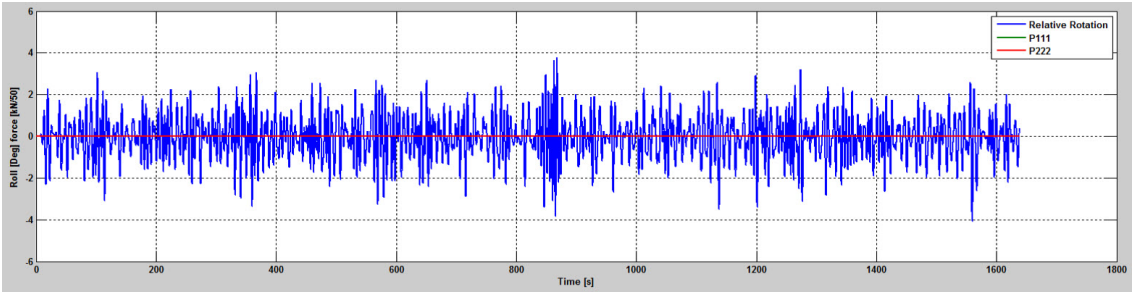

(c) Setup 1 roll

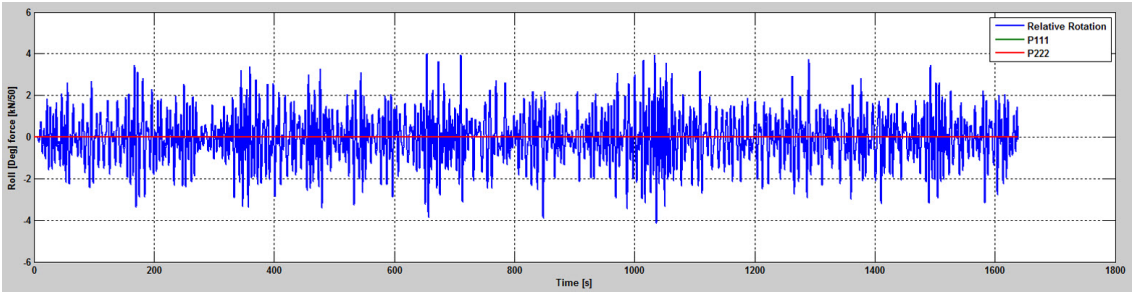

(d) Setup 4 roll

Figure 6.17: Test of couplings with friction. Without friction the rotation seem to be dampened by the friction force. The relative rotation seem to be greater when the radius of gyration is zero, as seen in (a)

6.8 Sea state limitations for setup 4

As discussed in section 6.7, setup 4 where the prongs are positioned close to the CGF, seem to be the preferred setup. Several analysis to give a check the limitations in sea state have been conducted. The results in fig. 6.18 show that setup 4 is sensitive to wave directions, especially for roll. The results also show only marginal difference between OP and PILT and that the relative rotation in a realistic heading (H1 and H2) is close to the limit value for H30T08. Setup 4 is also compared to setup 1 with the OP. From fig. 6.19 one can see that the relative rotation when using setup 4 is significantly lower than when original setup 1 is used.

The results in fig. 6.20 show that the operative sea state using setup 4 can be $H_S = 2.0$ for $T_P > 5.0s$ and a realistic wave direction (H2).

One should not that when different periods is analysed it seems like the result in fig. 6.7 does not match the results when setup 4 is used. This could be caused by the difference in cursor configuration or possibly the difference in stiffness of the CGF.

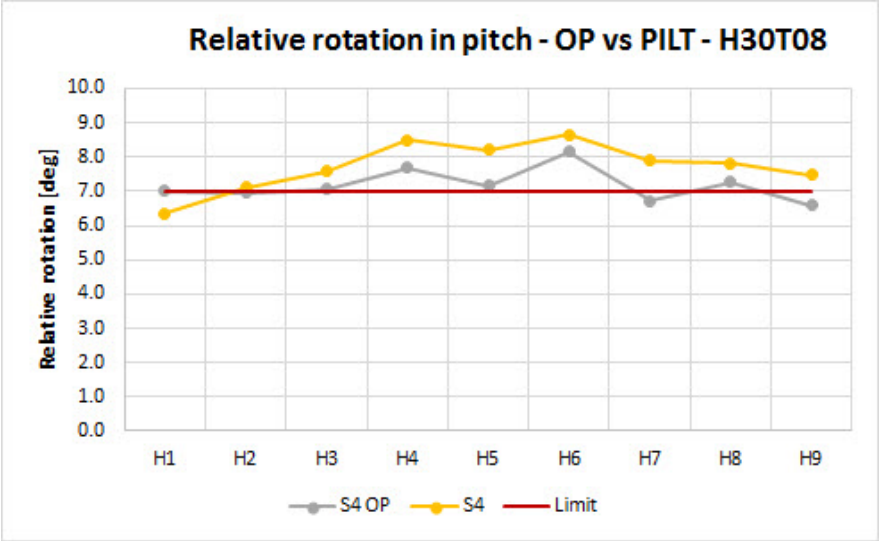

(a) Setup 4 pitch - OP vs PILT - H30T08

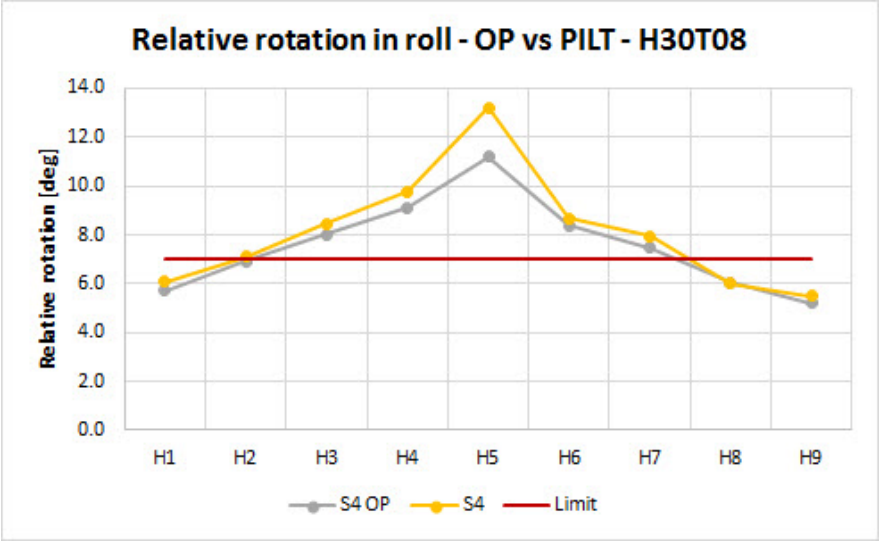

(b) Setup 4 roll - OP vs PILT - H30T08

Figure 6.18: Relative rotation in pitch and roll for different wave direction - Setup 4 - H30T08 - The results show only marginal difference between OP and PILT and that the relative rotation in a realistic direction (H1 and H2) is close to the limit value

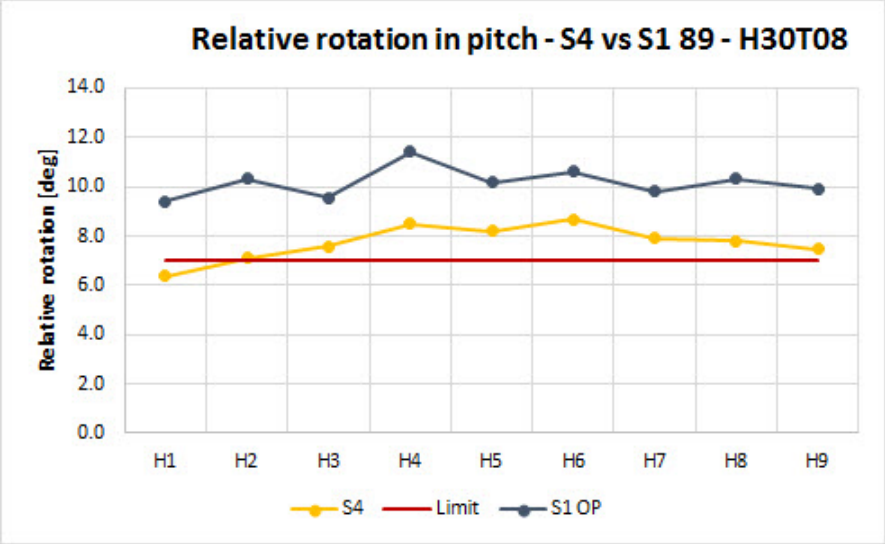

Figure 6.19: Comparison of setup 4 PILT and setup 1 OP - H30T08 - Setup 4 show less relative rotation for all wave directions

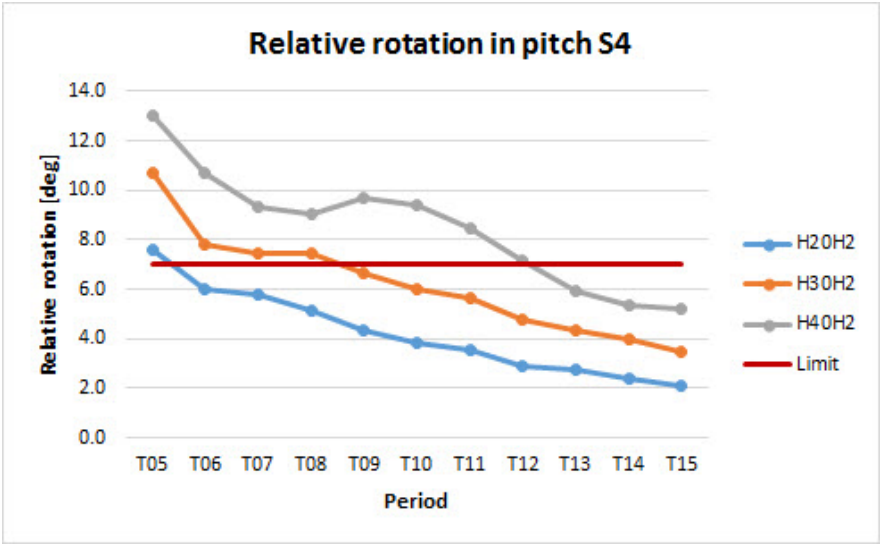

(a) Setup 4 pitch

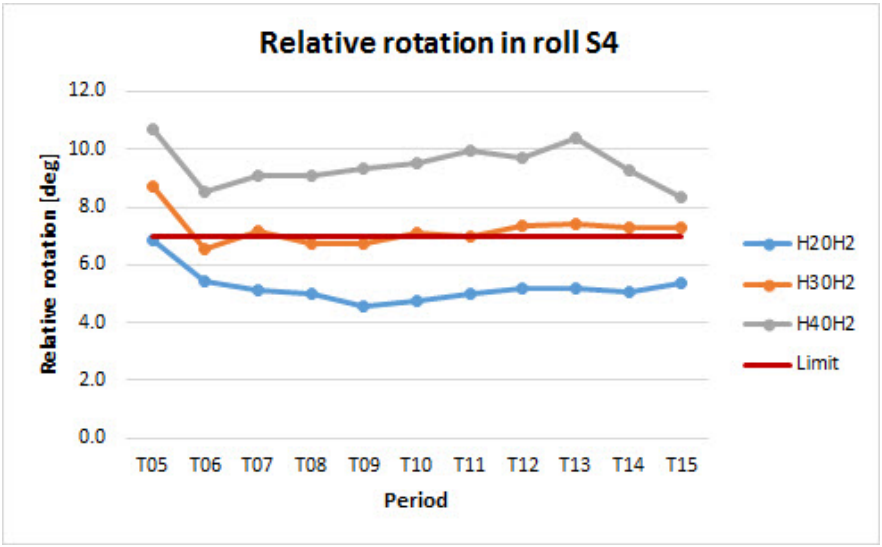

(b) Setup 4 roll

Figure 6.20: Comparison of wave heights in pitch and roll for different periods - Setup 4 - The relative rotation in pitch seem to decrease witch increasing periods. The relative rotation in roll seem to be at its maximum at a period of 5s and decrease to a approximately constant level for the other periods

6.9 Effect of CoG and geometry

The Statoil technical requirements state that the MHS cursor shall be able to handle tool/module with CoG at 5m below prongs for a module corresponding to maximum capacity of the MHS tower and shall have the capacity to lift 6mx6m footprint modules. In this section the standard module with a CoG of 3.0m, 4.25m and 5.0m and a footprint of 6mx6m is analysed and the effect of the altering CoG and different footprint is examined.

Altering the CoG and footprint will alter the moment of inertia of the module. Moment of inertia describes the torque needed to achieve a desired angular acceleration and is a measure of an object's resistance to changes in a rotation direction.

One should note that the module used in the simulation is based on a rectangular model with uniformly distributed mass. The moment of inertia of a real module will differ from the values used in this thesis.

The results showing the effect of altering CoG and footprint is given in table 6.14

Table 6.14: Effect of altering CoG and footprint -Setup 1 - H20T08H2 and H20T14H2. The relative rotation increase with increasing CoG and the change in relative rotation caused by altered footprint seems to be minimal

	H20T08H2 S1		H20T14H2 S1	
CoG	Pitch [Deg]	Roll [Deg]	Pitch [Deg]	Roll [Deg]
3	4.5	3.3	3.8	4.1
4.25	10.6	4.4	7.4	5.0
5	13.4	4.7	9.5	5.2
6x6 5	13.3	4.9	8.9	5.3

When comparing the results from figs. 6.21 and 6.22 with figs. 6.7 and 6.8 one would expect to see a slight change in relative rotation between T08 and T14 for pitch. The difference in roll would be expected to be minimal. This results seems to be consistent with the expectations, except for a module with setup 1 and CoG of 3m in pitch. The plot in fig. 6.21a show that the relative rotation for the given CoG is almost identical. The time series of the two scenarios is shown in fig. 6.23 and show that resonance occur when the period is 14s. If resonance was to

Table 6.15: Effect of altering CoG and footprint -Setup 1 - H20T08H2. The relative rotation increase with increasing CoG but the change in relative rotation caused by altered footprint is minimal

	H20T08H2 S4		H20T14H2 S4	
CoG	Pitch [Deg]	Roll [Deg]	Pitch [Deg]	Roll [Deg]
3	3.5	3.4	2.2	4.3
4.25	5.1	5.0	2.4	5.1
5	5.4	5.4	2.8	5.4
6x6 5	5.9	5.8	2.9	5.5

be disturbed, the relative rotation would be expected to be reduced.

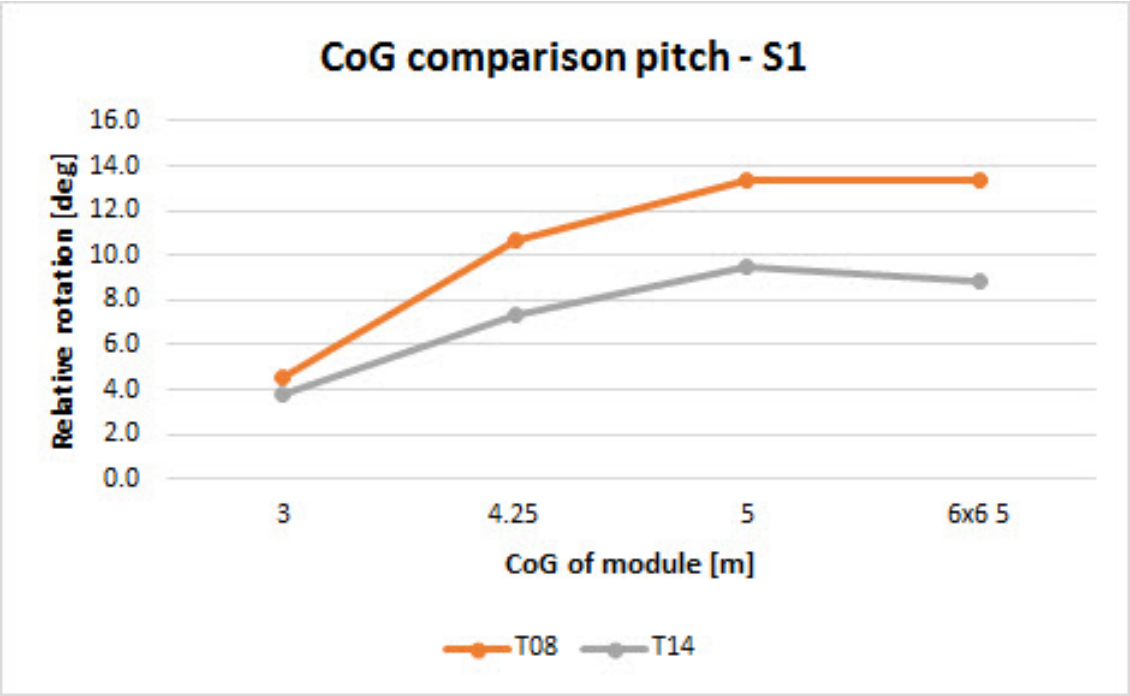

(a) Setup 1 pitch

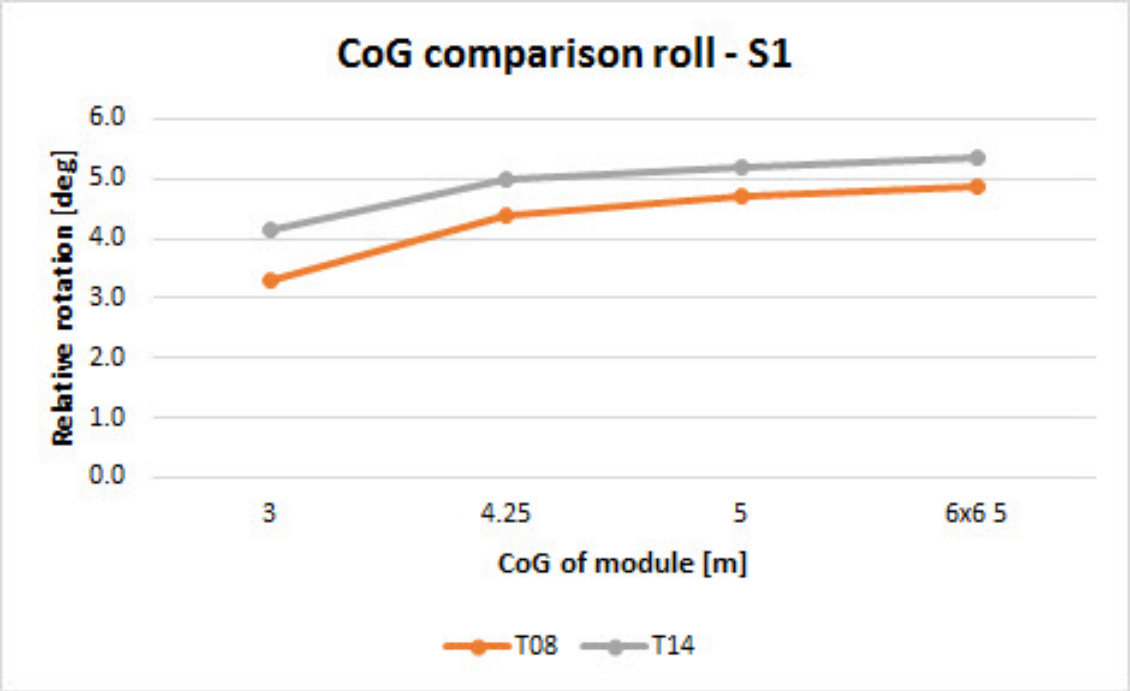

(b) Setup 1 roll

Figure 6.21: Effect of altering CoG and footprint -Setup 1 - H20T08H2 and H20T14H2. The relative rotation increase with increasing CoG and the change in relative rotation caused by altered footprint seems to be minimal

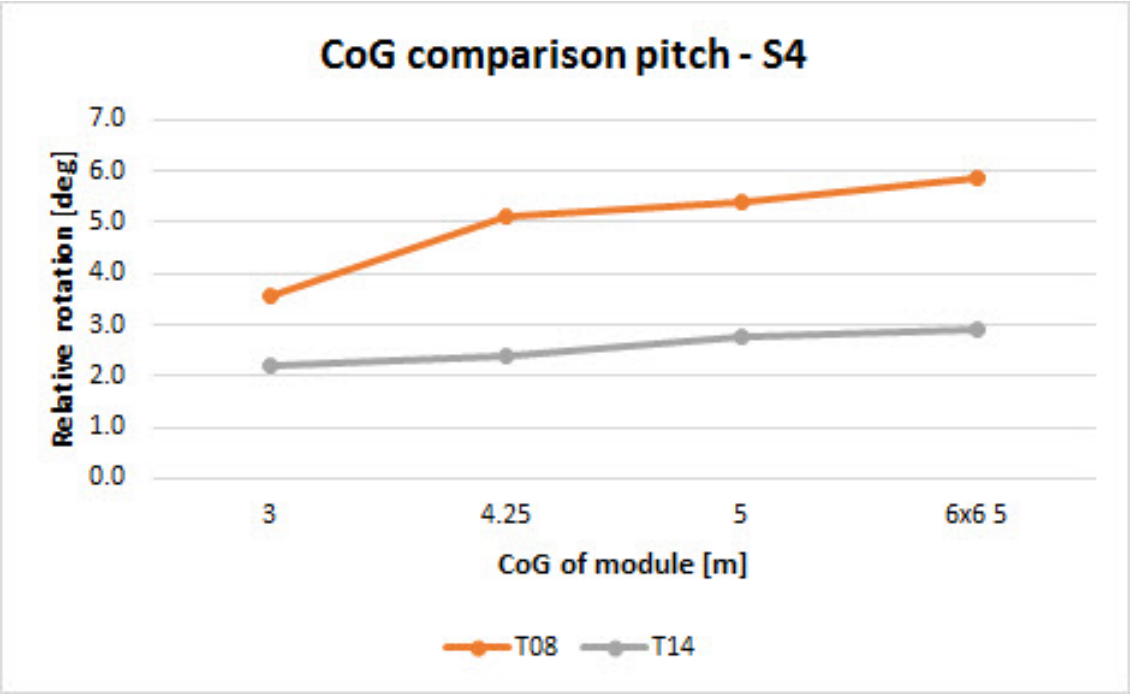

(a) Setup 4 pitch

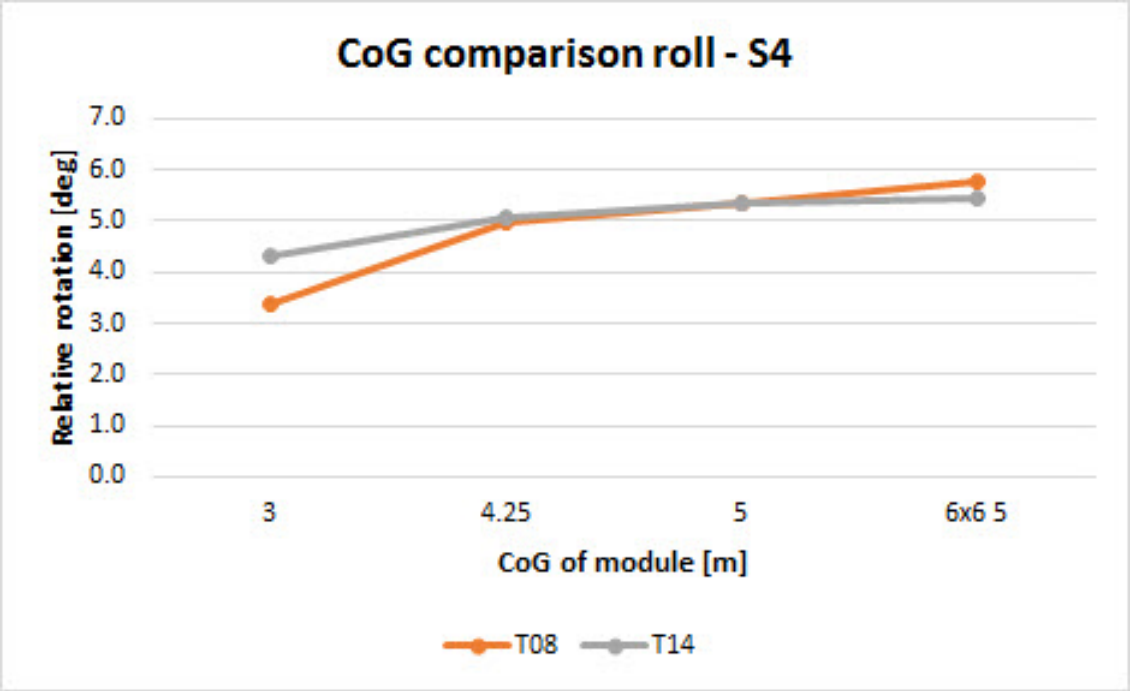

(b) Setup 4 roll

Figure 6.22: Effect of altering CoG and footprint -Setup 4 - H20T08H2 and H20T14H2. The relative rotation increase with increasing CoG and the change in relative rotation caused by altered footprint seems to be minimal

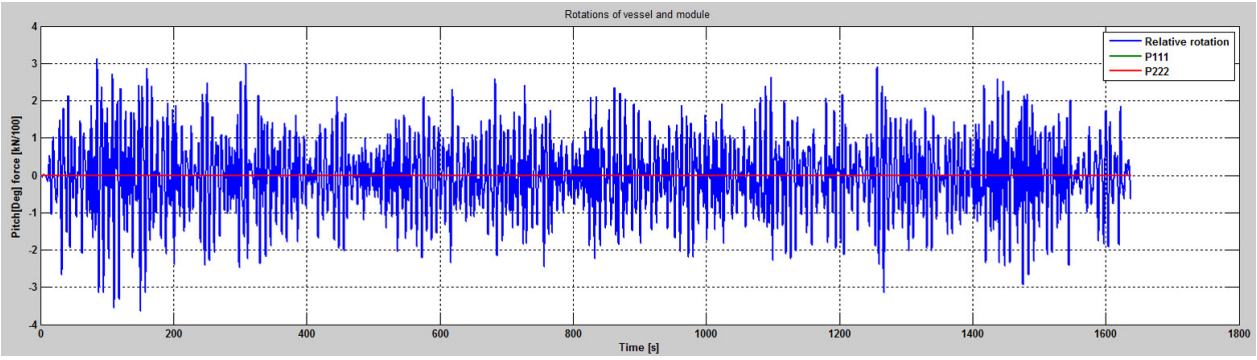

(a) Setup 1, CoG 3m, T08, pitch

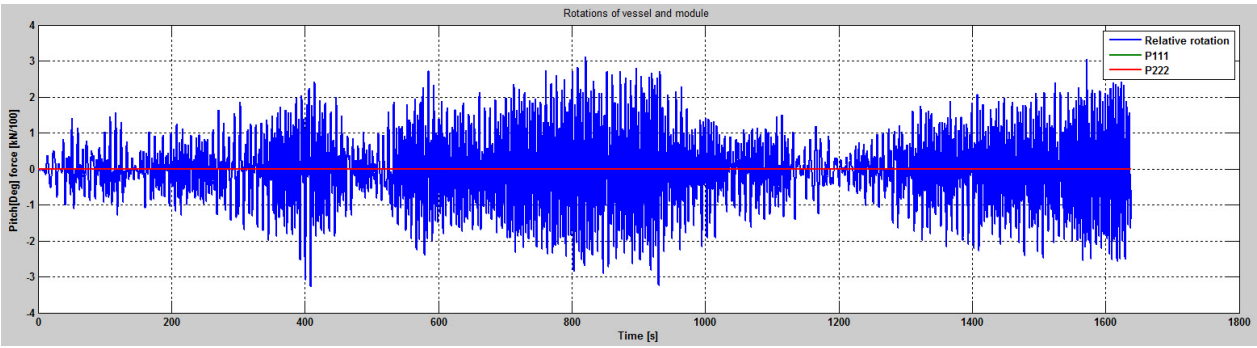

(b) Setup 1, CoG 3m, T14, pitch

Figure 6.23: Comparison of time series for module with CoG of $3m$ - H20T08H2 and H20T14H2. The plot in (b) show that resonance occur when the period is $14s$ and increase the relative rotation to the same level as in (a)

Chapter 7

Summary, Conclusion and Recommendations for Further Work

7.1 Summary and Conclusions

In this thesis a study of the MHS has been completed. The MHS is a lifting device capable of deploying and recovering subsea modules through moonpool. The main part of the study has been to use SIMO to simulate and analyse the critical phase where a module is suspended in air from the MHS tower. Conclusion regarding the deployment and recovery through moonpool have been based on the reports; Handling of Structures in Moonpool [14] and Modules Deployment and Recovery Analysis [15] by Næss.

7.1.1 Phase 1

The use of the new PILT design increase the maximum rotation of a module before momentum is exerted on the CGF By increasing the max allowed relative rotation the sea state for which a module can be deployed and recovered is also increased. For a module of 70Te, with

dimensions $4.2x4.2x8.5m$ using PILT design, the operative sea state will be $H_S < 2.0m$. For a lighter module of similar size , using the modified prong design, the operative sea state will be increased from $H_S < 1m$ to about $H_S = 1.5m$ [15].

Increasing the module CoG will also increase the relative rotation as seen in section 6.9, and hence lower the operative sea state. Greatest effect is seen when resonance is disturbed. Altering the size of the module have minimal or no significant effect on the relative motion.

Changing the cursor configuration can reduce the relative rotation. As the analysis show in section 6.7 the relative rotation is significantly reduced when moving the prongs close to the CGF. Figure 6.20 show that the operative sea state is $H_S = 2.0m$ for $T_P > 5.0s$ and a realistic wave direction.

The conclusion above show that all objectives in section 1.2 have been met.

7.1.2 Phase 2

Both the work with the UTA and the running tool show that the moonpool phase is not critical for realistic sea states, but this may not be representative for all modules and extensive testing and analysis of specific modules are required to decide the limitations for the specific case is needed. If a database with transfer functions for a wide range of objects and moonpools could be established, object forces will be easy to predict for any vessel where the moonpool responses are well documented [4].

7.1.3 Phase 5

The size of the UTA makes clearance between it and the moonpool walls a critical issue. For modules with a larger footprint larger than that of the UTA the sea state where recovery operations can be conducted would most likely have to be reduced compared to the UTA sea state limits.

By lowering the LWC, the clearance to the moonpool walls increase because of reduced relative rotation. The wave kinematics is not an important issue for the clearance. The relative motion between the module and the moonpool is mainly governed by the wave induced motion of the vessel Recovery of the UTA can be carried out in sea states with hs in the range of $2-3m$ depending on the sea state parameters. The dynamic tension in the lift wire will not be the governing case as long as a DAF of 1.3 is incorporated in the design.

7.1.4 Skidding system

The conclusion from the friction test was that as long as distance between the connectors of the skidding pallets are not increased, the skidding tracks and shifters should be able to handle modules up to $70Te$ [10].

7.2 Discussion

It seems like resonance plays an important role when the model is suspended in air. To increase the sea state where modules can be deployed, one should put effort into solutions that disturb and equalize the resonance effect. Using bumpers mounted on the cantilever beams of the CGF was suggested by Næss. The bumpers seem to effectively equalize the resonance. A negative effect of the bumpers is that forces acts on the cantilever beam at two positions, causing moment on the CGF. When the prongs are positioned close to the CGF they seem to give the same effect as the bumpers. Resonance seem to be equalized by the force acting in the opposite direction of the motion as described in section 6.7.2. It is hard to quantify absolute values for the sea state. The reason being that the governing issue is the vessel response and that small details in the numerical model of the sea state will influence the results significantly [15]. The results in phase 2-5 is based on the analyses done regarding the work with GSC project. The modules are used because they represent properties that is close to the requirements stated in TR1231.

Small changes in the SIMO model may have great impact on the relative rotation of the module. When comparing the simulations where the stiffness of the CGF is changed, crefseastate1 and fig. 6.20, it becomes evident that the results are highly sensitive to the input parameters

7.3 Recommendations for Further Work

During the work with the master thesis several interesting factors concerning operability of the MHS were identified. Some of these factors were not analysed in detail. The list of recommendations for further work is presented below:

- Do a comparison analysis of the bumpers and different cursor configuration
- Analyse the effect of changes in sea state by the use of different wave spectra (Torsethaugen and double-peaked JONSWAP)
- Analyse the effect of changes in module geometry
- Analyse the effect of changes in module mass
- Perform analysis of the different phases of deployment and recovery with a focus on the above mentioned factors
- Perform a structural analysis of the MHS with a focus on different cursor configuration

Bibliography

[1] (2004). SIMO - General Description. Technical report, Marintek Trondheim.

[2] (2008). *DP Operation Manual for Skandi Seven.* Global Maritime.

[3] (2009). SIMO - Theory Manual Version 3.6, rev: 2. Technical report, Marintek Trondheim.

[4] Berget, K. (2013). Subsea 7 Forced Heave Moonpool Tests. *MARINTEK.*

[5] DNV (2011a). DNV-OS-H101 Marine Operations, General.

[6] DNV (2011b). Rules for classification of ships, part 6 chapter 7.

[7] DNV (2014a). DNV-RP-C205 Environmental Conditions and Environmental Loads.

[8] DNV (2014b). DNV-RP-H103 Modelling and Analysis of Marine Operations.

[9] Gohin, F. (2013). Design Report , Module Handling System, 60806164-A-RP-0011, Rev. 02. *Subsea 7 Internal Note.* Subsea 7 Internal Document.

[10] Grødem, G. (2014). Technical Note, Seven Viking Shifter Friction, Gullfaks Compression, ES-ENG-R-TN-0006, Rev. 01. *Subsea 7 Internal Document.* Subsea 7 Internal Document.

[11] Haver, S. Prediction of Characteristic Response for Design Purposes , UiS.

[12] Hollund, B. S. (2013). Seven Viking Equipment Overvire. *Subsea 7 Internal Document.*

[13] Idsøe Næss, T.-B. (2012). FMC Multitool MFRT weather limitation study. *Subsea 7 Internal Document.*

[14] Idsøe Næss, T.-B. (2014a). HANDLING OF STRUCTURES IN MOONPOOL. *Subsea 7 Internal Document*.

[15] Idsøe Næss, T.-B. (2014b). MODULES DEPLOYMENT AND RECOVERY ANALYSES. *Subsea 7 Internal Document*.

[16] Jacobsen, T., Idsøe Næss, T.-B., and Karunakaran, D. (2012). COMPARISON WITH FULL SCALE MEASUREMENTS FOR LIFTING OPERATIONS. *2nd Marine Operations Specialty Symposium (MOSS 2012)*.

[17] Jacobsen, T. B. (2013). Technical Note, Skidding System, 60806164-N-TN-0010, Rev. 02. *Subsea 7 Internal Document*. Subsea 7 Internal Document.

[18] NORSOK (2007). NORSOK Standard N-003 Action and Action Effects.

[19] Torsethaugen, K. and Haver, S. (2004). Simplified double peak spectral model for ocean waves. In *The Proceedings of The Fourteenth (2004) International OFFSHORE AND POLAR ENGINEERING CONFERENCE*. International Society of Offshore and Polar Engineers (ISOPE).

[20] WPCI (2015). World Ports Climate Initiative, Environmental Ship Index (ESI). Available from: http://www.environmentalshipindex.org/Public/Ships [14.05.2015].

Acronyms

H_S Significant Wave Height

T_P Peak period

AHC Active Heave Compensator

ALW Auxiliary Lift Winch

CGF Cursor Guide Frame

CGFW Cursor Guide Frame Winch

CoG Center of Gravity

DAF Dynamic Amplification Factor

DNV Det Norske Veritas

DP Dynamic Positioning

FCM Flow Control Module

GSC Gullfaks Subsea Compression

GWW Guide Wire Winch

IMR Inspection, Maintenance and Repair

JONSWAP Joint North Sea Wave Observation Project

LWC Lift Wire Cursor

MHS Module Handling System

MLW Main Lift Winch

NORSOK Norsk sokkels konkurranseposisjon

OP Original prong

PILT Modified Prong

RAO Response Amplitude Operator

ROV Remote Operated Vehicle

SCM Subsea Control Module

SIMO Simulation of Marine Operations

STD Standard deviation

UTA Umbilical Termination Assembly

WROV Working Class ROV

Appendix A

Seven Viking Main Data

Seven Viking

7

Type:
IMR, Survey & Light Construction

Classification:
DnV 1A1 with the following class notations: SF, E0, DYNPOS-AUTR, CLEAN DESIGN, NAUT-AW, COMF-V(3), DEICE, ICE-C, HELDK-SH(CAA-N), WS, LFL*

The *Seven Viking* is a state-of-the-art vessel, with the innovative X-BOW® it is designed to meet the high demands of Inspection Maintenance and Repair (IMR), Survey and Light Construction in some of the harshest environments. The versatility of the vessel allows for Scale Treatment and Light Diving Support services.

- Length 106.5m x breadth moulded 24.5m
- Service Speed: 16.0 knots
- Accommodation: 90 persons
- AHC Offshore crane: 135 Te @13m
- 2 x Workclass ROVs
- 1 x Observation class ROV

Seven Viking

November 2012

General Information

Classification	DnV 1A1 with the following class notations: SF, E0, DYNPOS-AUTR, CLEAN DESIGN, NAUT-AW, COMF-V(3), DEICE, ICE-C, HELDK-SH(CAA-N), WS, LFL*
Built	Norway 2012
Flag State Authority	Norway

Dimensions

Length Overall	106.5m
Breadth moulded	24.5m
Draught (operational)	6.5m
Draught (max)	8.0m
Freeboard at operational draught	5.0m
Freeboard at max draught	3.5m

Main Data

Service Speed	16.0 knots
Accommodation	90 persons (64 single cabins, 13 semi-single cabins)
Personnel elevator	
Mid Ship Helideck for SuperPuma and Sikorsky S-92, Ø26.1m	

Power generation and propulsion

Generators	2 x 4,320 kW main diesel 2 x 1,824 kW main diesel 1 x 250 kW emergency generator
Propulsion	3 x 3 MW contra rotating azimuth
Thruster	1 x 1.4 MW retractable compass 1 x 1.4 MW combi retractable 1 x 1.7 MW tunnel SCR (NOx Catalyst) on exhaust

Tank Capacities (100%)

Fuel MDO	2,100m³
Fresh water (potable)	1,300m³
Fresh Water	200m³
MEG / Brine	600m³
Special Products, LFL	450m³

Working Deck

Deck strength	10t/m²
Deck area	approx 830m²

Weld-free seafastening

Twist locks are integrated in part of the working deck for quicker mobilisation/demobilisation of standard containers.

Cranes

Main Crane

AHC Offshore crane	135t @13m
Maximum reach	30m
Wire length	2,000m
AHC whip line	10t @ 31m
Whip line wire length	1000m
Operational limit	5.0m Hs Man riding

Auxiliary Cranes

Telescopic crane for provision	1 x 15 Te
Telescopic cranes in MHS hangar	2 x 3 Te
Telescopic crane on pallet	1 x 3 Te
Telescopic crane in ROV hangar	1 x 1 Te

Module Handling System

MHS fully integrated in hangar with cursor system for controlled launch and recovery of modules to 2,000msw in conditions up to 5m Hs.

Capacity to handle modules up to 70 Te and 10m height Skidding system with storage capacity of up to 8 skidding pallets, including 4 indoor storage positions.

Winches: 1 x 70 Te, 1 x 20 Te, 3 x 5 Te.

Integrated AHC winch with dedicated HPU for 12 lines hydraulic downline.

ROV

All ROV systems in enclosed ROV hangar
2 x Workingclass ROVs (Schilling HD), rated to 3,000 msw, launched over side by A-frames. AHC Umbilical winch, 2,500m umbilical

1 x Observation ROV (SubAtlantic Mohican), rated to 2,000 msw, launched by A-frame. AHC Umbilical winch, 1,800m umbilical.

Operational limit 5.0m Hs for all systems

Scale Treatment

Scale treatment pumping spread and special product tanks integrated in vessel
Pumping capacity 30-2,800 l/min @ 0-345 bar
Pre heating to 90 deg
Mixing units for small volumes of additives.

Operation control

Joint operation control room for Shift Supervisor, MHS control, ROV control, Scale Treatment control, third party control and survey with direct view to MHS.

Figure A.1: Seven Viking Main Data

Appendix B

Seven Viking Response Amplitude Operators

In this appendix graphic illustrations of the RAOs are presented.

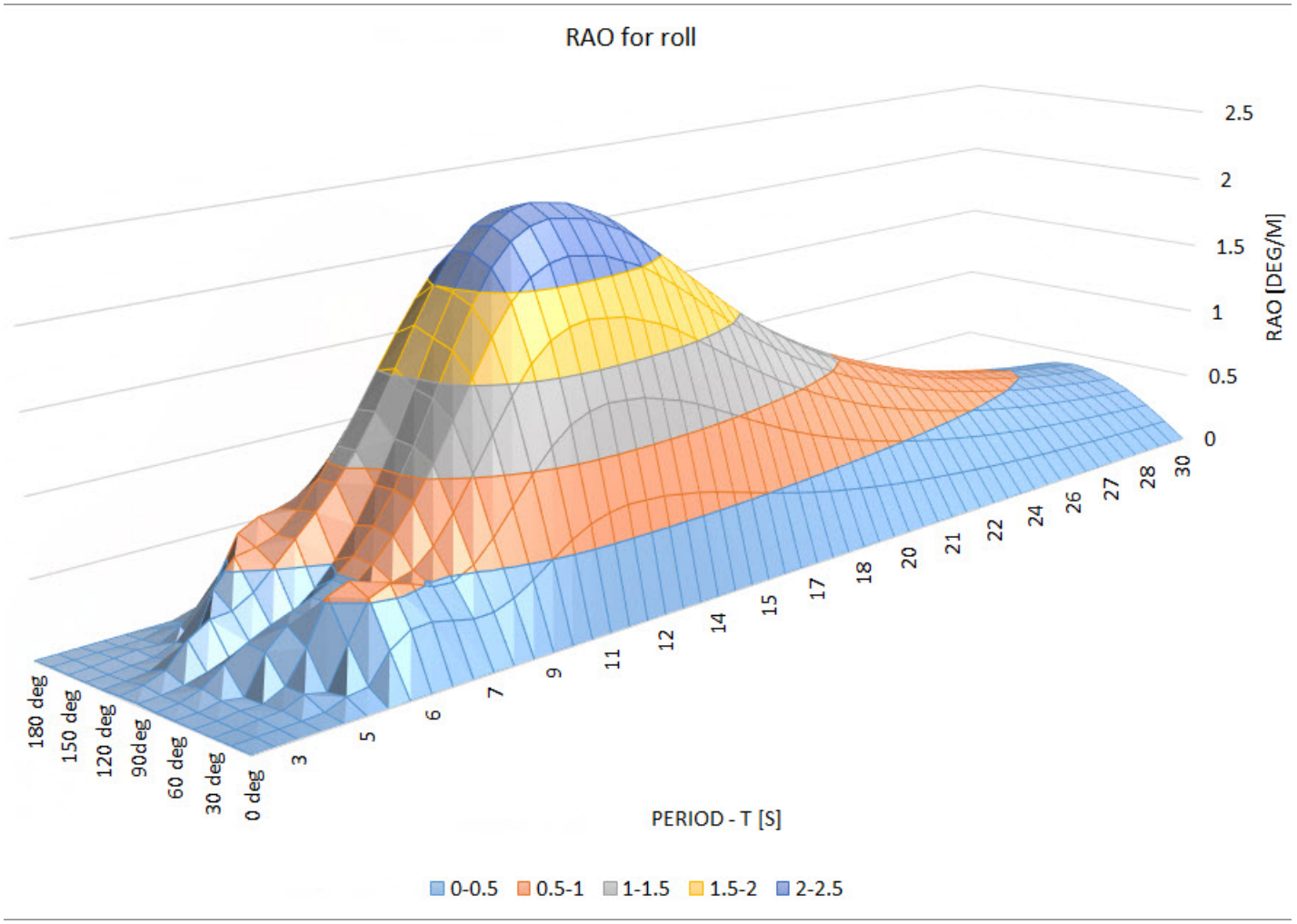

Figure B.1: RAO for roll

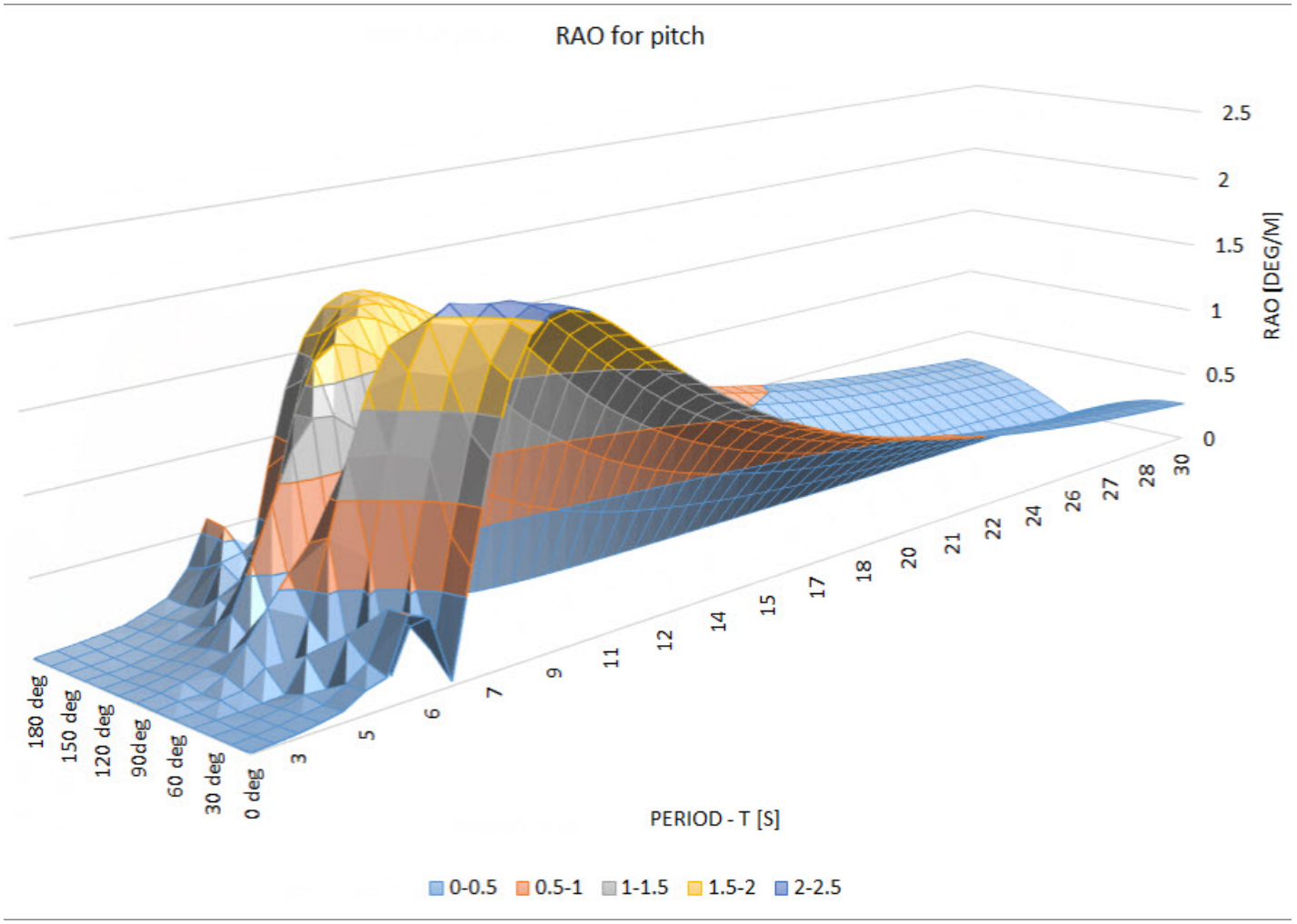

Figure B.2: RAO for pitch

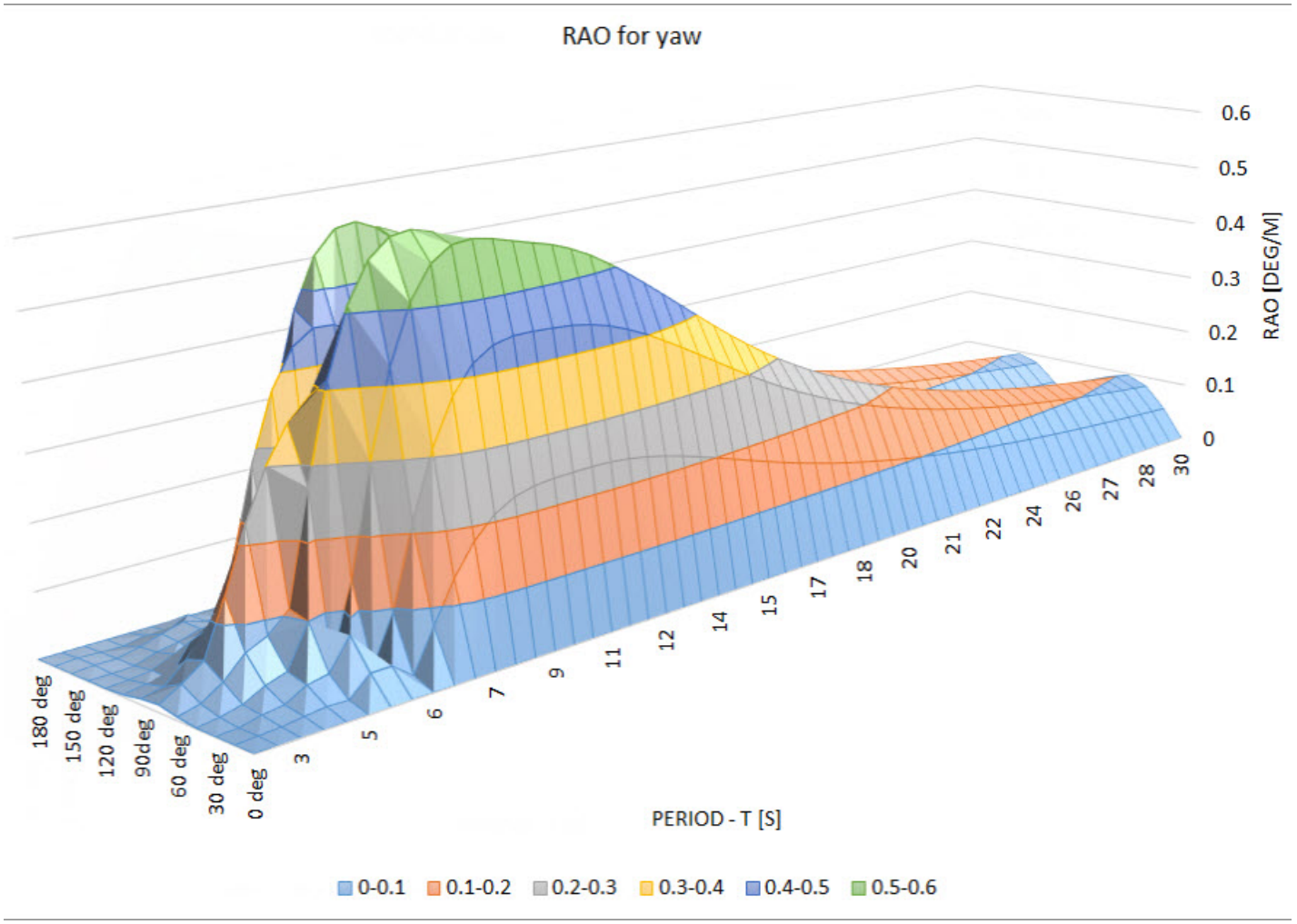

Figure B.3: RAO for yaw

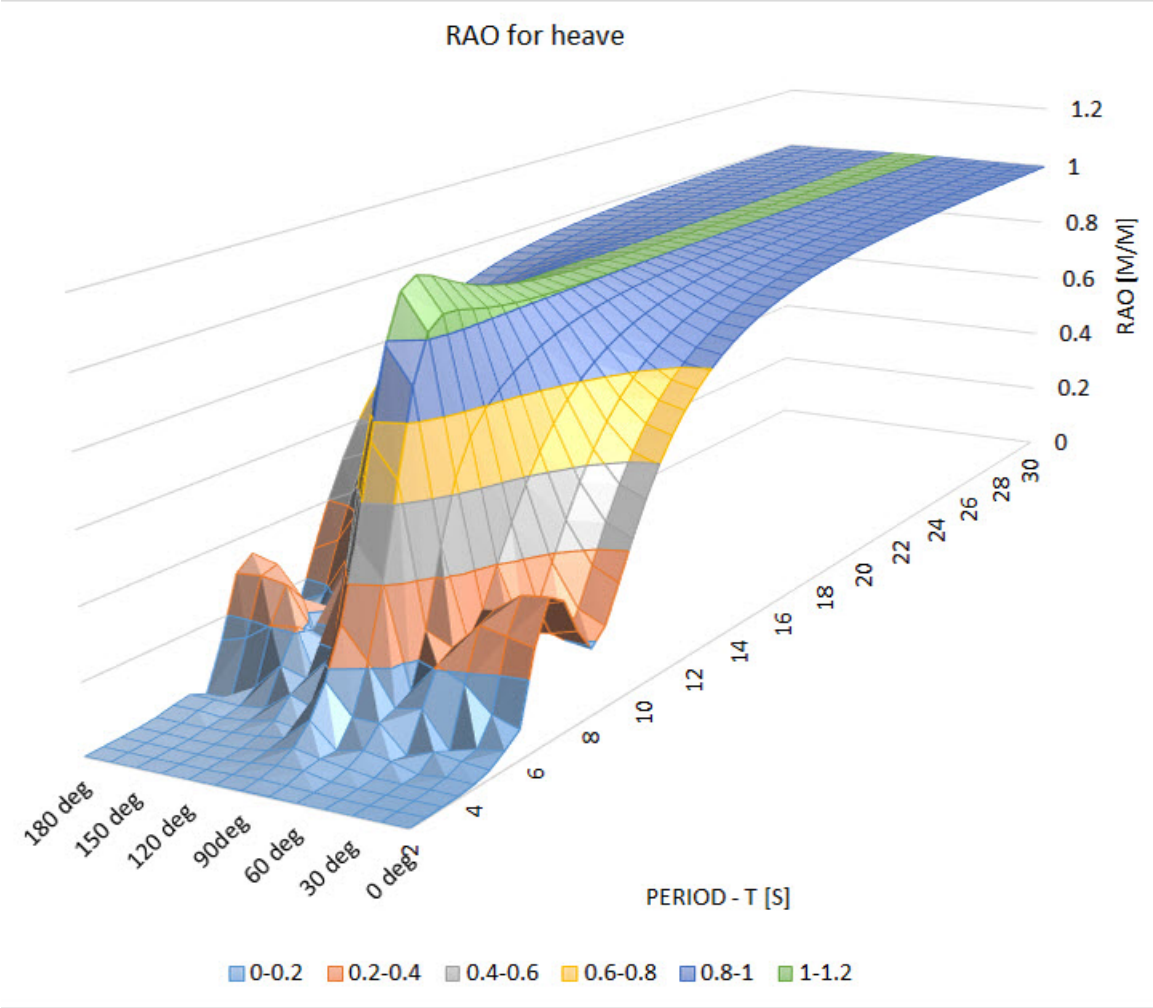

Figure B.4: RAO for heave

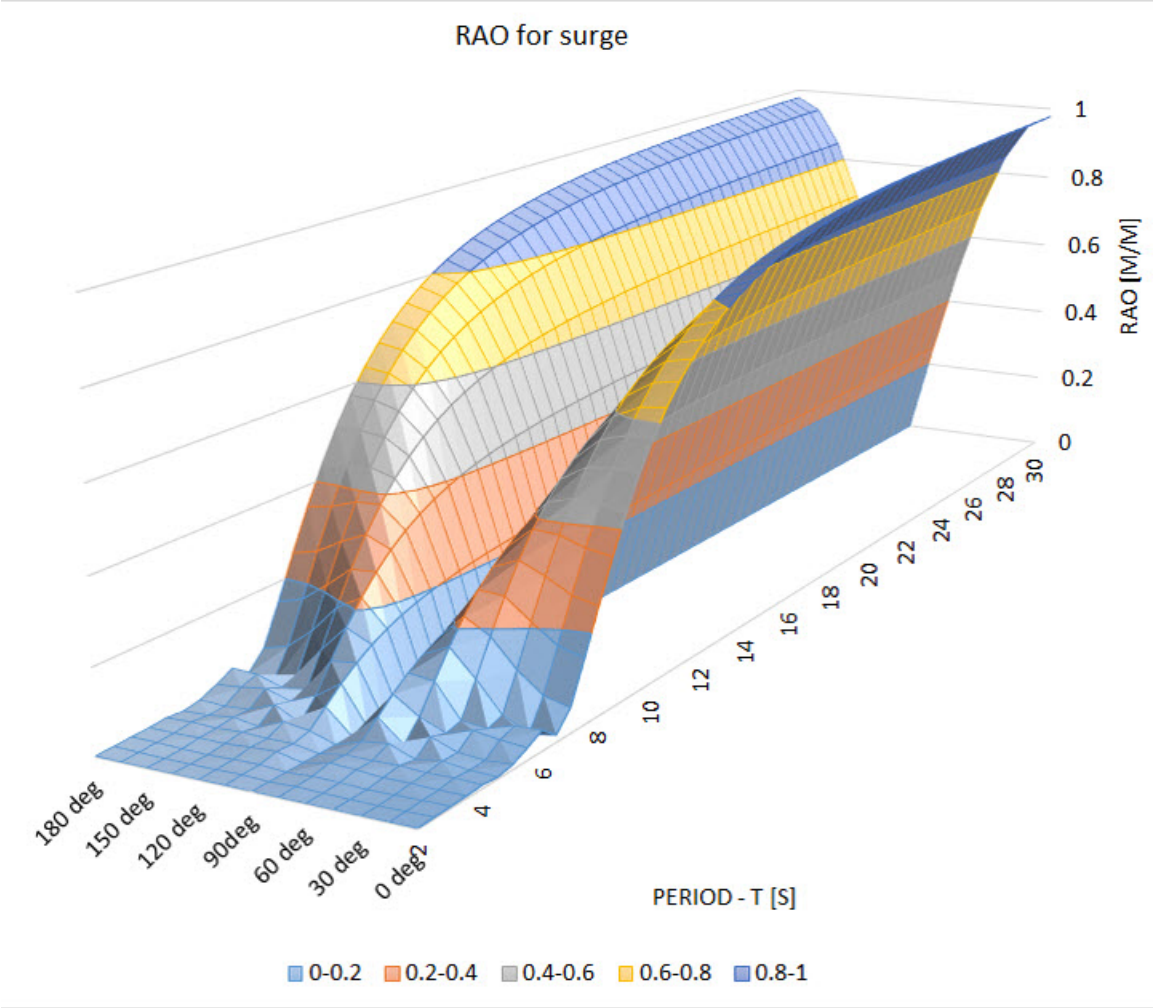

Figure B.5: RAO for surge

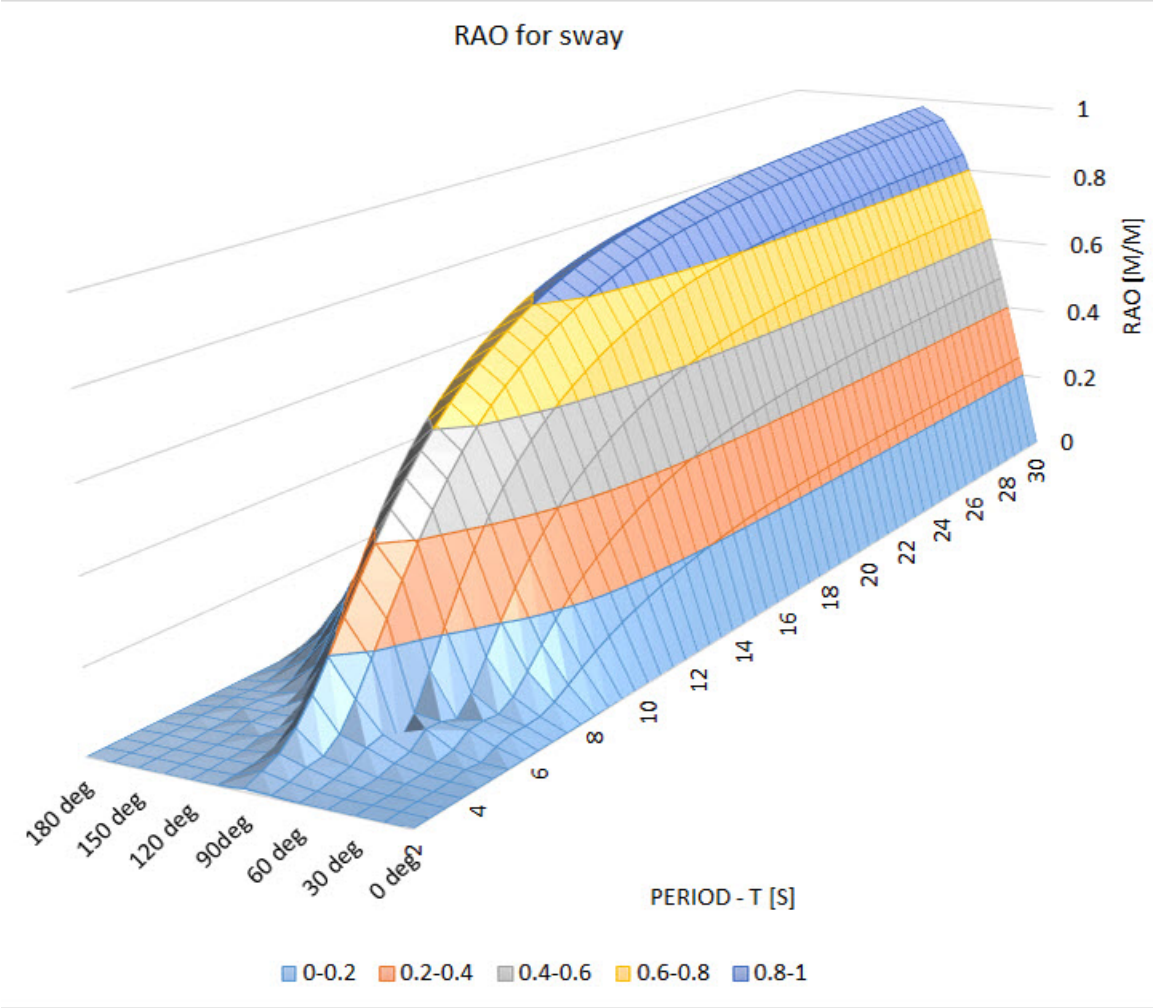

Figure B.6: RAO for sway